A New Model for the Generation of Photoplethysmographic Signal with Its Application to the Analysis of Beat-to-Beat Blood Pressure Variability

GU Yingying

A Thesis Submitted in Partial Fulfillment

of The Requirements for the Degree of

Master of Philosophy

in

Electronic Engineering

June, 2004

Acknowledgements

I would like to express my deepest gratitude to my supervisor, Prof. Y. T. Zhang, for his support and guidance throughout the two years of my master studies. Without his help this work could never be possible. I would also like to thank him for introducing me into this new field, biomedical engineering, which is appealing and exciting with various interesting topics. Meanwhile, I would like to express my deepest appreciation to Prof. C. Zhang for her support and tireless help at the final stage of my thesis work.

I would also like to express my appreciation to my colleagues in the BME lab for always being considerate and supporting each other. We together make efforts in constructing a nice atmosphere for our research. My special thanks go to Ms. T. Ma, whose ever lasting help and support makes me feel warm and happy. Warmest thanks also go to Mr. Chu, Mr. Kevin Hung, Mr. L. Yip, Mr. F Chen, Ms. Maggie Lee, Ms. Carmen Poon, Ms. X.Y. Zhang, Mr. Sunny Chu, Ms. X.F. Teng, Ms. Mico Wong, Mr. Y.S. Yan, Mr. Clifford Lui, and Mr. Rico Tai, for making me feel staying at home.

I would especially express my deepest thanks to my dearest parents for their ever lasting encouragement and their strongest support. With their deep love, I will never lose my confidence in experiencing any challenge in my life, and I will never feel lonely anytime, anywhere.

Abstract

The extensive use of the photoplethysmographic (PPG) technique in many clinical environments has raised great interest in understanding its underlying physiological process and therefore making better use of it. In this thesis, based on the Integral Pulse Frequency Modulation (IPFM) process mimicking neural physiological encoding mechanisms and the circuit theory describing the characteristics of cardiovascular system, a new model for the generation of PPG signals is developed, with the focus on the application of PPG signals to the analysis of the beat-to-beat blood pressure variability (BPV).

Low-pass filtering (LPF) technique has been suggested in literatures as a simple approach to recover the original input modulating information to an IPFM process. However, due to the non-linearity of the IPFM model and the difficulty in estimating the threshold value of neurons *in vivo*, it is practically impossible to recover precisely the input modulation information through a simple LPF. Instead, we found through a mathematical analysis that such demodulation is of special importance for studying the firing characteristics of neural and muscle cells. The results of the simulation with different patterns of modulating input to the IPFM model show that the firing rate function can be reconstructed with reasonable accuracy by a LPF-based demodulation method.

Taking advantage of the IPFM mechanism that reproduces event series of modulated cardiac periods, a new model is developed to mimic the generation of the PPG signal based on its physiological mechanism. By taking into account the characteristics of cardiovascular system, the influence of the sympathetic and parasympathetic branches of the autonomic nervous system, together with the transmission properties of pressure wave through arterial system, the novel model transforms a continuous input signal into event series representing ECG and PPG signals. Furthermore, based on the interaction with heart rate, the time-varying BP and PTT are realized in the new model. The model is tested by comparing the results of the simulation with experimental data from resting subjects. The comparison indicates that the proposed IPFM-based new model does plausibly capture a number of

important features of the PPG signal that are observed in the experiments. It also shows great potential in investigating certain characteristics associated with PPG signals under different physiological conditions The analysis on the relationship between the modulating inputs and the output of our IPFM-based model suggests that the spectra of PPG and ECG trains, which combine the information of firing rate with neural dynamics, may serve as a better substitute to evaluate heart rate variability (HRV) by analyzing the power of the sidebands.

Besides the physiological generation mechanism, certain characteristics on the waveform of PPG signals that were obtained from experimental data are investigated statistically. The results of this study indicate that there could be a significant correlation between the FY interval, representing the rising phase, of the PPG signal and pulse transit time (PTT) estimated as the time delay from ECG to PPG signals. Based on this new finding and the previously reported relationship between PTT and arterial blood pressure (BP), a new approach is proposed for the estimation of the beat-to-beat BPV, which plays a fundamental role for a better comprehension of the patho-physiological properties of the complex mechanisms. Compared with the AAMI standard, the results of both the multi-beat and the beat-to-beat estimations of BP based on experimental data are promising. The estimated BPV using the FY interval is consistent with that from FINAPRES device which indicates that the new FY-based method may provide an easy, low cost, and acceptable substitute of the existing techniques for analyzing non-invasively and continuously the beat-to-beat fluctuations in BP using PPG technique only. The potential application of this proposed new method could be huge, and thereby it may contribute significantly to both clinical diagnoses and home health care, which can not be achieved by the currently limited approaches for BPV analysis.

The semi-repetitive nature of the PPG signal has lead to another new application for human authentication. Distinctive features were extracted from PPG signals to generate the template for each subject. They are unique identifiers specific to different persons while they are similar enough to recognize the same person. The preliminary results with high successful rates for the group of subjects used in this study demonstrate that the new method is promising for human verification.

论文摘要

光电体积描记信号的广泛应用激发了人们对深入理解其产生机制，从而更好的发掘其应用价值的浓厚兴趣。本论文基于模拟神经编码机制的积分脉冲频率调制（IPFM）机制，建立了一个产生光电体积描记信号的新模型，并着重将该信号用于估测与每次心脏搏动相对应的血压变化率（BPV）。

低通滤波技术被人们认为是一种用于还原IPFM过程的起始调制输入信号的简单方法。然而，由于IPFM模型的非线性特征，以及从生物体上估计神经元阈值的难度，事实上是难以将起始调制输入信号通过简单的低通滤波来精确还原的。相反地，我们通过数学推导发现这样的解调方法对于研究神经和肌肉动作电位发放特性有着重要的意义。采用不同形式输入IPFM模型的仿真结果显示神经动作电位发放速度这一特性可以较为准确地通过简单的低通滤波来得到。

利用模拟产生心动周期的IPFM模型，本论文建立了一个可模拟每搏心跳并产生相应的光电体积描记信号的新模型。综合考虑心血管系统的特点和脉搏波在动脉系统中传输的特性，该模型将连续输入信号转化为离散事件序列，分别表示光电体积描记信号和心电信号。同时，基于心率与血压之间的关系，以及血压与脉搏波传输时间之间的近似线性关系，该模型还可以产生动态变化的血压和脉搏波传输时间。模型的可靠性通过将仿真结果与相应的实验结果相比较而判断。比较结果显示本模型合理地纳入了一些重要的光电体积描记信号特性。通过对该模型输入与输出之间关系的研究，我们进一步发现光电体积描记信号和心电信号的频谱可作为研究心率变化率的一种新途径。

除了光电体积描记信号的产生机制之外，本论文还从数理统计的角度对该信号波形上的某些特征进行了研究。研究结果显示光电体积描记信号的FY间距（代表上升延特性）在一定条件下与脉搏波传输时间（由心电信号和光电体积描记信号估算得到）有很高的相关性。基于脉搏波传输时间与动脉血压之间的关系，本论文提出了采用FY间距来估算与每次心脏搏动相对应的血压及其变化率的新方法。血压变化率对于了解人体的病态生理特征有着极其重要的意义。基于实验数据，我们分别作了不连续和连续（与每次心脏搏动相对应）的血压估算。通过与AAMI标准相比较，该方法的估测结果令人满意。此外，我们还对与每次心脏搏动相对应的BPV在时域和频域分别进行了分析。用FY间距估算的BPV结果与从另一种测量仪器（FINAPRES）上得到的结果基本一致，从而表明这种仅仅基于光电体积描记信号的方法将有可能替代现有技术而成为一种简单而又准确的血压测量新方法。

由于光电体积描记信号的波形的近似可重复性，本论文还提出了一种采用该信号进行人体身份识别的新方法。我们从信号中提取了一系列可区别不同个体的特征，并生成每一个个体的特征模版。初步的结果令人满意，从而表明这种方法将很有可能成为一种用于生物个体识别的新技术。

Contents

List of Figures

List of Tables

Chapter 1

Introduction

Photoplethysmographic (PPG) technique has been widely used for a variety of applications to provide useful information for the evaluation of clinically valuable physiological parameters. Mathematical modeling based on the physiological generation process of the PPG signal would certainly provide an insight into better understanding of the signal and therefore making better use of it. However, many researchers just employed this technique without exploring or elaborating the underlying generation mechanism of the PPG signal. In this chapter, an overview on the generation mechanism of the PPG signal will be provided, which is closely related to features described by the Integral Pulse Frequency Modulation (IPFM) and the Windkessel model, as well as some other properties of the cardiovascular and the arterial system. The IPFM model and the Windkessel model will be reviewed based on previous work. This is followed by an introduction on the current research status of the beat-to-beat blood pressure variability (BPV) analysis which may result in a promising new application of the PPG technique. Finally, the main purpose of this study is given and the organization of this thesis is outlined.

1.1 IPFM Model

1.1.1 Description of the IPFM Model

Essentially, the IPFM model is a physiologically plausible device to transform a continuous non-negative input signal into an event series representing the timings of cardiac activity [1] [2]. In the IPFM model, any two consecutive event-occurrence times t_i and t_{i+1} satisfy the relationship [3]:

$$V_{th} = \int_{t_i}^{t_{i+1}} (m_0 + m_1(t))dt \qquad (1\text{-}1)$$

where $m_1(t)$ is the information or modulating input signal, m_0 is the constant input signal, t_i is the incidence of the ith impulse , and V_{th} is the integration threshold. As illustrated by Fig.1-1 (a), the non-negative time-continuous input signal, which consists of a DC component m_0 and a modulating signal $m_1(t)$, is integrated; whenever the integrated value exceeds a threshold V_{th} , a unitary spike is generated and the integrator is reinitialized. Fig. 1-1(b) shows an integration process denoted by $x(t)$ and an output pulse train denoted by $y(t)$ when $m_1(t) = A\cos(2\pi f_m t + \theta)$ is applied as the input modulation signal to the IPFM model.

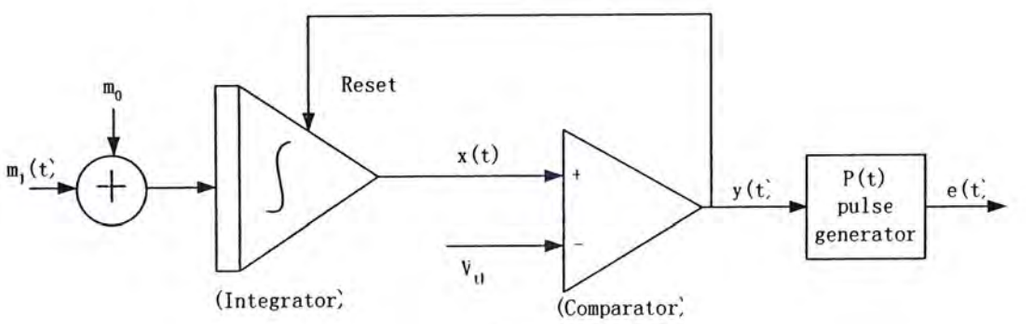

(a)

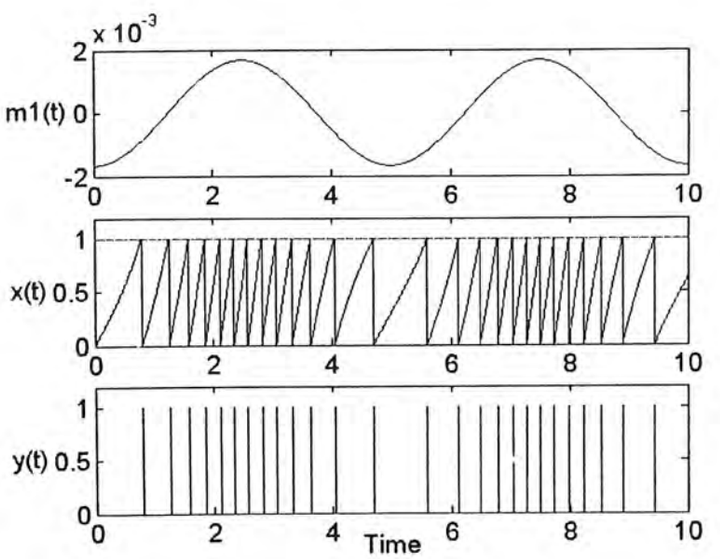

(b)

Fig. 1-1: IPFM model: (a) Schematic diagram of the IPFM model; and (b) the input and output of the IPFM model for $m_1(t) = A\cos(2\pi f_m t + \theta)$.

To mimic the action potential sequence generation process and various coding schemes of neurons, different neuronal models can be built by choosing a specific integrator with different parameters reflecting neural electrical behaviors to replace the unspecified integral operator as shown in Fig.1-1 (a). The integration process is determined by membrane electrical properties, neuron anatomical structure, etc. The membrane threshold V_{th} depends on neuronal geometry and the membrane voltage depolarization level at the site of the origin required for action potential initiation. The input signals to the IPFM model can be different for different applications, representing the input variation, such as stretch, force, pressure, synaptic current, etc. In the neuron case, for example, the integrated signal is the neuronal membrane potential, which rises until the threshold is reached and consequently a pulse is generated. The resetting function corresponds to the reestablishment of resting membrane voltage over much of the neuron surface after the passage of a neuronal spike or action potential [3].

The spectral analysis of an IPFM process could provide insights into the mechanisms of encoding and decoding in nervous systems. There is evidence that the major features of the spectrum describing an IPFM process are similar to that observed in the nervous system, as investigated by Bayly [3]. More importantly, Bayly had pointed out that with a single sinusoidal signal $m_1(t) = A\cos(2\pi f_m t + \theta)$ as the input modulation signal to the IPFM model and under certain restrictions, it is theoretically possible to recover the input modulation signal through a simple LPF.

1.1.2 Background of the IPFM Related Modeling

The IPFM model, capturing some of the crucial neuronal behaviors, but at a much reduced complexity, is a powerful tool in studying neural coding aspects. Many signals due to physiological event, such as nervous pulse trains and cardiac

contractions, can be appropriately interpreted by the IPFM model. Particularly, the heart rate variability (HRV) signal, which is recognized as one of the most valuable measures reflecting various important cardiovascular pathologies with which an alteration of the autonomic nervous system (ANS) may be associated, has been extensively studied. On the other hand, due to the possibility in recovering the input modulation information through a simple LPF, the IPFM model has become especially important when the recovering of a hidden modulation signal behind an observed set of events is of interest. As a result, the IPFM model has been used for mainly the following two purposes. First, it has been utilized to verify the correspondence between the spectral structures of autonomic input and the estimated spectrum of the HRV, relying mainly on the theoretical work of Bayly (1968). Second, the IPFM model provides a framework for evaluating how precisely the proposed method for the HRV analysis could reflect the activities of the ANS.

Many studies have been carried out to investigate the feasibility of extracting the hidden dynamics of the cardiac nervous system from the observable characteristics of the HRV obtained from the output of the IPFM model [2]. In these studies, the input modulating signal $m_1(t)$ is the signal representing the autonomic nervous function, and the constant input signal m_0 is the mean heart rate which determines the duration of each RR-interval when there is no autonomic modulation of the sino-atrial (SA) node's intrinsic firing rate. The output is thus an RR-interval series. If the IPFM model provides a realistic representation of the autonomic regulation of the HRV, and if Bayly's theory is applicable to the analysis of the HRV, the spectral structure of the HRV, at least in the lower frequency range well below the mean heart rate, would faithfully reflect that of the autonomic regulatory input. In fact, Hyndman et al. [4] have already confirmed the applicability of this theory to the HRV analysis, and many researchers have made use of this approach in their studies [5] [6] [7] [8]. In other

words, the IPFM model has greatly facilitated the studies on extrapolating the hidden dynamics of autonomic regulation from a series of heart beats (or RR intervals).

Recently, further studies are being carried out to improve the IPFM model to better simulate the HRV signals. On the other hand, several new methods or algorithms are emerging to improve the analysis of the HRV signal based on the conventional IPFM model or its modified versions. In [9], an improved IPFM model for the simulation of the HRV signals is proposed so as to implement an algorithm for the signal decomposition. Fig. 1-2 shows the basic structure of the improved model: $m(t)$ is a non-negative modulating function that controls heart rate, $m(t) = k + m'(t)$, where k controls the average heart rate and $m'(t)$ controls the fluctuation of HRV; and $m(t)$ is uniformly sampled. After a reciprocal calculation, $1/x$, the sampled values are stored in the memory as a time sequence, $1/m_0, 1/m_1, \cdots, 1/m_k, \cdots$ where $m_k = m'(t_k)$. Triggered by the reset signal from the output $x(t)$, the sampled values are outputted sequentially to the integrator, controlling the rate of integration. The output of the integrator, $y(t)$, is then compared with a threshold value, V_T. Whenever the value of $y(t)$ exceeds V_T, a positive going jump is generated at the output, $x(t)$, which then serves to reset the integrator. Thus a positive impulse, $\delta(t)$ (i.e., a point event), will be produced in $x(t)$ at this moment. Meanwhile, the next memory value, $1/m_{k+1}$, will be applied to the input of the integrator.

Mathematically,

$$y(t) = \begin{cases} \int_k \frac{dt}{m_k}, & when\ y(t) < V_T,\ or\ t_k < t < t_{k+1} \\ 0, & when\ y(t) = V_T,\ or\ t = t_{k+1} \end{cases} \tag{1-2}$$

In Eq. (1-2), t_{k+1} is obtained from:

$$V_T = \frac{1}{m_k} \int_k^{k+1} dt = \frac{t_{k+1} - t_k}{m_k} = \frac{\tau_k}{m_k} \tag{1-3}$$

where $\tau_k = t_{k+1} - t_k$ is the time interval between two consecutive point events. The

output point process, $x(t) = \sum_k \delta(t - t_k)$, is the signal simulating the beat-to-beat heart rate, which is often represented as a uniform time series, called an HRV signal (from Eq. 1-3):

$$HRV(k) = \{\tau_k ; k = 0,1,2\cdots\} - \{V_T m_k ; k = 0,1,2\cdots\} \qquad (1\text{-}4)$$

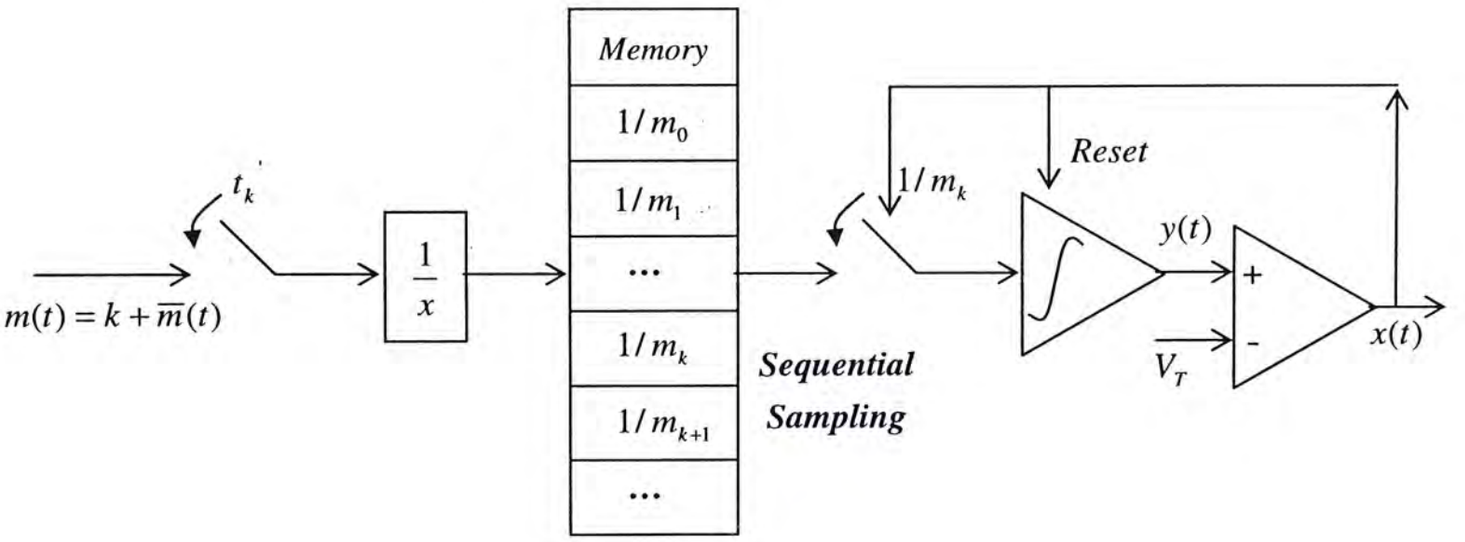

Fig. 1-2: Improved IPFM model of HRV signals.

Based on this modified IPFM model, a decomposition method based on wavelet transform is proposed in this work to obtain the individual frequency components of the HRV signals. The simulation results show that the model is able to not only faithfully represent the physiological process of the HRV signal, but also generate the signal that can well approximate the experimental data in both time and frequency domains. Therefore, it helps us to better understand the individual frequency components of the HRV signal and to further study the underlying mechanism of this signal.

A more recent study [10] presented a new model, which was formed by the combination of the Warner model and the IPFM model, to further clarify the relationship between the autonomic nervous activity and the HRV signal. As generally

known that autonomic nerves release the neurotransmitters that influence the automaticity of SA nodal cells, and thereby the timing of a heartbeat generation is changed. Since the Warner model can appropriately describe the kinetics of the neurotransmitters released from autonomic nerves, it was combined with the IPFM model to better describe the characteristics of beat-to-beat fluctuations in heart rate under autonomic nervous control. Fig. 1-3 shows the block diagram of this model. Inputs, $f_S(t)$ and $f_V(t)$, are the instantaneous neural activities on sympathetic and vagal nerves, respectively. The kinetic part of the Warner model is used to produce the effective concentrations of neurotransmitters NE (t) and Ach (t). The concentrations of NE (t) and Ach (t) are combined to form a modulating signal, $m(t)$, in the IPFM model. Finally, the heartbeat interval series, $HI[n]$, is generated by the IPFM model. (For more detailed information about the Warner model, please refer to [10].) Through the simulation using this model, the LPF effects on both sympathetic and vagal inputs are revealed. Secondly, the effects of mean autonomic tone on the HRV were studied, and the results show that an increase in the mean sympathetic tone decreases the HRV induced by perturbation of sympathetic activity, and an increase in mean vagal tone causes a decrease in the HRV resulting from perturbation of vagal tone. In summary, this new model indicates that the fluctuant strength, the fluctuant frequency, and its mean value are three major quantities in fluctuant autonomic activity that have an effect on the HRV.

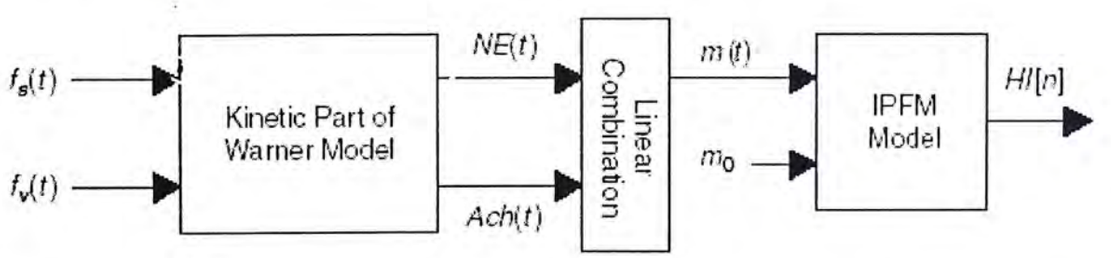

Fig. 1-3: Diagram of the new model: $f_S(t)$, $f_V(t)$, NE (t), and Ach (t) are the same as those in the Warner model. NE (t) and Ach (t) are linearly combined to form a modulating

signal, $m(t)$, the input of the IPFM model.

The IPFM model has also been applied successfully in the analysis of neonatal respiratory sinus arrhythmia (RSA) at high respiratory rates [11]. Recently, an important mathematical framework was reported by [12] to unveil the complexity and nonlinearity of the relationship between the mean heart rate, RSA, and vagal activation, and to explain conflicting experimental results previously published.

Indeed, the IPFM model with a simple but useful structure can be of great potential to simulate a complex neural system for investigating neural coding process. It represents a reasonable tradeoff between simplicity and faithfulness to key attributes of the neural coding. However, it should be pointed out that since Hyndman et al. [4] showed the applicability of Bayly's result to the HRV analysis, many researchers just followed the idea that the input spectral structure could be fully recovered by LPF the output pulse train of the IPFM model. Nevertheless, the limitations of this method have also been recognized [5]. Thus, it is worthwhile to further investigate that whether it is practically plausible to recover precisely the input modulation amplitude or intensity information through a simple LPF. On the other hand, it is quite necessary to further explore the physiological mechanisms of other important neural or cardiac events based on the IPFM model or its modified versions.

1.2 Windkessel Model

The simplicity of the Windkessel model in interpreting pressure and flow behavior of the arterial system has extended its use to much of last century. Modern development of theories in analyzing BP and flow waveforms, and in explaining pulse transmission characteristics, have been focused on the improvement of the original Windkessel model [13].

1.2.1 Background of the Windkessel Model

Lumped model of the arterial circulation was first described by Hales back in 1733. Although mostly qualitative, his model did emphasize the storage properties of large arterials and the dissipative nature of small peripheral resistance vessels. In this manner, the blood ejected by the heart during systole into the arterial system distends the large arteries (primarily the aorta). During diastole, the elastic recoil of these same arteries propels blood to perfuse the smaller peripheral resistance vessels. This idea initiated the earlier conceptual understanding that the distensibility of large arteries is important in allowing the transformation of intermittent outflow of the heart to steady outflow throughout the peripheral vessels. In other words, the large compliance of the larger arteries protects the stiff peripheral vessels of organ vascular beds from the large swing of BP caused by pulsations. The latter view is still held by some until this day. The significance of arterial pulsations continues to be debated. The necessity of pulsatile perfusion, however, is well rooted, and demonstrated in both experimental and clinical studies.

Quantitative description of Hale's concept was not provided until Frank [14] [15], whose interest was originated in obtaining stroke volume, or the amount ejected by the ventricle per beat, from the measured aortic pressure (AoP) pulse contour. Indeed, even decades later, methods to determine the flow from pressure measurement or the so-termed pressure-derived flows [16] [17], continued to attract considerable interest until the advent of the popularity of electromagnetic blood flow and ultrasonic blood velocity measuring devices. Utilizing Frank's air-bellows description of the arterial system, the ventricle ejects into a compliant chamber representing the aorta, where blood flow is stored in systole, and, on its elastic recoil in diastole, the stiff peripheral vessels are perfused.

In the Windkessel model, the amount of blood flow, Q_s, stored during each

contraction, is the difference between inflow, Q_i, to the large arteries and the outflow, Q_o, to the small peripheral vessels (Fig. 1-4),

$$Q_s = Q_i - Q_o \qquad (1\text{-}5)$$

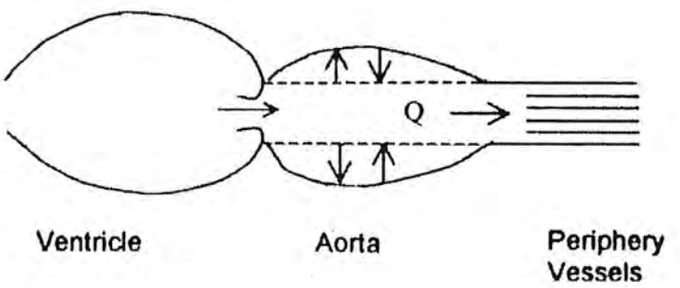

Fig. 1-4: Diagrammatic representation of the LV and the arterial circulation, based on the idea of the Windkessel. The ventricle ejects into a compliant chamber representing aorta, blood flow is stored in systole (solid line), and, on elastic recoil in diastole (dotted line), the stiff peripheral vessels are perfused.

The amount of outflow rate is equivalent to the pressure drop from the arterial side (P) to the venous side (P_v) due to the peripheral resistance, R_s,

$$Q_o = (P - P_v)/R_s \qquad (1\text{-}6)$$

Assuming that the flow is steady and P_v is small, we obtain a familiar expression for estimating the peripheral resistance, R_s,

$$R_s = \overline{P}/\overline{Q} \qquad (1\text{-}7)$$

where $\overline{Q}$ is the mean total flow rate and $\overline{P}$ is the mean arterial pressure. With pressure having the unit of mmHg and flow rate in mL/s, R_s has the unit of mmHg /mL/s.

The storage property can be described by the use of arterial compliance, which expresses the amount of change in blood volume (dV), due to a change in distending pressure (dP) in the artery. So,

$$C = dV/dP \qquad (1\text{-}8)$$

Here C represents the total compliance of the arterial system. With volume measured in mL, the arterial compliance has the unit of mL/mmHg. Both peripheral resistance and arterial compliance have both are the most popular parameters for clinical assessment of the properties of the arterial system.

The amount of blood flow stored, or Q_s, because of arterial compliance, is related to the rate of change in pressure that distends the artery,

$$Q_s = CdP/dt \qquad (1\text{-}9)$$

Substituting Eq. (1-9) and (1-6) into (1-5), an expression relating the arterial pressure to the flow rate, incorporating the two Windkessel parameters, C and R_s can be obtained:

$$Q(t) = CdP/dt + P/R_s \qquad (1\text{-}10)$$

In diastole, when inflow rate is zero, as is the case when diastolic aortic flow rate equals zero, then

$$0 = CdP/dt + P/R_s \qquad (1\text{-}11)$$

or

$$dP/P = -dt/R_sC\,. \qquad (1\text{-}12)$$

This equation states that the rate of diastolic aortic pressure drop depends on both the compliance of the arterial system and the peripheral resistance. Both of which also determine the flow. Integrating of both sides of Eq. (1-12) gives:

$$P = P_o e^{-t/R_sC} \qquad (1\text{-}13),$$

Eq. (1-13) is valid for the diastolic period, or $t = t_d$.

This last equation is seen to be equivalent to

$$P_d = P_{es} e^{-t_d/\tau} \qquad (1\text{-}14)$$

Eq. (1-14) indicates that the decay of the diastolic aortic pressure from end-systolic pressure (P_{es}) to end-diastolic pressure (P_d) follows a mono-exponential manner, with a time constant τ. The time constant of pressure decay τ, is determined by the

product of resistance and compliance, i.e.,

$$\tau = R_s C \tag{1-15}$$

It can also be expressed in terms of measured AoP,

$$\tau = \frac{t_d}{In\frac{P_{es}}{P_d}} \tag{1-16}$$

The latter expression has been extensively used, and is a popular approach to estimate the total arterial compliance when peripheral resistance and aortic pressure pulse contour are known. Combining Eq. (1-15) and (1-16) yields

$$C = \frac{t_d}{R_s In\frac{P_{es}}{P_d}} \tag{1-17}$$

Analysis, utilizing simple electric analog, has given the Windkessel model a two-element representation. Arterial compliance is represented by a capacitor, which has storage properties, in this case, the electric charge. Peripheral resistance, with its viscous properties, is represented by a resistor that dissipates energy. The electrical analog of the Windkessel model for the arterial system is given in Fig. 1-5.

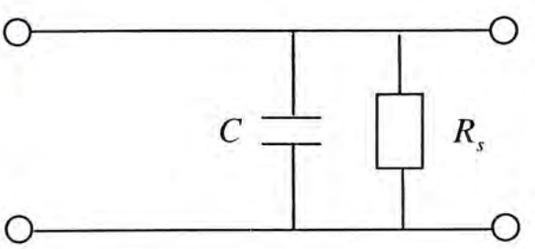

Fig. 1-5: The two-element resistance-capacitance electrical analog model of the Windkessel model. Compliance is represented by a capacitor and the peripheral resistance by a resistor.

The two element Windkessel model was found to be insufficient to describe the vascular impedance to blood flow and to characterize the gross arterial tree properties. A modified Windkessel model (Fig. 1-6), which has three elements, was proposed by

Westerhof et al. in 1969. It consists of a characteristic impedance of the proximal aorta in addition to arterial compliance and peripheral resistance.

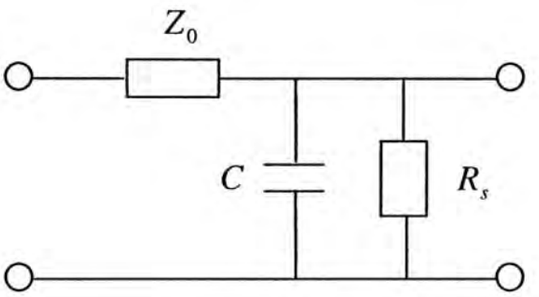

Fig. 1-6: A modified Windkessel model with three elements.

1.2.2 Modeling using Windkessel models

The three-element Windkessel (WK3) model for the systemic arterial tree has been widely used [18] [19] to study the transmission properties of arterial pulses. It contributes to understanding the differences in pulse and flow waveforms in different parts of the vascular tree in a human body. The distinct features of pulse and flow waveforms as the pulse wave travels away from the heart and their explanations are significant in understanding the functional aspects of the arterial system. Consequently, considerable diagnostic information can be derived from these pulse and flow waveforms.

By the acquisition of only two pressure pulse waveforms at proximal and distal, respectively, A.S. Ferreira *et al.* proposed the use of the WK3 model for the determination of the arterial compliance from the brachial to radial arterial segment. With the impulse response of the WK3 model, and an experimental version of the proximal pressure pulse, a theoretical output pulse (theoretical distal pulse) can be obtained from the convolution of proximal pulse and the impulse response function. This theoretical output is compared with its experimental counterpart. The arterial compliance can be determined through an optimization algorithm. Similar approaches

have been used by many researchers for the estimation of not only the arterial compliance, but also the peripheral resistance and the characteristic impedance of the proximal aorta [7], [20].

Cavalcanti, S. *et al.* (1996) had developed the Windkessel model to analyze the influence of time delay in the baroreflex control of the heart activity as shown in Fig. 1-7. The mean arterial pressure in the Windkessel model is controlled by a nonlinear feedback driving a non-pulsatile model of the cardiac pump in accordance with the steady-state characteristics of the arterial baroreceptor reflex. A pure time delay is placed in the feedback to simulate the latent period of the baroreceptor regulation. By changing the value of the time delay within a range of physiological importance, dynamics with different patterns of behavior is observed. As a result, the nonlinear characteristics of the cardiovascular system are better understood in terms of the time delay influence on the baro-reflex control.

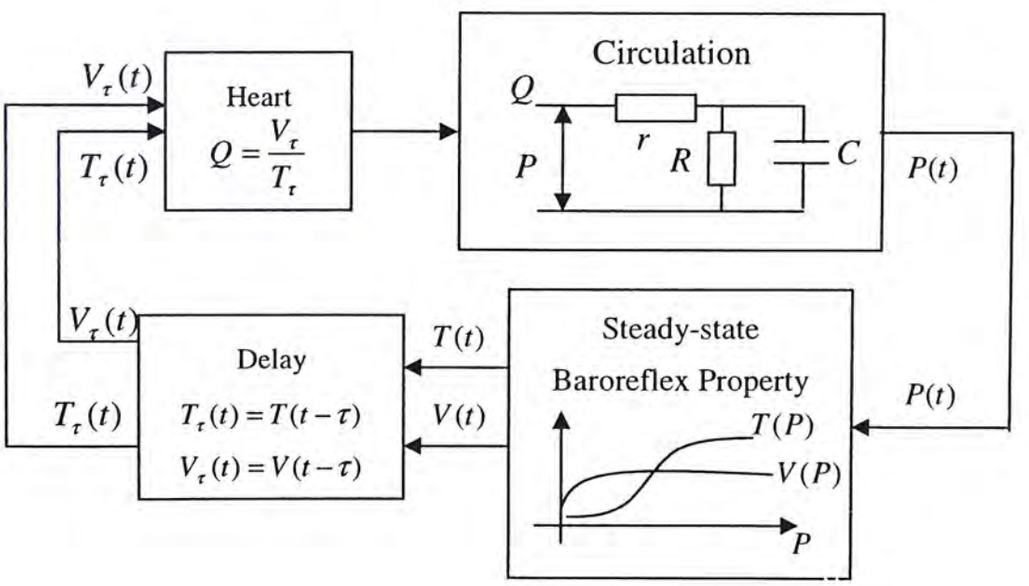

Fig. 1-7: Schematic representation of the mathematical model employed to study the influence of the time delay in the baroreflex control of the heart activity [18].

1.3 Photoplethysmogram (PPG)

1.3.1 Principle of the PPG

The radial stretch of the ascending aorta brought by the left ventricular ejection initiates a pressure wave that is propagated down the aorta and its braches [21]. As mentioned before, pulse and flow waveforms at different sites of a human body have distinct features which could be significant in understanding the functional aspects of the arterial system. With advanced technologies, it is easy to obtain arterial pressure contours at various sites along the aorta. Therefore it can be used to the extract the pulse transmission information, such as pulse wave velocity (PWV) which has been widely used as an index of the elastic properties of arteries, and to interpret of hemo-dynamic alterations under diseased conditions [13].

The pulse wave at peripheral sites has attracted considerable interest among many researchers in recent years. This is probably due to the advantage that it can be measured at the peripheral sites, such as fingers, ears, toes, etc. A number of techniques are employed to obtain the distal pulse waves, such as the ultrasonic Doppler method [22], the electronic palpation method [23], the MRI technique [24], the impedance plethysmography [25], and the PPG [26] [27] [28], etc. Among these techniques, the PPG offers remarkable convenience and advantages, and is one of the most widely used approaches for a variety of applications, including monitoring of arterial BP [26] and compliance [29], recording of heart and respiratory rates [30], oxygen saturation measurement [31], detecting anxiety [32], etc.

The PPG was first used by Hertzman [33] for studies of blood volume pulsations in the skin. It is a non-invasive technique that utilizes an optical sensor that produces a signal associated with the change in the volume of red blood cells in the peripheral micro-vascular bed with each pressure pulse initiated by the heart. More specifically, it consists of a light source, a photo-detector, and an AC amplifier and can be used to detect flow variations in the periphery during the cardiac cycle. The light is impinging

on the skin surface, and is then absorbed, scattered and reflected by tissue and blood. The perfusion and structural changes modulate the intensity of the light received by the photo-detector [34]. Thus the signal from the photo-detector is closely related to blood volume changes in tissue. The repetition of PPG pulses should be the same as that of ECG signals over the same cardiac cycles. Therefore, it seems to be promising that PPG signals can also be interpreted based on the IPFM mechanism coupled with certain transmission characteristics of the pressure wave through the arterial system.

1.3.2 Characteristics of the PPG Signal

Based on the principle of the PPG technique, as reported in several literatures, the intensity variations of the PPG signal mainly arise from the change in blood volume in the peripheral micro-vascular bed with each pressure pulse initiated by the heart. In spite of its simple waveform, the time intervals, such as those reflecting the rising or falling phases, of the PPG signal could contain important information that is corresponding to the periods of systole and diastole [23] [26]. Specifically, the signal of the photo-detector decreases when tissue blood volume increases, as during heart systole – the heart contraction, when blood is ejected from the heart to the tissue; while the PPG signal increases with the decrease in the volume of red blood cells, as during heart diastole [38] [39]. Thus, the rising phase and the falling phase of the PPG signal could to some extent reflect the periods of systole and diastole respectively.

Besides, the PPG technique provides a complement to existing methods for the non-invasive measurement of pulse transit time (PTT). PTT is defined as the difference in time between two pulses detected at two different locations from the heart. It can be measured in two ways. One method employs two arterial pulse pickups located at different locations from the heart. The other method, which really measures pulse arrival time, employs one arterial pulse pickup and the R-wave of

electrocardiogram (ECG) as a timing signal [36]. Current non-invasive methods for the measurement of PTT rely on the time lag between features on ECG and PPG taken at the finger. The advantage of this technique is in its simplicity and the ease of use. It has been shown that using such technique could yield accurate estimations of PTT [37]. Recently, it has been reported in several literatures that PTT assessed by the time delay between the characteristic points on ECG and PPG signals are being used for non-invasive estimation of arterial BP [26][36][38]. It has been shown by several studies that there is statistically high linear correlation between PTT and arterial BP. As generally known, arterial BP is routinely measured in patients, and it provides an important clue to the cardiovascular status. Most of the currently used approaches for BP estimation are still based on 1) the auscultatory measurement, which detects the Korotkoff sound using an occlusive cuff and a stethoscope. The cuff is inflated to a pressure exceeding the expected systolic arterial pressure (P_s) so that the segment of the artery under the cuff is forced to collapse. During the deflation, the first vascular sounds that emerge are generally referred to as the P_s phase, and when the vascular sounds become muffled or disappeared completely, the diastolic pressure (P_d) is obtained; 2) the oscillation method, which measures the mean arterial pressure when the oscillation of the cuff pressure is maximal. The P_s and P_d is then obtained using empirical derivations; 3) ultrasound method, which records BP waveforms by detecting Doppler signals received as the motion of the blood vessel varies under different states of occlusion; or 4) intra-arterial approaches, which most commonly utilize the fluid-filled catheter to monitor the pulsatile BP waveforms in cardiac chambers and major vessels; etc. However, these methods are either incapable of providing continuous BP measurement, or they are difficult to operate and make patients feel uncomfortable since they are invasive. In order to avoid all these problems, the PTT based BP measurement could probably provide a breakthrough as

a non-invasive and non-encumbering means to monitor beat-to-beat variations in BP.

More and more researchers are making use of the PPG technique in extensively various applications. Mathematical modeling based on the physiological generation process of the PPG signal would provide an insight into better understanding the underlying mechanism of the signal. It could also be helpful in clarifying the relationship between PPG signals or PPG related information and other cardiovascular signals. On the other hand, it is worthwhile to investigate systematically certain characteristics of the PPG waveform, such as the rising phase, falling phase, and PTT, for the evaluation of clinically useful physiologic parameters. The variations in the systolic or diastolic portions of the pressure wave, as well as that in PTT, may be, to some extent, correlated to the time-varying properties of the vascular and peripheral systems, as suggested by the Windkessel model. However, the complex interactions among these important parameters are not yet fully established. Thus, it is necessary to investigate whether the parameters extracted from the waveform of the PPG are correlated with each other, and how these parameters are associated with the properties of cardiovascular or arterial systems.

1.4 A Study on the Beat-to-Beat BPV

As one of the most important cardiovascular parameters, BP has been studied extensively. The oscillatory behavior of BP has been known for long time. The analysis of the oscillations in BP plays a fundamental role for a better comprehension of the patho-physiological properties of the complex mechanisms which act through neural, mechanical, vascular, humoral factors and others [40]. Particularly, considerable attention has been focused on the fluctuations occurring at frequencies in the range of approximately 0.04-0.35 Hz, which are believed to reflect intrinsic vascular activity and neural modulation of the vascular tone.

Essential to the study on the beat-to-beat BPV is the availability of a continuous recording of the BP. However, as mentioned before, there are certain limitations in the beat-to-beat measurement of BP. The auscultatory and oscillation approaches, although simple and commonly used, are not able to provide continuously BP monitoring. The intra-arterial recordings allow accurate beat-to-beat measurement, but the invasive procedure limits the widespread use of such methodologies and the repetition of the tests in different conditions. Thus, a continuous non-invasive BP monitoring would be preferable.

Since its introduction in clinical research in the early 80's, the FINAPRES device (from FINger Arterial PRESsure) or the Finometer has raised great interest for its ability to provide non-invasive beat-to-beat BP recordings. It operates through a cuff wrapping the middle phalanx of the finger, and BP is recorded by a PPG measuring arterial blood flow. Studies performed in a laboratory setting and during surgical interventions have shown that the BP values continuously provided by this device are similar, although not identical, to those simultaneously recorded by an inter-arterial catheter. However, it is undeniable that there is noise from the measuring instruments. Moreover, there also exists the physiological disturbance particularly from the respiratory rhythm.

BP estimation based on PTT or other beat-to-beat parameters could provide an alternative to existing approaches for the non-invasive continuous BP monitoring. These methods can be even simpler in implementation and easier to use than the FINAPRES device. However, such methods have not been carried one step further to measure the beat-to-beat variability of BP, which is still an unknown.

1.5 Main Objectives of the Study

The original motivation of this work is triggered by the extensive use of the PPG

technique, and its potential applications to the analysis of the beat-to-beat BPV and etc. The study on the underlying physiological process of PPG activity could be important in better understanding the signal, and therefore making better use of it. The main objectives of this study are listed as follows:

1) To investigate the generation process of the PPG signal from physiological point of view, and to develop a new mathematical model for the generation of the PPG signal based on its physiological mechanisms.
2) To test the mathematical model by comparing simulation results from the model the experimental data from testing subjects, and to do analysis on the relationship between the modulating inputs and the output of our newly developed model.
3) To look into certain characteristics of the PPG waveform from experimental data, to further understand the physical generation mechanism of the PPG signal and to investigate its potential applications.
4) To explore new applications of the PPG signal based on the understanding of its physiological mechanism and the features on its waveform for the analysis of the beat-to-beat BPV and the human authentication.

1.6 Organization of the Thesis

This thesis is mainly divided into five parts. The first part is a theoretical study on the neural firing rate function based on the IPFM model. The second part is the development and analysis of the new model for the generation of the PPG and ECG signals. The third part is focused on a correlation study on the features related to PPG signals. The fourth part is on investigating new approaches for the beat-to-beat BPV estimation. Finally, a new application of the PPG and ECG signals for human verification is introduced. This thesis consists of 7 chapters. The following is the ouline of each chapters.

Chapter 1 provides the background information on some basic models used in this study, the history and current status of the related works, and an overview of this thesis.

Chapter 2 presents a study on the spectral analysis of the IPFM process. In this chapter, further investigation is carried out on whether it is practically plausible to recover precisely the input modulation amplitude or intensity information from the IPFM model through a simple LPF. An expression approximating the instantaneous firing rate as a function of the input intensity for the IPFM model is also derived.

Chapter 3 introduces the details of the new model, and provides the theoretical analysis and simulation results using this new model. In the first part of this chapter, the physiological and mathematical background of this model is given. It is followed by the elaboration on the theoretical analysis and computer simulation.

Chapter 4 focuses on a correlation study from statistical point of view to investigate the relationship between the PPG related parameters and their association with the parameters from ECG signals such as RR interval.

Chapter 5 presents a new approach for the BP estimation as well as for the analysis on the beat-to-beat BPV based on the results from Chapter 4. The feasibility of the new approach is investigated by using the data obtained from the FINAPRE device as reference.

Chapter 6 presents a new approach for human verification using PPG signals. Experiments were carried out to obtain PPG signals from different subjects. The preliminary results demonstrate that the new approach is promising for human verification.

Chapter 7 concludes the original contributions in this thesis and provides some potential research directions based on the current work.

Chapter 2

Spectral Analysis on the IPFM Process

2.1 Introduction

The IPFM model has been widely used for encoding physiological or physical information into variable spike intervals. This is a very simple but yet powerful tool in exploring a relationship between the input modulation signal and the events generated by the neural encoding system. It is especially useful when the recovering of the hidden modulation information in a set of observed events is interested in. Therefore, many physiological events, such as nervous pulse trains and the signals associated with cardiac contractions, can be appropriately interpreted by the IPFM model.

The spectral analysis of the IPFM process has played an important role in understanding the mechanisms of encoding and decoding in nervous systems. It was reported in many early studies [3] [4] that, if the modulation depth and frequencies were suitably restricted, demodulation of the IPFM process by a simple LPF could be used to recover the input modulation information attached with physiological meanings. In fact, many researchers have made use of this approach in their studies without further justifications. However, it is found that in order to fully recover the input modulating signal, the knowledge of the threshold of the IPFM model is necessary. Indeed, in a complex biological living system, the threshold very much depends on the cell geometry and the membrane voltage depolarization level at the site of the origin required for pulse initiation, and is therefore difficult to obtain without extensive exploration of the physiological mechanism of the pulse generation in the nerve cells. As a result, it is practically implausible to recover precisely the

input modulation amplitude or intensity information by a simple LPF. However, demodulation by LPF can be useful in reconstructing some important features, such as firing rate functions, which is closely related to the original input information. In the first part of this chapter, the spectral characteristics of the IPFM process is studied from demodulation point of view.

On the other hand, the information-carrying train of events at the output of an IPFM model is often simplified as a series of stereotyped impulses, which provide only the information of their occurrence times. However, in reality, the significance of the modulated series of events is also attached to the detailed dynamics of the event itself. Indeed, when the detailed properties of the event itself are taken into account, the spectrum of the whole IPFM process can be quite different, which complicates the process of reproducing the original modulation signal. Therefore a simple LPF for demodulation could no longer be satisfactory to recover the important hidden neural information unless appropriate pre-processing is applied. In the second part of this chapter, a study on the nature of the interaction between the detailed neural dynamics and the neural coding processes is presented.

2.2 A Theoretical Study on the Neural Firing Rate Function

In this section, the spectrum of the IPFM model is studied from demodulation point of view. An expression approximating the instantaneous firing rate as a function of the input intensity is derived. The theoretical work provided by Balay is also introduced on the spectral analysis of the IPFM process. Comparing with the spectral results from the corresponding IPFM model shows that the firing rate function can be recovered by a simple LPF.

2.2.1 Mathematical Derivation of the Neural Firing Rate

In the IPFM model shown in Fig. 2-1(a), the occurrence times of the ith and $(i+1)th$ pulses, t_i and t_{i+1}, satisfy the relationship

$$V_{th} = \int_{t_i}^{t_{i+1}} (m_0 + m_1(t))dt \qquad (2\text{-}1)$$

where $m_1(t)$ is the information or modulating input signal, m_0 is the constant input signal, and V_{th} is the integration threshold. The non-negative input signal $m_0 + m_1(t)$ is integrated, and whenever the integrated value exceeds the threshold V_{th}, a unitary spike is generated and the integrator is reinitialized. Fig. 2-1(b) shows an integration process denoted by $x(t)$ and an output pulse train denoted by $y(t)$ when $m_1(t) = A\cos(2\pi f_m t + \theta)$ is applied as the input modulation signal to the IPFM model.

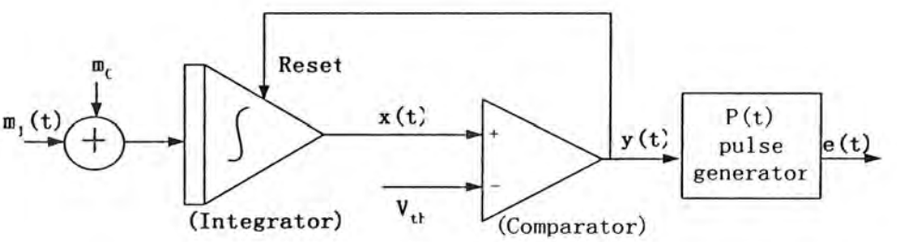

(a)

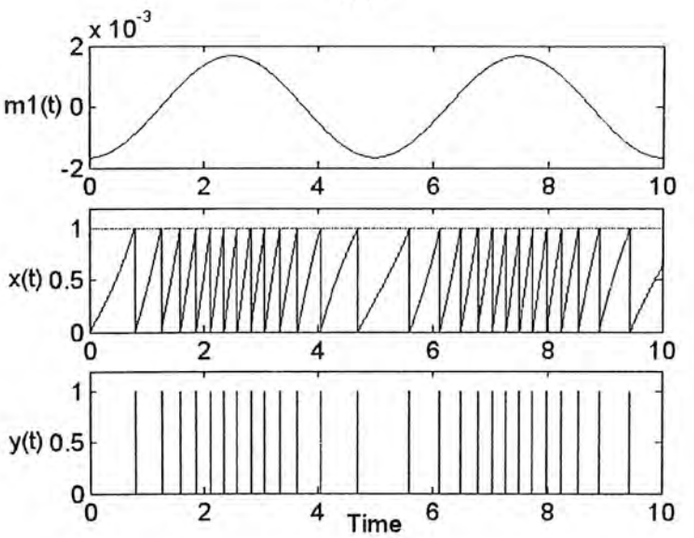

(b)

Fig. 2-1: IPFM model: (a) Schematic diagram of the IPFM model; and (b) the input and output of the IPFM model for $m_1(t) = A\cos(2\pi f_m t + \theta)$.

By converting the input modulating signal that mimics the physical process (pressure, current, etc.) into a time series, the output of an IPFM model clearly reflects the important features of a neuron with close relevance to the physical input such as firing rate. Considering $m(t)=m_0$ with the input modulating signal $m_1(t)=0$ as a simple example, the expression of the firing rate can be easily derived as $r_0=m_0/V_{th}$ according to Eq. (2-1). It is clear that the firing rate r_0 is proportional to the DC input component m_0 and inversely proportional to the threshold V_{th}. More generally, if $m(t)=m_0+A\cos(2\pi f_m t+\theta)$ ($A\le m_0$ such that $m(t)$ is ensured nonnegative) is the input signal to the IPFM model, Eq. (2-1) becomes:

$$\begin{aligned} V_{th} &= \int_{t_i}^{t_{i+1}} (m_0 + A\cos(2\pi f_m t+\theta))dt \\ &= m_0(t_{i+1}-t_i)+\frac{A}{\omega_m}[\sin(2\pi f_m t_{i+1}+\theta)-\sin(2\pi f_m t_i+\theta)]. \end{aligned} \tag{2-2}$$

Considering that $\sin a-\sin b=2\sin(\frac{a-b}{2})\cos(\frac{a+b}{2})$, we have

$$V_{th}=m_0(t_{i+1}-t_i)+\frac{A}{\pi f_m}\sin(\pi f_m(t_{i+1}-t_i))\cos(\pi f_m(t_{i+1}+t_i)+\theta). \tag{2-3}$$

This can be further simplified by the Taylor series of the sinusioidal function given by

$$\sin x = x-(\frac{x^3}{3!})+(\frac{x^5}{5!})-(\frac{x^7}{7!})+\cdots. \tag{2-4}$$

In fact, the difference between $\sin x$ and x is less than 4% when $x<0.5$. For x with values less than 0.75, the deviation is not greater than 10% and for x with values closer to one, the difference can become as high as 16%. On the other hand, in most physiological situations, the time interval between two consecutive firings is less than or close to one. For example, in nervous system the interpulse intervals are normally ranged from the order of 10ms to the order of 100ms, while for neuro-cardiac case, the normal range of heart rate is 60 to 100 beats per minute [41]. If the frequency of the modulation signal can be restricted such that $x=\pi f_m\Delta t_i$ is much less than one, the

first order approximation of $\sin(\pi f_m \Delta t_i)$ by $\pi f_m \Delta t_i$ will be reasonable. The actual physiological series of point events, e.g. neural spike trains or series of heart beats, are often influenced by slow modulation, such as respiration which has a frequency f_m around 0.3Hz [42]. Hence, the resulting firing rate sequence is approximated by

$$\frac{1}{t_{i+1}-t_i} \approx \frac{m_0}{V_{th}} + \frac{A}{V_{th}} \times \cos(2\pi f_m \tilde{t}_i + \theta), \qquad (2\text{-}5)$$

where $\tilde{t}_i = \frac{t_i + t_{i+1}}{2}$.

In order to facilitate the discussions, the parameter $\tilde{t}_i$ is replaced by the continuous time variable t. Therefore the approximated firing rate can be expressed as:

$$r = \frac{1}{T} = \frac{1}{t_{i+1}-t_i} \approx \frac{1}{V_{th}}[m_0 + A \times \cos(2\pi f_m t + \theta)], \qquad (2\text{-}6)$$

Eq. (2-6) gives the relationship between the firing rate and the input intensity of the modulation signal.

As schematically depicted in Fig.2-2(a), the time interval between two consecutive firings will be lengthened as $m_1(t)$ decreases, and vice versa. Fig.2-2(b) gives the approximated firing rate as a function of time under different thresholds. It is obvious that smaller values of threshold result in higher firing rates for a given intensity, and vice versa. This result supports the experimental observations on the relation between the firing rate and the intensity reported before [43] [44]. When the intensity of the input stimulation (synaptic current, stretch, or pressure, etc.) increases, the time for the integrate-to-fire process will be shorten, which results in a corresponding increase in the firing rate. Conversely, when the fixed threshold V_{th} representing the depolarization level of membrane potential required for potential initiation increases, the integration process will last for longer time, resulting in a

decrease in the firing rate.

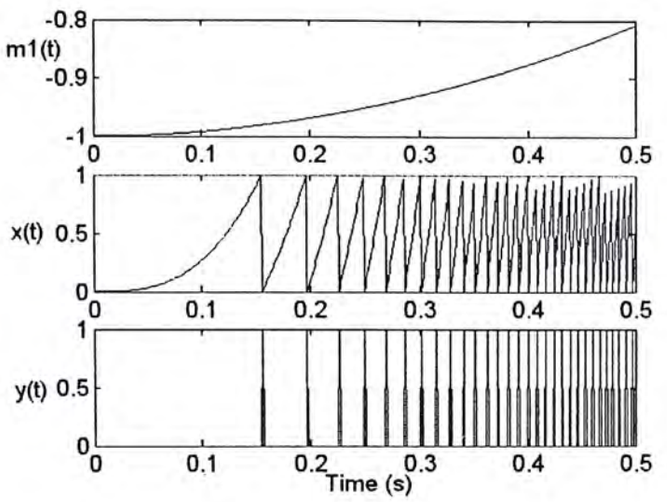

(a)

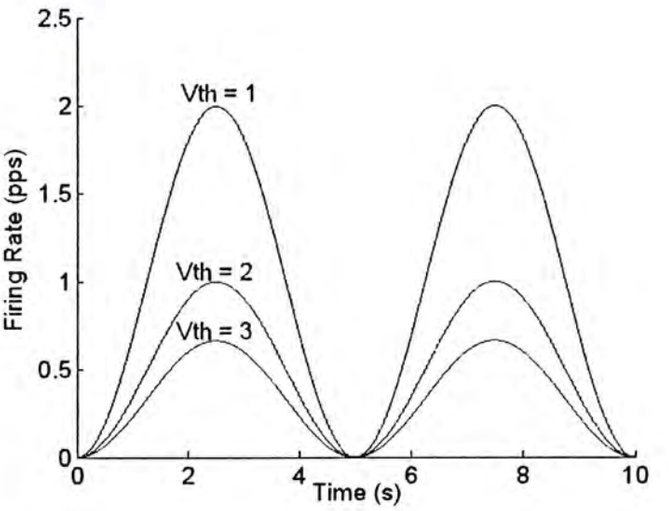

(b)

Fig. 2-2: (a) The output of the IPFM model when the modulating input signal is given by $A\cos(2\pi f_m t+\theta)$, the parameters used are: $A=1, f_m=0.2Hz, \theta=\pi, m_0=1, V_{th}=1$. (b) The approximated firing rate as a function of time for different threshold values with the other conditions remaining unchanged.

2.2.2 Spectral Analysis of the IPFM Process

The spectral analysis of the IPFM process could provide insights into the mechanisms of encoding and decoding in nervous systems. For simplicity, it is assumed that the impulses have a surface area of unit. Using Parseval relation and Bessel function, Bayly [3] derived the spectrum of the IPFM process:

$$Y(f)=\frac{m_0}{V_{th}}\delta(f)+\frac{A}{2V_{th}}\cdot\delta(f\pm f_m)\cdot\exp(\mp j\theta) + \frac{m_0}{V_{th}}\sum_{k=1}^{\infty}\sum_{n=-\infty}^{\infty}b_{k,n}\cdot\delta\{f\pm(kf_0+nf_m)\}\cdot\exp(\mp j\phi_{k,n})\,. \tag{2-7}$$

in which $b_{k,n}=J_n(\frac{kAf_0}{f_m})(1+\frac{nf_m}{kf_0})$, and $\phi_{k,n}=2k\pi f_0\alpha+n\theta+\omega$ with $\omega=\frac{kAf_0}{f_m}\sin(2\pi f_m\alpha-\theta)$, where J_n is the Bessel function of the first kind of the order

n, α denotes an arbitrary initial time instant as mentioned before, f_m is the frequency of the modulating signal, and f_0 is the pulse mean firing rate (or carry frequency) proportional to the DC signal component m_0.

If the ratios, $\frac{A}{V_{th}}$ and $\frac{f_m}{f_0}$, are properly restricted, the spectrum of the IPFM signal will have the form as shown in Fig.2-3 [3]. From this figure and Eq. (2-7), three clusters of frequency components can be identified as follows:

1) The DC component represents the average value of the pulse train.
2) The modulation or input information related to the signal component at the modulating frequency, f_m, next to the DC component, is given by $A/2V_{th}$. Demodulation is, therefore, possible through the estimation of the firing rate by LPF without any harmonic distortions if the threshold V_{th} is known.
3) The components at harmonics of the mean sampling rate kf_0 are surrounded by a cluster of side components at sums and differences of the mean firing rate and modulating frequency, i.e., $kf_0 \pm nf_m$. These harmonic components and sidebands are attributed to the nonlinearity of the IPFM model, specifically the threshold operation for the integrate-to-fire process.

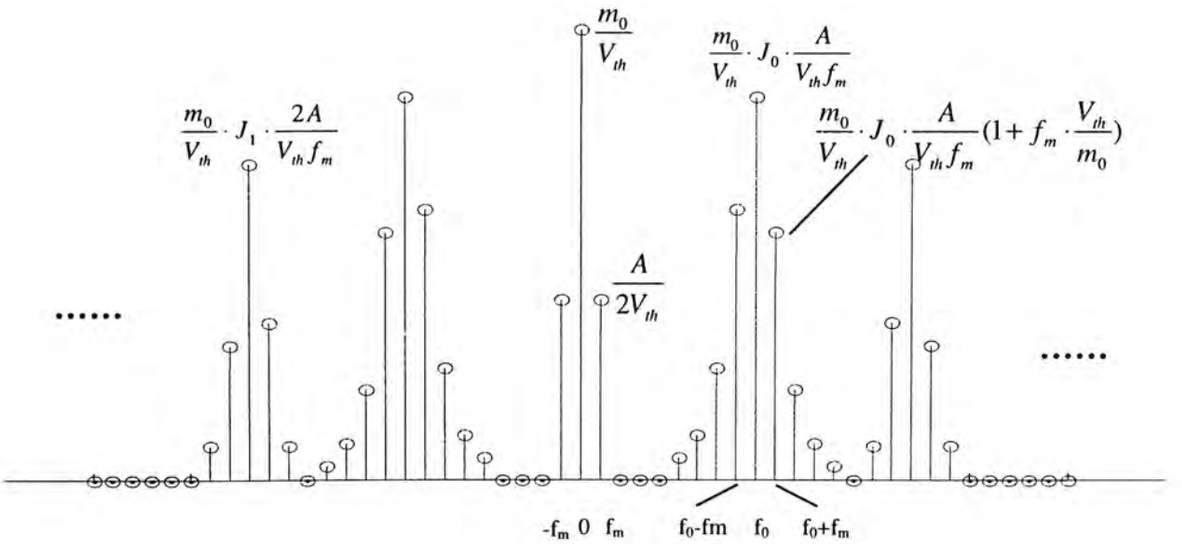

Fig. 2-3: The spectrum of the IPFM signal.

Accordingly, a demodulation method using LPF with a proper cut-off frequency is illustrated in Fig.2-4, where the main requirement on the filter is that its cut-off frequency be high with respect to the frequency of the modulation and low with respect to the carrier frequency [3]. Fig.2-4 (a) gives the schematic diagram of the demodulation of an IPFM pulse train by LPF. The actual output is

$$\frac{A}{V_{th}}|G|\cos(2\pi f_m t + \theta + \phi) + Noise, \qquad (2\text{-}8)$$

where $|G|$ is the gain of the low-pass filter. Therefore, it is theoretically possible to recover the input modulating information ($m_1(t) = A\cos(2\pi f_m t + \theta)$), with the knowledge of V_{th} and $|G|$.

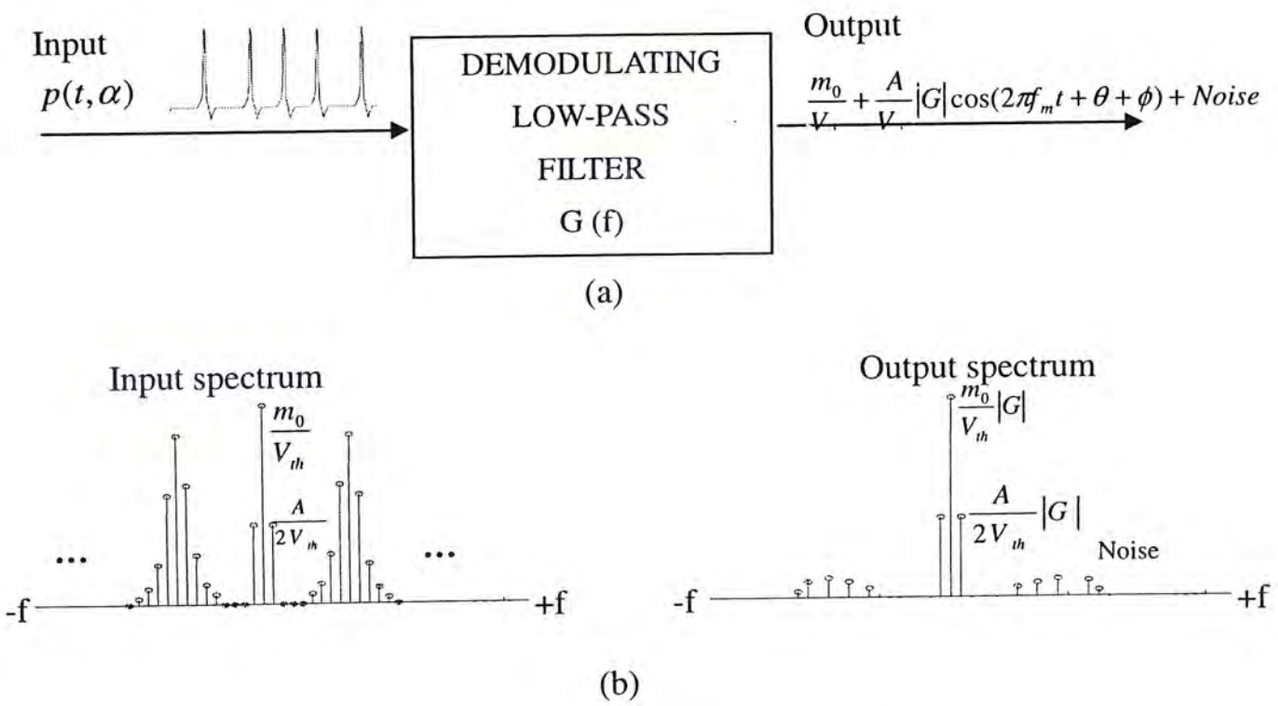

Fig. 2-4: (a) Schematic diagram of the IPFM demodulation by LPF; and (b) the corresponding input and output spectra. Distortion at the output occurs when the first carrier component at f_0 and its lower sidebands are not completely removed by the LPF. $|G|$ is the gain of the filter.

However, the threshold very much depends on the neuronal geometry and the membrane voltage depolarization level at the site of the origin required for pulse

initiation. Therefore, it is practically difficult to be obtained without extensive exploration of the physiological mechanism of the pulse generation in the neurons. The qualitative aspects of the thresholds *in vivo* cannot be captured at present, although much has been speculated on this topic. Therefore, it is physiologically implausible to recover precisely the input modulation amplitude or intensity information by a simple LPF due to the difficulty in estimating the exact value of the threshold value V_{th} in the complicated living biological systems.

2.2.3 Reconstruction of the Neural Firing Rate through LPF

Though it is implausible in practice to recover precisely the input modulation amplitude or intensity information to the IPFM model, demodulation by LPF can be of special importance for studying the firing rate characteristics of a neuron. In comparison with the approximated firing rate by Eq. (2-6), the output of the IPFM demodulator without noise is actually the instantaneous firing rate with both the DC component proportional to m_0 and the AC component to the modulating signal, as shown in Fig.2-4(b). Therefore, the demodulation by LPF is possible in reality for the estimation of the firing rate which is closely related to the intensity of input signals.

Simulations were carried out to evaluate the feasibility to reconstruct the firing rate using a simple low-pass filter. Different patterns of input modulation signals were used in simulations as illustrated in Table 2-1. In Simulation A, a sinusoidal signal was used as the modulation input, which was also employed in Bayly's studies. In Simulation B and C, more complicated signals were generated from Gaussian random sequence to investigate the applicability of this approach using more generalized input signals. Two different thresholds were selected for each simulation. For demodulation, a low-pass filter with a cutoff frequency at 0.1Hz was applied.

Table 2-1: Different patterns of inputs for simulations.

Simulations	Input signals	V_{th}
A	$m_0 = 1$; $m_1(t) = 2\times10^{-2} \cdot \cos(0.2\pi t + \pi)$	0.8, 1.2
B	$m_0 = 1$; A zero-mean unit variance Gaussian random sequence is generated. $m_1(t)$ is obtained by filtering the sequence with a low pass filter at a cutoff frequency at 0.1Hz multiplied by 4.	0.8, 1.2
C	$m_0 = 1$; A zero-mean unit variance Gaussian random sequence is generated. $m_1(t) = 4 \cdot m_{11}(t) - 2 \cdot m_{12}(t)$, in which $m_{11}(t)$ is obtained by filtering the sequence with a low pass filter at a cutoff frequency at 0.1Hz, and $m_{12}(t)$ by filtering the sequence with cutoff frequencies at 0.1Hz and 0.5Hz.	0.8, 1.2

The results of Simulations A, B, and C are given in Fig. 2-5. The dotted line in each simulation represents the input signal $m_0 + m_1(t)$; the dashed line is the corresponding firing rate function of the IPFM process; and the solid line is the signal generated by demodulating the output of the IPFM model using a low-pass filter. It is clear that without scaling the output of the demodulator by the threshold V_{th}, it is certainly unable to recover precisely the amplitude of the original input, neither the amplitude of the constant input signal nor the oscillation amplitude of $m_1(t)$. On the contrary, it is observed that the theoretical firing rate function tallies almost perfectly with the output signal of the low-pass filter especially in Simulations A and B, regardless the value of the threshold. In Simulation C, with a more generalized input

signal, the difference between the dashed line and solid line is magnified to some extent. Nevertheless, even under a higher threshold (Fig. 2-5 (f)), the error is still reasonable. It therefore suggests that demodulation by a simple LPF can be useful to recover the firing rate function not only under a special condition when the modulating input signal is given by $A\cos(2\pi f_m t+\theta)$, but may also for other cases.

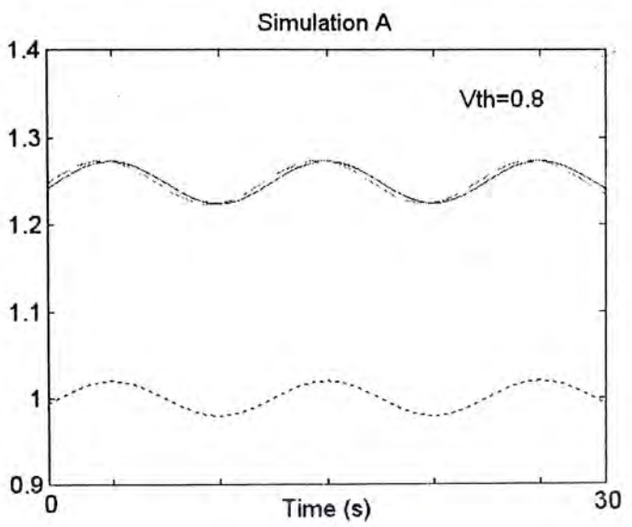

(a)

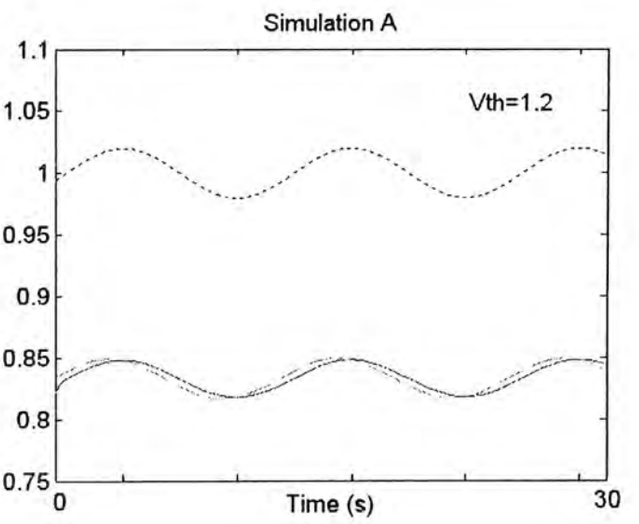

(b)

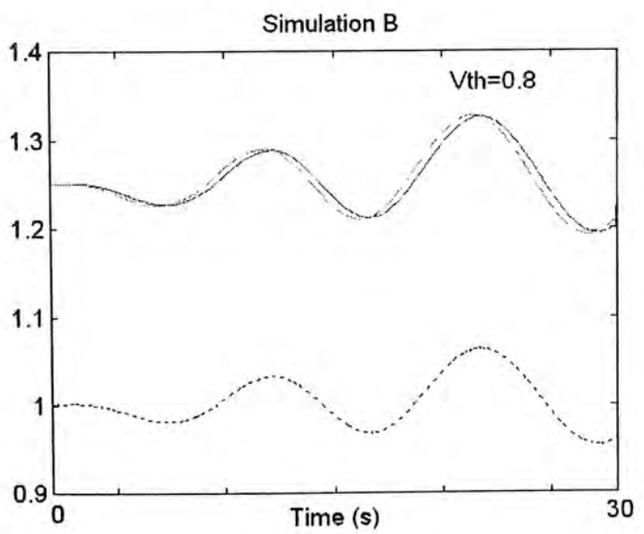

(c)

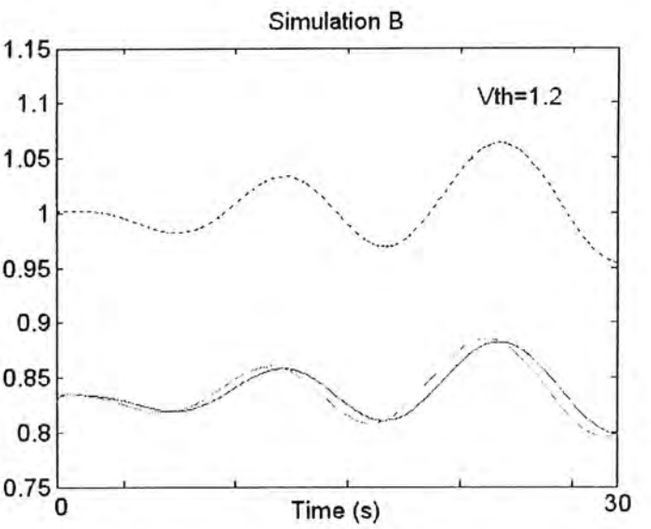

(d)

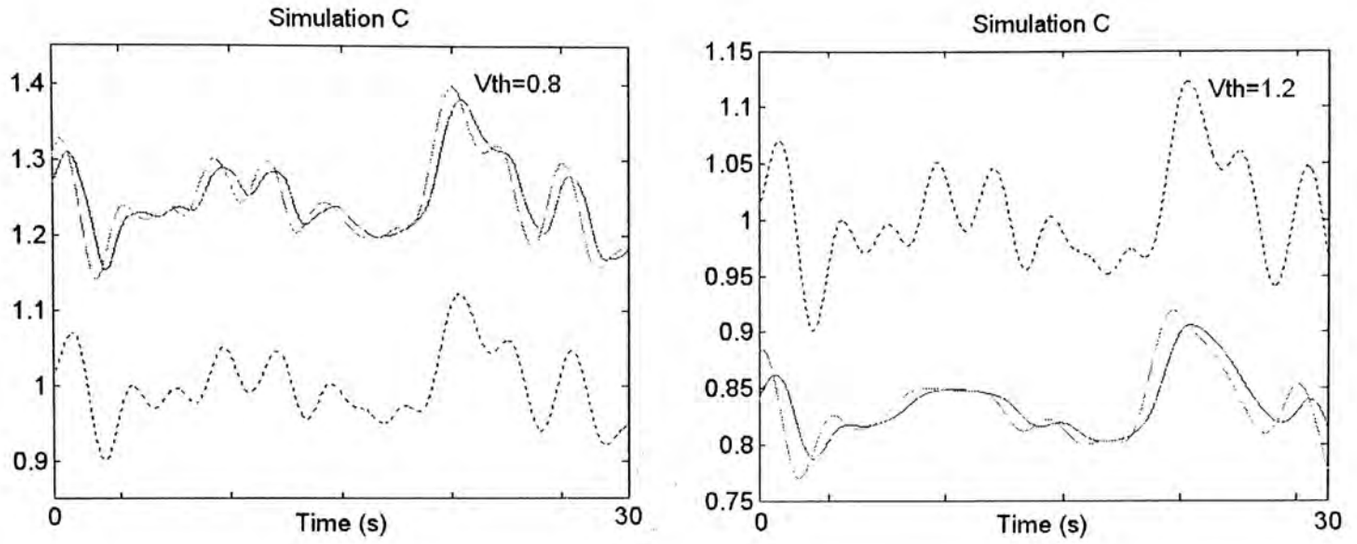

(e) (f)

Fig. 2-5: The results of simulation A, B, and C under different thresholds. Dotted line: the input signal; dashed line: the theoretical firing rate of IPFM model; and solid line: the output of the low-pass filter.

2.3 Effects of the Neural Dynamics

The specific characteristics of the pulse may contain the important information of dynamic changes in physiological systems, including the variations of ionic currents in the underlying ionic channels and the changes in the membrane permeability. Therefore cannot be neglected in order to better understand of the coding of neural information. As a result, the ultimate output spectrum of the IPFM process integrated with neural dynamics is determined by the multiplication of the action potential spectrum with the spectrum given by Bayly.

Let $P(t)$ represents the function of an action potential. Eq. (2-7) and $p(t)$ together yield the ultimate output spectrum of the IPFM process integrated with neural dynamics:

$$E(f) = Y(f) \times P(f) = \frac{m_0}{V_{th}} P(0) \cdot \delta(f) + \frac{A}{2V_{th}} P(f \pm f_m) \cdot \delta(f \pm f_m) \exp(\mp j\theta) + \frac{1}{V_{th}} \sum_{k=1}^{\infty} \sum_{n=-\infty}^{\infty} b_{k,n} \cdot P(\pm(kf_0 + nf_m)) \cdot \delta\{f \pm (kf_0 + nf_m)\} \cdot \exp(\mp j\phi_{k,n}) \quad (2\text{-}9)$$

It is clearly indicated by Eq.(2-9) that the amplitude of the frequency components in the IPFM spectrum given by Eq. (2-7) are modulated by $P(f)$. As illustrated in Fig.2-6, with different action potentials P_1 and P_2, the information signal AC component around $f_0 = 1Hz$ may be distorted to different extents. From the point of view of the demodulation process, the interaction of the action potential with the IPFM process results in a scaling factor and it complicates the process of recovering any original information. Hence, demodulation by a single LPF can no longer be able to recover either the simplified firing rate function, or the original input modulation signal. In order to solve this problem, pre-whitening techniques can be considered to offset the influence of the "dynamic waveform" before LPF.

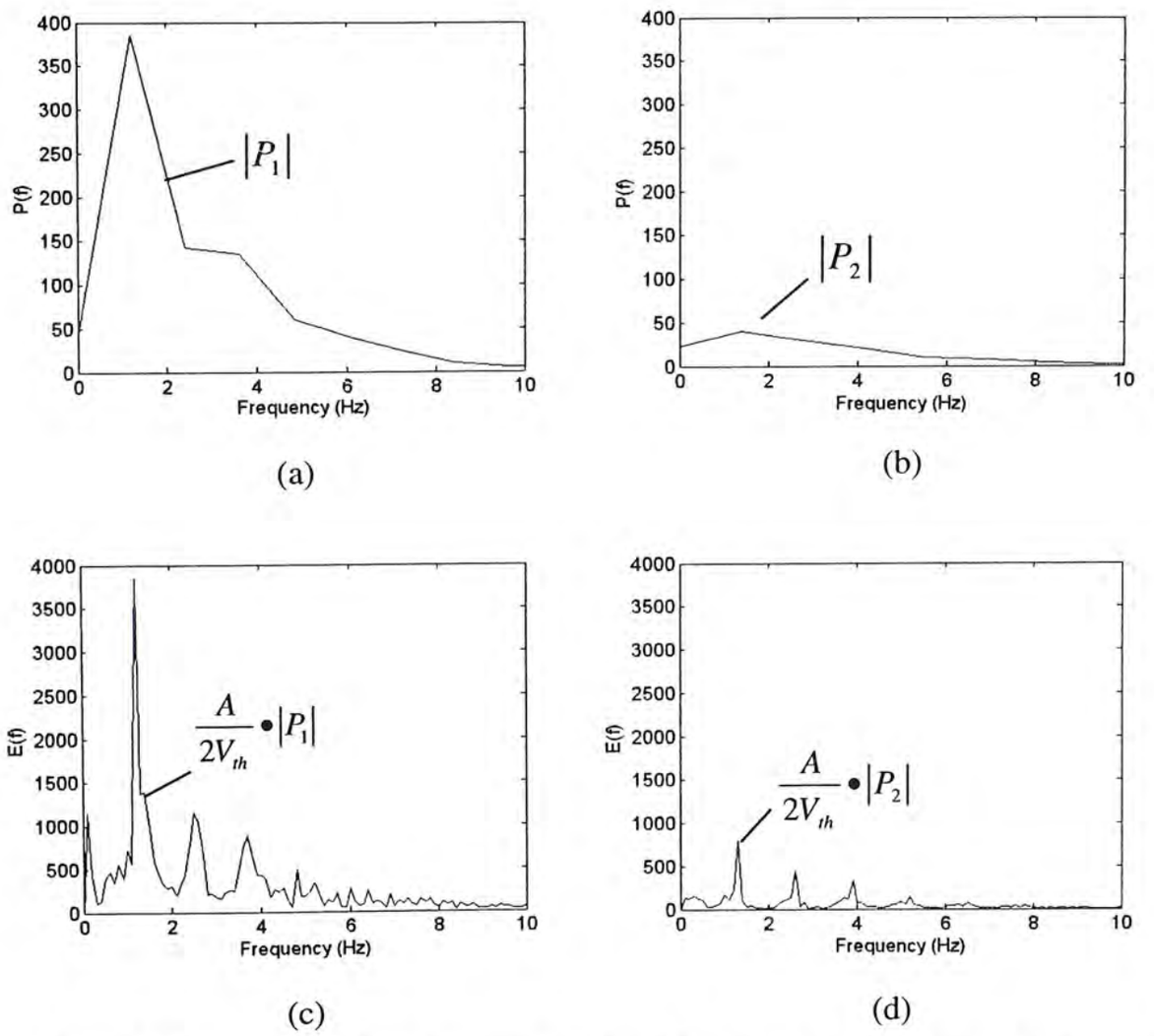

Fig.2-6: The spectra of the frequency modulated pulses taking into account the neural dynamics.

2.4 Discussion & Conclusions

In this chapter, with a single sinusoidal signal as the input modulation signal to the IPFM model, a mathematical expression approximating the instantaneous firing rate as a function of the input intensity is derived. Meanwhile, the corresponding output spectrum of the IPFM process is studied, particularly from demodulation point of view. Comparing with the spectral components as shown in Fig. 2-3, it is interesting to note that the DC component is exactly the mean firing rate given by $\frac{m_0}{V_{th}}$ as shown in Eq. (2-6). Furthermore, the modulation or input information related to the signal component at the modulating frequency, given by $A/2V_{th}$, is proportional to the AC component of the firing rate function defined by Eq. (2-6).

Using a simple LPF, it is found that the output of the IPFM demodulator without noise is actually the approximated instantaneous firing rate, rather than the original input modulation signal as reported by Bayly. In our simulations, the modulation frequency to carrier rate ratio $f_m / f_0 (f_0 = m_0 / V_{th})$ was appropriately selected, so that the modulation signal component can be isolated in frequency from other spectral components, and in this case, demodulation by LPF is reasonable [3]. The simulation result with different patterns of input signals demonstrates that without the knowledge of the threshold, it is impossible to recover precisely the input amplitude or intensity information, neither the amplitude of the constant input signal, m_0, nor the oscillation amplitude of $m_1(t)$. It also shows that reconstruction of the firing rate function through LPF can be applicable for more generalized inputs besides the single sinusoidal signal. Therefore, this theoretical analysis provides an insight into the quantitative evaluation of mean firing rate and the rate variability at the physiological modulating frequency. The results could be useful in exploring underlying relevant modulation mechanisms of a biological living system. However, when either or both

the modulation frequency to carrier rate ratio, f_m / f_0, or modulation depth to carrier rate ratio are large, the signal recovery for both the modulation input and the firing rate function becomes more difficult.

Taking into account the detailed properties of the output events, another important aspect beneficial to better understanding of the IPFM process for neural decoding has been addressed in this chapter. The results show that the neural dynamics may induce some serious distortions to the amplitude at the original modulation frequency components. This study suggests that a proper processing before LPF, e.g. pre-whitening, is necessary in order to recover the original neural information accurately. The details about the preprocessing technique will be under further investigation.

Chapter 3

A New Model for the Generation of PPG

3.1 Introduction

Triggered by the simple but yet powerful structure of the IPFM model, it is quite necessary to further develop this model for exploration of the physiological mechanisms of other neural or cardiac related events, such as PPG signals. The PPG signal measured using a photo-detector on the skin surface of human body is associated with the change in the volume of red blood cells in the peripheral micro-vascular bed with each pressure pulse initiated by the heart. In other words, the repetition of PPG pulses should be the same as that of ECG signals over the same cardiac cycle. Therefore, it seems to be promising that PPG signals can also be interpreted based on the IPFM mechanism coupled with certain transmission characteristics of the pressure wave through the arterial system.

Due to its advantage in the ease of measurement at the peripheral sites and in providing useful information on some physiological parameters, PPG signals have been widely used for a variety of applications, including monitoring of arterial pressure and compliance in human [45], recording of heart and respiratory rates [30], oxygen saturation measurement [31], detecting anxiety [32], etc. However, many researchers just made use of PPG signals without elaborating or exploring their generation mechanism. Consequently, it remains controversial on what contributes to the generation of those peripheral signals. Weinman *et al.* [46] concluded that scattering, reflection, absorption and movement of the vessel wall all play a role in producing PPG signals. Most recently, Moyle described that there are four

absorption strata at a PPG site. The majority of light produced by the light source is scattered by tissue, venous blood and arterial blood; while a small portion of light experiences variable scatter due to the pulsation of arterial blood [47]. The first objective of this chapter is to clarify the fundamental mechanism of PPG signals in terms of the characteristics of the cardiovascular system and the arterial system, and the principles of fluid mechanics.

Despite the complex source which affects only the details in the waveform, the repetition of PPG pulses should be strictly consistent with that of heart beats. In fact, PPG signals have already been used for heart rate monitoring for a long time. In the second part of this chapter, the mathematical modeling taking the advantage of the IPFM mechanism is carried out to provide an insight into better understanding the underlying mechanism of the PPG signal.

3.2 Principles of PPG

In this section, the elementary principles for the generation of the PPG signal are provided. Though the actual composition of the PPG signal could be complex, the explanation based on hemodynamics and certain characteristics of the biological systems would be of great importance in understanding this signal. The basic laws or equations in fluid mechanics with certain assumptions, though cannot be rigorously applied to biological systems, they perform almost certainly as a close and practical approximation for understanding the interrelationship among the oscillatory pressure wave, blood flow and arterial properties in a biological system.

3.2.1 Relationship between Pressure and Flow

A small shift of fluid elements in a compressible media will induce in due course similar movements in adjacent elements and that in this way a disturbance, called

acoustic wave or pressure wave, which propagates at a relatively high speed, the speed of sound, through the media. It is therefore easy to imagine that with the onset of the ejection phase during a cardiac cycle, giving rise to a sharp increase in aortic pressure, a pressure wave is initiated in the radial stretch of the ascending aorta and it is propagated down the aorta and its branches [21].

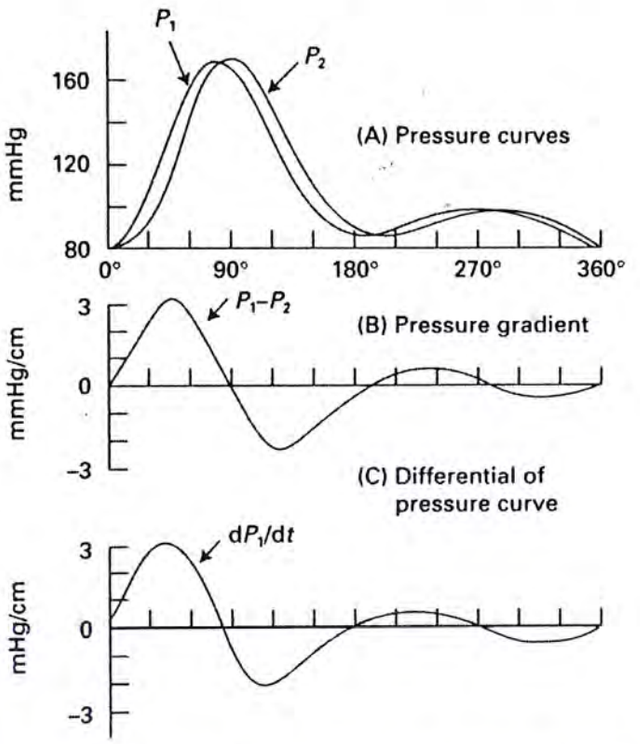

Fig. 3-1: A diagram that shows how a traveling pressure wave creates an oscillatory pressure gradient. (A) Two pressure waves recorded a short distance apart along the femoral artery of a dog; (B) The pressure gradient derived by subtracting the pressure at the downstream site from that at the upstream site at 15° intervals and dividing by the distance between the recording sites; and (C) The derivative with respect to time of the upstream pressure wave (dP_1 / dt).

The pulsatile flow rate depends on the pressure gradient along the artery [48]. The calculation of the pressure gradient is explained by Fig. 3-1. Owing to the fact that the pressure pulse generated in the aorta due to expulsion of blood by the ventricle travels along the arteries, the crest of the wave reaches the upstream recording site a short time before it reaches the downstream site. At this time, the pressure is higher at the first set than that at the second site and the pressure gradient

occurs in this direction. The situation rapidly reverses, and when the crest has reached the second site the pressure gradient is in the opposite direction. The resultant pressure gradient, therefore, is one that oscillates about a mean as shown in Fig. 3-1 (B). As there are traveling waves in all arteries, pressure gradients in all arteries will be of this form.

Pressure is one of the principle determinants of the rate of flow rate. Based on Poiseuille's law, for the steady, laminar flow of a Newtonian fluid through a cylindrical tube, the flow rate, Q, varies directly with the pressure difference, ΔP, and the fourth power of the radius, r, of the tube, and it varies inversely with the length, L, of the tube and the viscosity, μ, of the fluid. The expression of Poiseuille's law is

$$Q = \frac{\pi r^4 \cdot \Delta P}{8\mu L} \qquad (3\text{-}1)$$

where $\pi / 8$ is the constant of proportionality [21].

Obviously, the blood itself is not simple, homogeneous solution but instead is a complex suspension of red and white corpuscles, platelets, and lipid globules dispersed in a colloidal solution of proteins [21]. Besides, the aorta, the pulmonary artery, and their major branches constitute a system of conduits with considerable volume and distensibility. As a result, the mathematical equation to describe the relationship between the oscillatory pressure gradient and the blood flow in the arteries differs from Eq. (3-1) (For the details of the derivation of the relationship between the oscillatory pressure gradient and the flow, please refer to [48]). Nevertheless, the pressure gradient is directly related to the flow just as that in Poiseuille's law. The relationship between pressure and flow velocity, which depends on the pressure gradient, can be represented by Fig. 3-2. It can be seen that a considerable similarity exists between the simultaneously recorded pressure and

flow waveform.

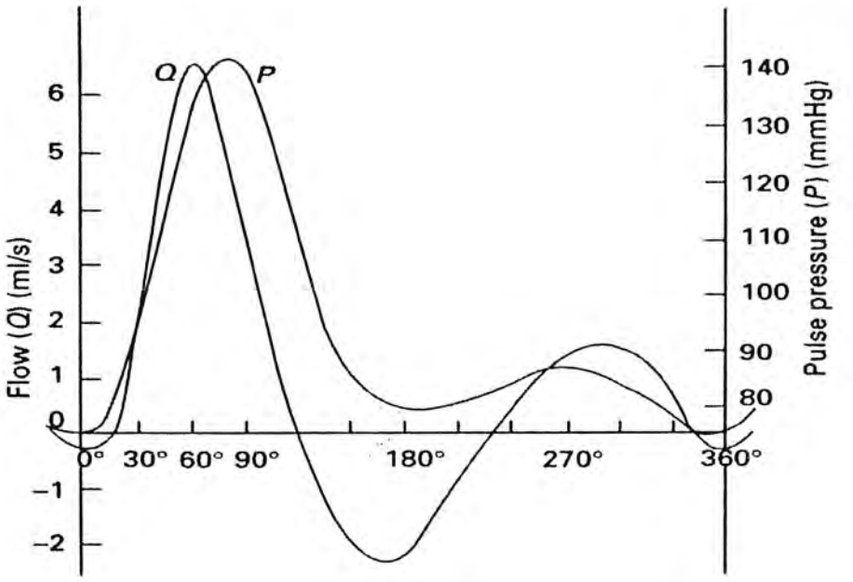

Fig. 3-2: The flow velocity (Q: ml/s) determined by the pressure gradient and the arterial pressure pulse (P) recorded simultaneously in the femoral artery of a dog [48].

3.2.2 Peripheral Pressure and Flow Curves

Structural and geometric non-uniformities give rise to differences in pressure and flow contours in different anatomic locations in the arterial system. As the pulse wave is transmitted down the arterial system, simultaneous recordings of pressure and flow waveforms in different parts of the vascular tree have clear distinct features. The changes in configuration of the pressure and flow pulses with distance are shown in Fig. 3-3 [48]. Aside from the increasing delay in the onset of the initial pressure rise, three major changes occur in the pulse contour as the pressure wave travels distally. First, the high frequency component of the pulse, such as the incisura (the notch that appears as a result of an aortic valve closure at the end of ventricular ejection), is damped out and soon disappear; and a hump may appear on the diastolic portion of the pressure wave [21]. Second, the systolic portion of the pressure wave becomes narrowed and elevated; that of the flow waveform behaves

in just the opposite manner. Third, the pulse pressure increases and the flow amplitude decreases progressively, though the mean pressure falls very slowly until reaching the arteriolar beds [13]. On the other hand, in general, pressure and flow waveforms are similar at corresponding anatomic sites among many mammalian species [49].

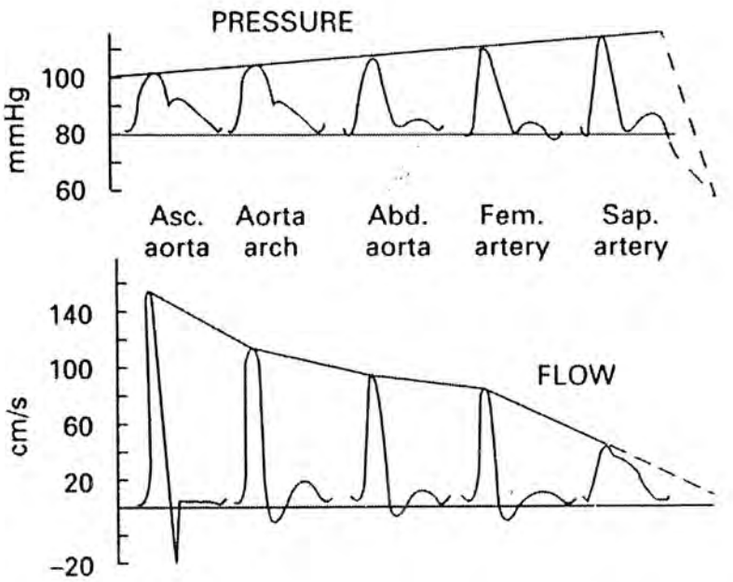

Fig. 3-3: Pressure and flow waveforms in the ascending, thoracic, and abdominal aortas, as well as the femoral and saphenous arteries.

These changes in the pressure contour are mainly caused by the differences in total peripheral resistance and arterial compliance in different sites of the arterial system. Since the arteries become less compliant with advancing in age, the changes of the pressure contour are more pronounced in young individuals. The pulse wave of elderly patients maybe transmitted virtually unchanged from the ascending aorta to the periphery. Furthermore, the precise mechanism for the peaking of the pressure wave is controversial. Probably several factors affect the peaking of the pressure, including reflection, tapering, resonance, and changes in transmission velocity with the pressure level.

3.2.3 Generation of the PPG Signal

As the pressure wave travels from the ascending aorta toward the periphery, the corresponding pulsatile flow occurs with the oscillatory pressure gradient. The pulsations of the arterial blood can be detected by an optoelectronic detector, and hence generating the PPG signal.

As shown in Fig. 3-4, there are four absorption strata at a PPG site indicated. The majority of light produced by the LED (light source) is scattered by tissue, venous blood and arterial blood. A small portion of the light experiences variable scatter due to the pulsation of arterial blood. Some portion of the light is detected by an optoelectronic detector, and therefore, contains the signature of the pulsatile component of the arterial blood flow.

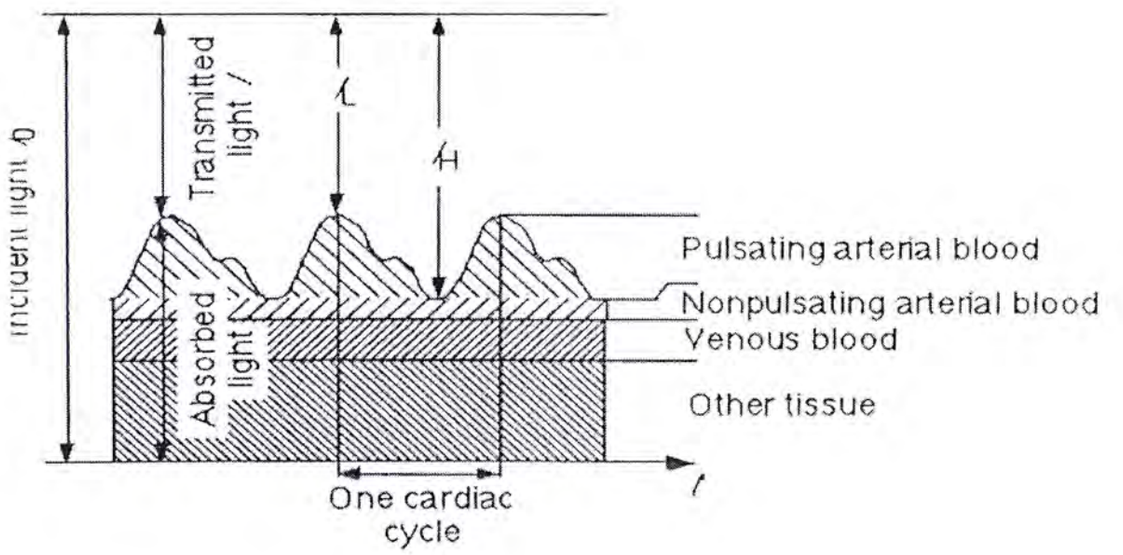

Fig. 3-4: The principle of the PPG technique [47].

It is also indicated by Fig. 3-4 that the intensity of the light passing through the tissue during diastole is at the high peak (I_H). The absorbers that are present during diastole are the DC component. The optical path length in the arteries increases during the systole, therefore the transmitted light reaches the low peak (I_L).

In summary, the PPG signal is associated with changes in the volume of arterial blood in the peripheral micro-vascular due to the pressure pulse initiated by the heart. Particularly, the variations in the intensity of the signal reflect the pulsations of arterial blood flow occurring as the pressure wave travels along the arteries. However, as the detected light that contains the pulsatile component is only a fraction of the total received light, the PPG signal could give only a rough representation of the peripheral flow waveform, which may differ a little bit from that detected at aorta, and it so far only yields a qualitative description of BP or flow. Nevertheless, the generation and properties of PPG signals are closely related to that of the pressure wave. Mathematical modeling based on such physiological mechanism is just under way.

3.3 Model Description

As described in the last section, the elementary generation mechanism of the PPG signal can be concluded as: 1) the onset of the ventricular contraction coincides with the peak of the R-wave of the ECG signal. There is a time interval between the start of the ventricular contraction and the opening of the semilunar valves (when ventricular pressure rises abruptly), which is termed as isovolumic contraction or the pre-ejection period (PEP). After the PEP, the opening of the semilunar valves marks onset of the blood ejection phase that gives rise to a sharp increase in aortic pressure, and a pressure wave is initiated in the radial stretch of the ascending aorta; 2) the pressure wave is then propagated down through the arterial system, including the aorta and its branches; 3) and finally, as the pressure wave travels distally, the corresponding pulsation of the blood flow at the periphery is detected by the photo-detector which generates the PPG signal. Such a mechanism for PPG signal generation is the basis of the model in this study. Since the IPFM model is widely

used to mimic the mechanism of heart beat generation, the timing of the occurrence of the R peaks (or the ventricular systoles) can be determined by using this model. On the other hand, the Windkessel model can be used to describe the arterial system, through which the pressure wave is transmitted. Therefore, a mathematical model is constructed for the generation of the PPG signal based on these two models.

3.3.1 IPFM Model

The details of the IPFM model have already been introduced in the last chapter. As a physiologically plausible model, it transforms a continuous non-negative input signal, representing the ANS activity on the SA node, into a series of cardiac events (firing events). Here, it is utilized as a realistic model of RR intervals.

The occurrence times of any two consecutive R peaks satisfy the relationship:

$$V_{th} = \int_{t_i}^{t_{i+1}} (m_0 + m_1(t))dt \qquad (3\text{-}2)$$

where $m_1(t)$ is the modulating input signal, m_0 is the constant input signal, V_{th} is the integration threshold, and t_i .and t_{i+1} are the occurrence time of the ith and $(i+1)th$ pulses, respectively. The structure of the IPFM model is given in Fig. 3-5. The output firing pulses are represented by a discrete time series $y(t)$ .The pulse generator $p(t)$ can be a QRS complex generator.

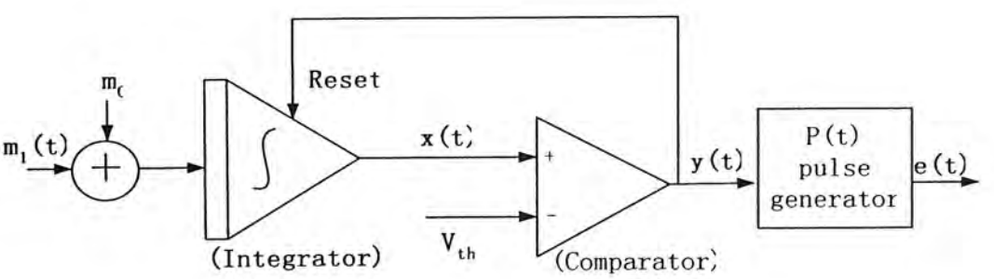

Fig. 3-5: Schematic diagram of the IPFM model.

3.3.2 Windkessel Model

A three-element Windkessel (WK3) model is utilized to represent the characteristics of the aorta and its branches, through which the pressure wave is propagating. Arterial compliance is represented by a capacitor, C, which has the storage properties, in this case, the electric charge. Peripheral resistance, with its viscous properties, is represented by a resistor, R, that dissipates energy. In addition, a characteristic impedance of the proximal aorta, or the input impedance to the arterial system, is also represented by a resistor, r. The electrical analog of the Windkessel model for the arterial system is shown in Fig. 3-6.

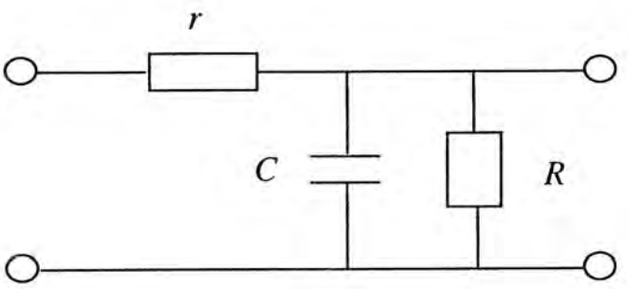

Fig. 3-6: A Windkessel model with three elements.

This three-element Windkessel model for the systemic arterial tree has been a useful tool in studying the transmission properties of arterial pulses [13] [18] [19]. It helps to understanding the differences in pulse and flow waveforms in different parts of the vascular tree in a human body. More specifically, through this model, the distal pressure pulse can be interpreted as the output, being the proximal pressure pulse the input. Such interpretation is illustrated in Fig. 3-7: the pressure wave generated at the ascending aorta propagates through the arterial trees represented by the Windkessel model, and the peripheral pulse is therefore obtained which has some distinct features from that of the original one. The differences in the

configuration of the pulse contour have been elaborated in section 3.2.2.

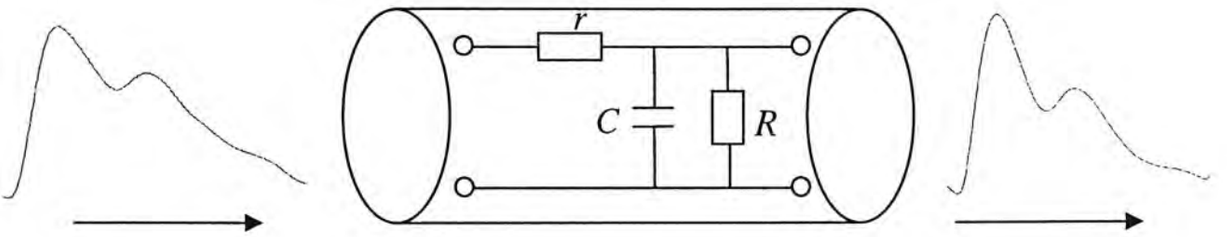

Fig. 3-7: Three-element Windkessel modeling the arterial system, with the proximal pulse as the input and the distal pulse as the output.

Once the proximal pulse is applied to the model, the distal pressure pulse can be determined by the model parameters. In other words, the output distal pulse is the convolution of the input proximal pulse with the impulse response, $h(t)$, of the WK3 model. Similar to the derivations in Chapter 1, the relationship between the pressure and flow rate, incorporating the WK3 parameters, r, C, *and* R, can be expressed as:

$$Q(t) = C \cdot dP_C(t)/dt + P_C(t)/R, \tag{3-3}$$

and

$$P(t) = P_C(t) + Q(t) \cdot r \tag{3-4}$$

in which $P(t)$ and $Q(t)$ are the input aortic BP and flow rate, respectively; $P_C(t)$ represents the peripheral systemic pressure.

Substituting Eq. (3-3) into Eq. (3-4), we have:

$$P(t) = C \cdot r \cdot dP_C(t)/dt + (1+\frac{r}{R})P_C(t) \tag{3-5}$$

By using the analytic solution of Eq. (3-5), the impulse response of the WK3 model can be obtained:

$$h(t) = F^{-1}(\frac{P_C(f)}{P(f)}) = k \cdot (\frac{1}{rC}) \cdot \exp(-\frac{R+r}{R \cdot r \cdot C} \cdot t) \tag{3-6}$$

in which the constant k is used to scale the proximal to distal pulses, considering that the proximal pressure pulses have lower amplitude than that of the distal ones.

With this impulse response function and an input pressure pulse, a theoretical distal pulse can be calculated.

3.3.3 ANew Model for the Generation of PPG

Based on the IPFM model and the WK3 model with a pulse generator and a time delay generator, a new model for the generation of the PPG signalis constructed. The diagram of this model is illustrated in Fig. 3-8.

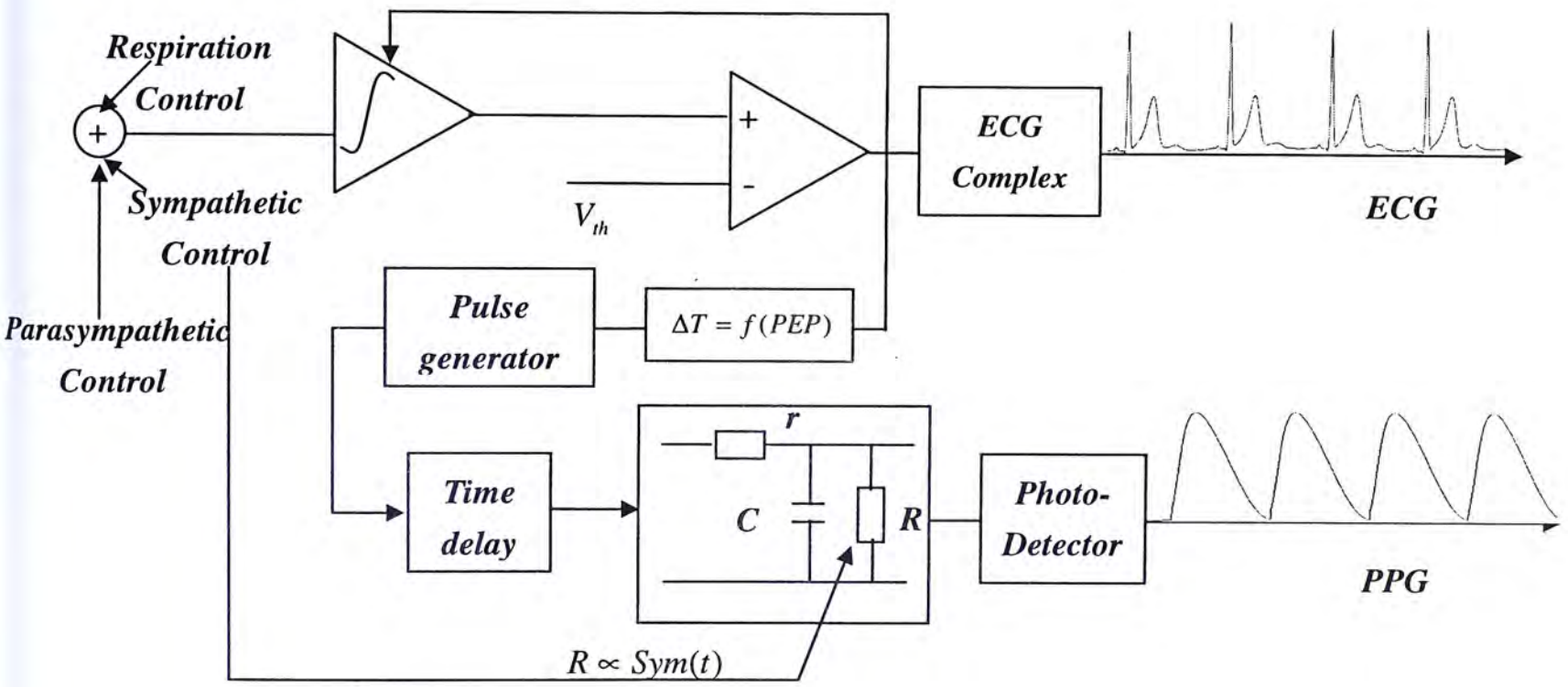

Fig. 3-8: The schematic diagram of the new model for the generation of PPG.

The upper part of Fig. 3-8 is a conventional IPFM model mimicking the generation process of SA firings. The continuous non-negative input modulating signal, consisting of the autonomic nervous activity and the respiration effect, is integrated. The ANS is represented by its two branches, the sympathetic and the parasympathetic nervous activities, which decreases and increases the interval between depolarizations of the SA node, respectively. Once the integrated value

exceeds the threshold, V_{th}, a unitary spike is generated at the output of the comparator and the integrator is reset to zero. This nerve spike series is regarded as the timings of the peak of the R-wave in the ECG signal. By the convolution of the nerve spikes with the ECG dynamics, a train of the ECG signal is generated at the output of the complex generator.

The lower part in Fig. 3-8 extends the conventional IPFM model for the generation of the PPG signal. As the firing time of the nerve spikes coincides with the onset of the ventricular contraction, and after a time interval *PEP*, the semilunar valves open that marks the onset of the blood ejection phase and gives rise to a pressure wave in the ascending aorta. A time interval (*PEP*) and a pulse generator are also connected to the output of the IPFM model. Through the convolution of the nerve spikes with the time interval *PEP* and the pulse waveform, a series of pressure wave is generated which synchronizes with the corresponding heart beats. The time interval *PEP* is assumed to be a constant under normal physiological conditions.

The pressure wave is then propagated down the aorta and its branches. Since the pulse transmits with a finite speed, the speed of sound in the arterial system, there is an increase in the time delay in the onset of the initial pressure rise with the increase in the distance from the heart. In other words, at certain anatomic locations in the arterial system, the occurrence of the pressure wave during the same heart cycle is some time after that at the proximal. This time delay could be attributed to several factors that may affect the transmission velocity, such as the elastic modulus of the arterial wall, the thickness of the wall, the lumen radius, and the density of blood, etc. It could also be associated with temperature, age, or other physical status. In our model, this time delay is defined as the interval between the occurrences of the proximal and peripheral pressure waves. Here, the time delay is assumed to depend on factors other than the arterial compliance, peripheral resistance, and the

vascular impedance which are included in the WK3 model. These factors are relatively stable under normal physiological conditions. Therefore, a time delay generator is connected to the pulse generator, which gives a constant.

Aside from the delay in the onset of the initial pressure rise, changes also occur in the pulse contour as the pressure wave travels distally. These changes, as mentioned in section 3.2.2, are mainly caused by the differences in total peripheral resistance and arterial compliance in different sites of the arterial tree. The WK3 model, representing the major features of the systemic arterial tree, is therefore included in our model. With the proximal pulse as the input, the WK3 model is able to render the possible changes in the pulse contour by convoluting of the proximal wave with its impulse response, $h(t)$. Finally, the PPG signal, which is regarded as the peripheral pulse in our model, is generated at the output of the photo-detector.

3.4 Simulation

In this section the simulation will be carried out using the new model with the numerical input, mimicking the sympathetic and the parasympathetic nervous activities, as well as the respiration signal. The parameters of the WK3 model either fixed or controlled by certain neural activity.

3.4.1 Generation of the ECG Signal

To simulate the SA firings, the input time-varying signal to the IPFM model is expressed as [50]:

$$m(t) = k_0 + k_1(k_2 S(t) - k_3 PS(t)) + k_4 RS(t) + AT \qquad (3\text{-}7)$$

The interpretation of the parameters is as follows:

$S(t)$: The time-varying sympathetic nervous activity on the SA node;

$PS(t)$: The time-varying parasympathetic nervous activity on the SA node;

$RS(t)$: The time-varying respiration activity on the SA node;

k_0 : The intrinsic rate of the rise of the SA node cell potential;

k_1 : The weight that adjust the ANS effect on the SA node;

k_2 : The weight of the SA sympathetic influence;

k_3 : The weight of the SA parasympathetic influence;

k_4 : The weight of the SA respiratory influence;

AT : The tonic autonomic activity at the SA node.

The standard physiological interpretation of this model is that $m(t)$ resembles the membrane potential of the SA node cells, and V_{th} (as shown in Fig. 3-8) is the threshold level for initiation of an action potential. From Eq. (3-7), the rate of the increase of the membrane potential is controlled by a rate k_1, the autonomic neural influence $S(t)$, $PS(t)$ and AT, and the respiratory modulation $RS(t)$. The parameter AT represents the tonic autonomic (sympatho-vagal) activity, while $S(t)$ and $PS(t)$ represent the phasic sympathetic and parasympathetic responses. Sympathetic influence is prevalent when $S(t) > PS(t) + AT$, and will cause an increase in the rise of the cell potential, and therefore a decrease in the interval between two successive firings. Parasympathetic dominance is evident when $PS(t) > S(t) + AT$, and will result in a decrease in the rise of the cell potential, and hence prolong the firing intervals [49].

The signals, $S(t)$, $PS(t)$ and $RS(t)$, are created by first generating zero-mean unit variance Gaussian random sequences. Sympathetic signals are obtained by filtering the Gaussian random sequence with a low pass filter at a cutoff frequency at 0.1Hz, reflecting the slower time dynamics of sympathetic innervation. Parasympathetic signals are obtained by filtering the sequence with cutoff frequencies at 0.1Hz and 0.5Hz. Respiratory signals are obtained by filtering a second zero-mean unit variance Gaussian random sequence with a band-pass filter

between 0.25 and 0.3Hz [50].

The full set of the parameters used for the simulation is given in Table 3-1. Through such suitable choice of scaling variables, the threshold V_{th} can be approximately equal to the mean RR interval. The ECG complex is constructed from experimental data to represent general P-QRS-T dynamics. Since the purpose is not to investigate the details of the neural dynamic, a uniform ECG complex is used for each pulse. Simulations can also be carried out for different mean heart rates by changing the threshold and adjusting other parameters.

Table 3-1: Simulation parameters for the IPFM model.

Variable	Value
k_0	1
k_1	0.8
k_2	5
k_3	0.5
k_4	2
AT	0.05
V_{th}	0.8

A data segment of 20 seconds was simulated by using MATLAB. The input modulation signals, $S(t)$, $PS(t)$ and $RS(t)$, and the simulated RR intervals are illustrated in Fig. 3-9. The RR intervals as a discrete time series are plotted at their corresponding time of firings. It can be observed that the RR intervals in Fig. 3-9 (d) oscillate almost at the same low frequency, around 0.1Hz, as the sympathetic input signals in Fig. 3-9 (a). There is a phase shift of about π, however, which

demonstrates that an increased sympathetic nervous activity leads to a decrease in RR intervals, and vice versa. The parasympathetic signals and the respiratory signals contribute to the relatively high frequency fluctuation in RR intervals. The parasympathetic signals in Fig. 3-9(b) are almost in phase with the RR series, while there is also a phase shift of about π between the respiratory signals in Fig. 3-9(c) and RR series. Therefore, the heartbeat intervals generated by the IPFM process indeed carry the information of all the input signals, which can be clearly reflected by spectral analysis as discussed later.

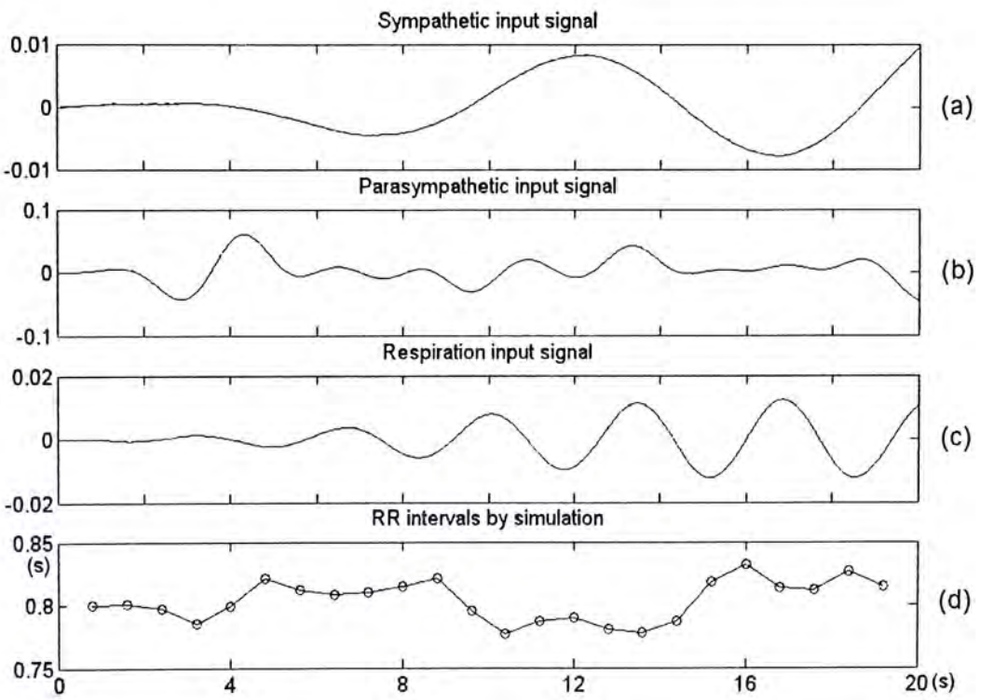

Fig. 3-9: a) Sympathetic signals $S(t)$; b) Parasympathetic signals $PS(t)$; c) Respiratory signals $RS(t)$; and d) The simulated RR intervals.

The simulation results of the integration process and the output neural spike series, as well as the corresponding ECG signals are shown in Fig. 3-10 (a), (b), and (c), respectively. Only one fourth (5 seconds) of the total simulated results are displayed. It is clearly illustrated that whenever the integrated value reaches the threshold Th in Fig. 3-10 (a), a unitary impulse is generated in Fig. 3-10 (b). Fig. 3-10 (d) shows the generation process of the neural dynamics. The ECG complex is

obtained by averaging several ECG complexes extracted from experimental data of a healthy subject. The neural spikes are convoluted from the given ECG complex, and the ECG signals with uniform P-QRS-T complexes ($p_{QRS}(t)$) are generated, in which the R peaks are located at the timings of neural firing. The output train of ECG signals can be expressed as:

$$e_{ECG}(t) = y(t) * p_{QRS}(t) \tag{3-8}$$

where $y(t)$ is the neural spike train generated by the IPFM model.

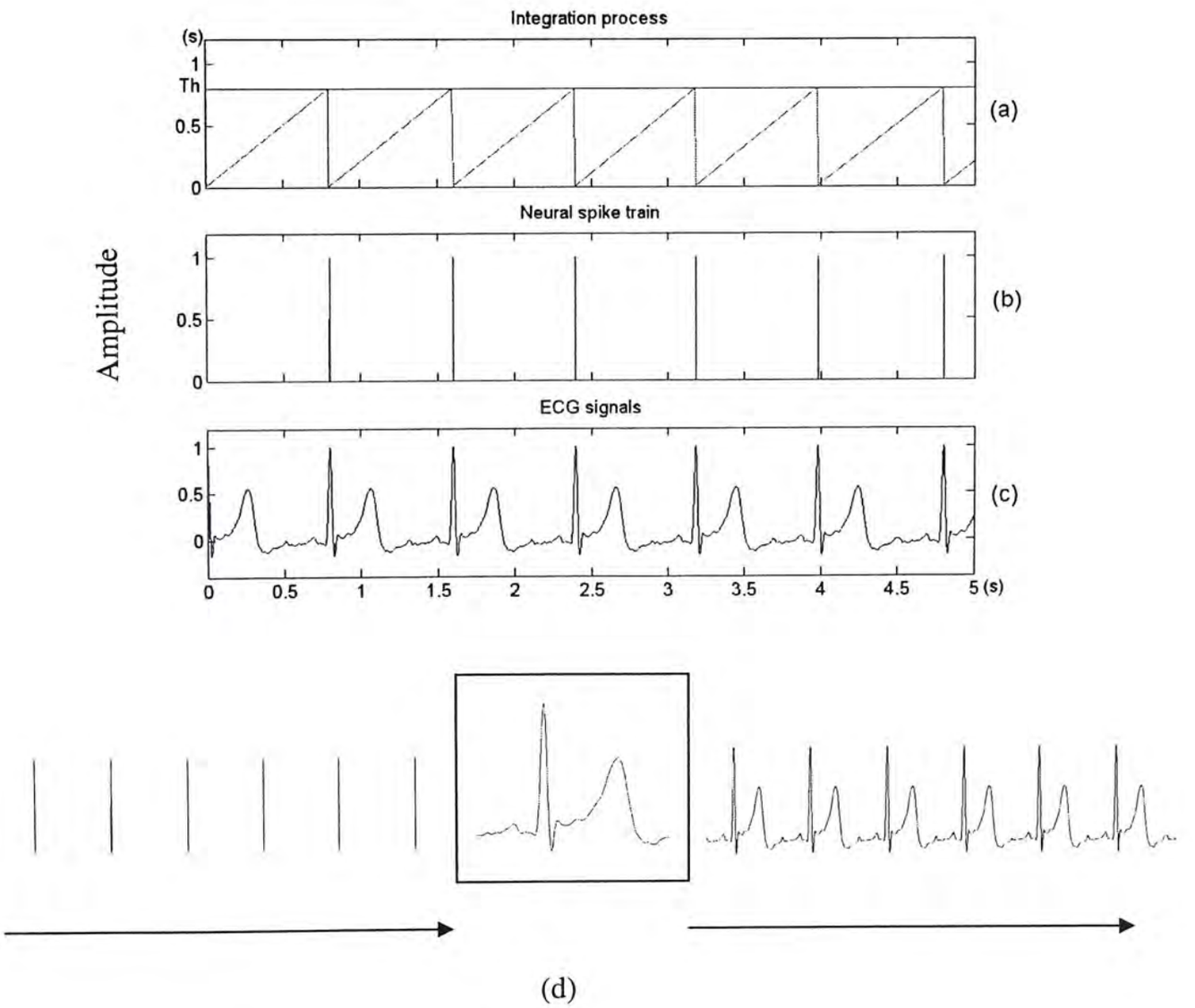

Fig. 3-10: (a) The integration process of the simulated IPFM model; (b) The neural spike train at the output of the comparator; (c) The corresponding ECG signals; and (d) The generation process of the neural dynamics of the ECG signals.

The spectral analysis of the simulation results could provide useful information in better understanding the characteristics of the signal itself; and by comparing with that of experimental results, it could also justify the feasibility of the new model. The spectra of RR intervals from simulation and experimental data are given in Fig. 3-11(a) and (c), respectively. It is clearly observed in Fig. 3-11(a) that the spectrum of the RR interval, calculated from the total simulation data of 20-second using FFT, reflects apparently the rhythms of the input modulation signals: the low-frequency component centered around 0.1Hz is mainly contributed by the sympathetic input signals; while the high-frequency component, generally between 0.25-0.3Hz, is mainly determined by the respiratory frequency with the contribution of the parasympathetic signals. Fig. 3-11(c) is the spectrum from a healthy subject with the same data length of 20-second using FFT. Frequency components at similar regions with similar powers can be identified from these two spectra. The difference in the magnitude of the spectra is due to the difference in mean heart rate between the simulation and the experimental data.

The ultimate output spectrum of the IPFM process integrated with neural dynamics of ECG can be expressed as:

$$E_{ECG}(f) = Y(f) \times P_{QRS}(f) \tag{3-9}$$

where $P_{QRS}(f)$ is the spectrum of the given P-QRS-T complex $p_{QRS}(t)$. The magnitude spectra of ECG signals with neural dynamics from the simulation and experimental data are given in Fig. 3-11(b) and (d), respectively. Again, apparent similarity can be observed between these two spectra, which contain peaks at the mean heart rate and its multiples. There are fewer noises in Fig. 3-11 (b) because the ECG signal from the simulation contain a uniform and smoother P-QRS-T complex.

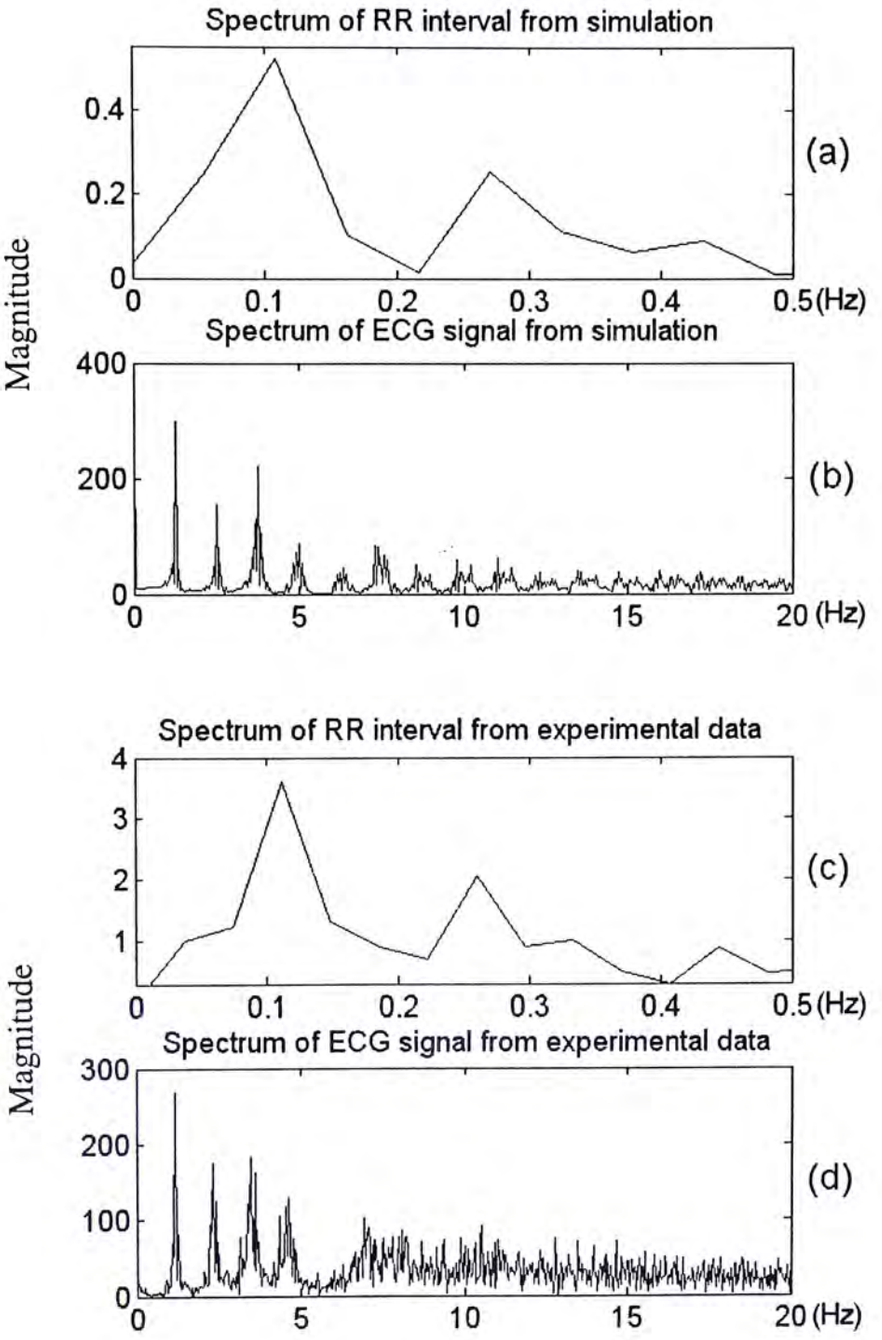

Fig. 3-11: (a), (b) The spectra of the RR interval and ECG signal from the simulation; and (c), (d) The spectrum of RR interval and ECG signal from experimental data of a normal subject.

3.4.2 Generation of the PPG Signal

Since we do not concern much about the details of the pressure waveform is not a concern here, a pulse with a simple waveform is synchronously generated at the firing of each neural spike at the output of the IPFM model. With the knowledge of

the cardiac period, RR interval, an aortic pressure wave is synthesized by means of two cubic splines [51]. Suppose the length of the RR interval is T, the coefficients of the two cubic splines are determined by satisfying the following conditions:

a) Passage through three points of coordinates $(0, P_d)$, (t_m, P_s), and (T, P_d), where t_m is the time interval between the diastolic (P_d) and systolic (P_s) pressure values (P_s and P_d are assumed as constants), and is roughly determined as one fourth of the cardiac period T [21];

b) Zero time derivative in the same three points.

In this way, similar pulse waveforms are generated depending on the length of the corresponding RR intervals. An example of such spline interpolation is shown in Fig. 3-12. The diastolic and systolic pressures are 80mmHg and 120mmHg, respectively.

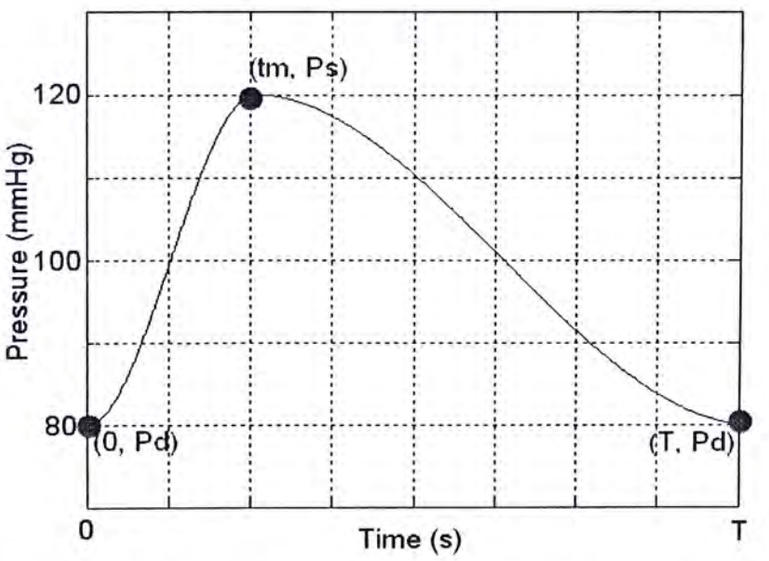

Fig. 3-12: Example of the spline interpolation to generate a pulse waveform.

Base on the knowledge of the cardiovascular physiology and the foot-to-foot transmission velocity of the pressure wave in arterial system, a constant PEP=50 ms and a constant time delay $t = 130ms$ are used in the simulation [37].

The WK3 model parameters, the large vessel compliance C and the proximal

aorta impedance, r, are assumed constant in our model [52]; while the peripheral resistance, R, is under the modulation of sympathetic nervous activity [53]. The dynamic change of R is in accordance to the actual physiological mechanism, i.e., t during a cardiac cycle, the ANS reacts to the baro-receptors not only by modulating the autonomic resting tones to heart through sympathetic and parasympathetic activities, but also by modulating peripheral resistance through sympathetic control [53]. On the contrary, the vessel compliance, C, and the proximal aorta impedance, r, are of constant values remains a reasonable approximation in many studies, and it is proved to be adequate to usual measurement and model errors [18] [52]. Therefore, the constant C was calculated from the radial artery cross-sectional compliance and the mean superficial length of the forearm of all subjects [54]. The r value was obtained by Poiseuille's equation [48] from the radial artery radius [54], and the DC value of R from [55]. It is generally known that the peripheral resistance varies proportionally with the sympathetic activities. Thus, the ac value of R is directly proportional to the input sympathetic signals. The impulse response $h(t) = k \cdot (\frac{1}{rC}) \cdot \exp(-\frac{R+r}{R \cdot r \cdot C} \cdot t)$ is also determined by appropriate selection of k. The values of these parameters are listed in Table 3-2.

Table 3-2: Values of the parameters in the WK3 model.

Parameter	Value
C	$6.22\times10^{-7}\ cm^5/dyn$
r	$1.15\times10^{5}\ dyn\cdot s/cm^5$
R (DC)	$6.81\times10^{5}\ dyn\cdot s/cm^5$
R (AC)	$\propto S(t)$
k	10^{-2}

Fig. 3-13 shows an example of the distal pulse wave generated through the convolution of proximal pressure wave with $h(t)$. It is clearly indicated that the systolic portion of the pressure wave becomes narrowed and elevated, which is consistent with the practical situation. Other changes expected can not be reflected due to the simplicity of the waveform itself. The distal pulse waves, though not exactly the PPG signals, are strictly synchronized with PPG pulses with similar contours (see Fig. 3-2). In other words, the distal pulses generated by the new model can be regarded as PPG signals.

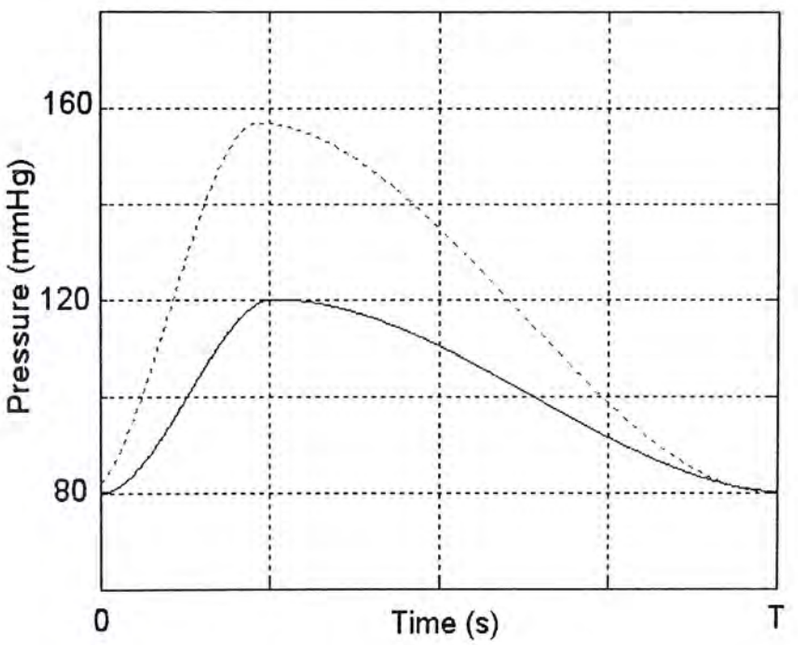

Fig. 3-13: An example of the distal pulse wave (dotted line) compared with the proximal pressure wave (straight line).

The output train of PPG signals can therefore be expressed as:

$$e_{PPG}(t) = y(t - \Delta t - PEP) * h(t) * p_{BP}(t) * c(x) \qquad (3\text{-}10)$$

where $p_{BP}(t)$ is the pulse waveform generated with the firing of each neural spike at the output of the IPFM model, Δt is a constant provided by the time delay generator, and $h(t)$ is the impulse response of the WK3 model, and

$c(t) = (-1) \times I_0 e^{-\varepsilon(\lambda)[d+x(t)]}$(Beer-Lamber's law, in which $x(t)$ is exactly determined by the instantaneous amplitude of the distal pressure wave at time t [61].) is the impulse response of the photo-detector. In this way, ECG and PPG signals can both be obtained, as shown in Fig. 3-14 (a). There is a delay between the R peak of ECG signals and the onset of PPG signals, which is induced by the time delay constant Δt in the model. Obviously, this is in accordance to the reality, in which the delay in time between the characteristic points on ECG and PPG signals is regarded as PTT.

The ultimate output spectrum of PPG signals can be expressed as:

$$E_{PPG}(f) = Y(f) \times e^{-j\omega(\Delta t + PEP)} \times H(f) \times P_{BP}(f) * C(f) \qquad (3\text{-}11)$$

where $H(f)$ and $C(f)$ are the transfer functions of the WK3 model and the photo-detector, $P_{BP}(f)$ is the PSD of an individual BP waveform. The magnitude spectra of ECG and PPG signals are given in Fig. 3-14 (b), which contain the first sharp peak at the same mean firing rate with smaller peaks at its harmonics. This is absolutely in consistence with reality that the repetition of PPG pulses is the same as that of ECG signals over the same cardiac cycles, as represented by the first peak.

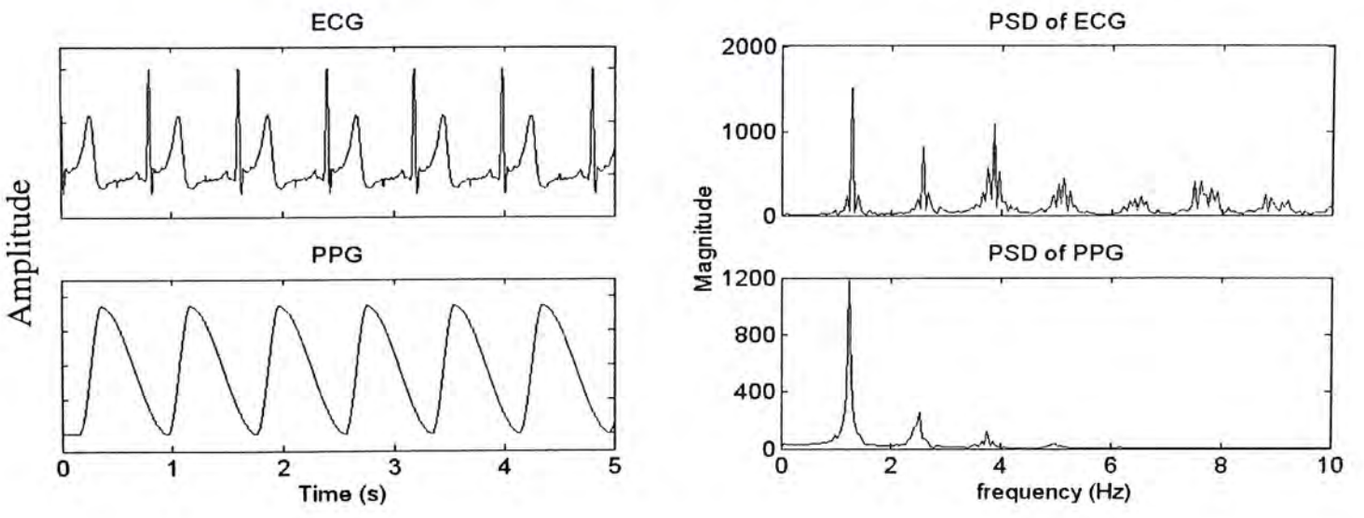

(a) (b)

Fig 3-14: (a) ECG (upper panel) and PPG (lower panel) signals generated by the new model; and (b) the spectra of ECG and PPG signals in (a).

The magnitude of the spectra of ECG and PPG signals from the simulation and experimental data are given in Fig. 3-15. Apparent consistence can be observed between these two sets of spectra, which contain peaks at the mean heart rate and its harmonics with decaying amplitudes. It should also be emphasized that besides the same location of the first sharp peak in the PSD of ECG and PPG signals, the corresponding harmonics are also located at the same frequencies—the multiples of the mean heart rate, which is already realized by the new model.

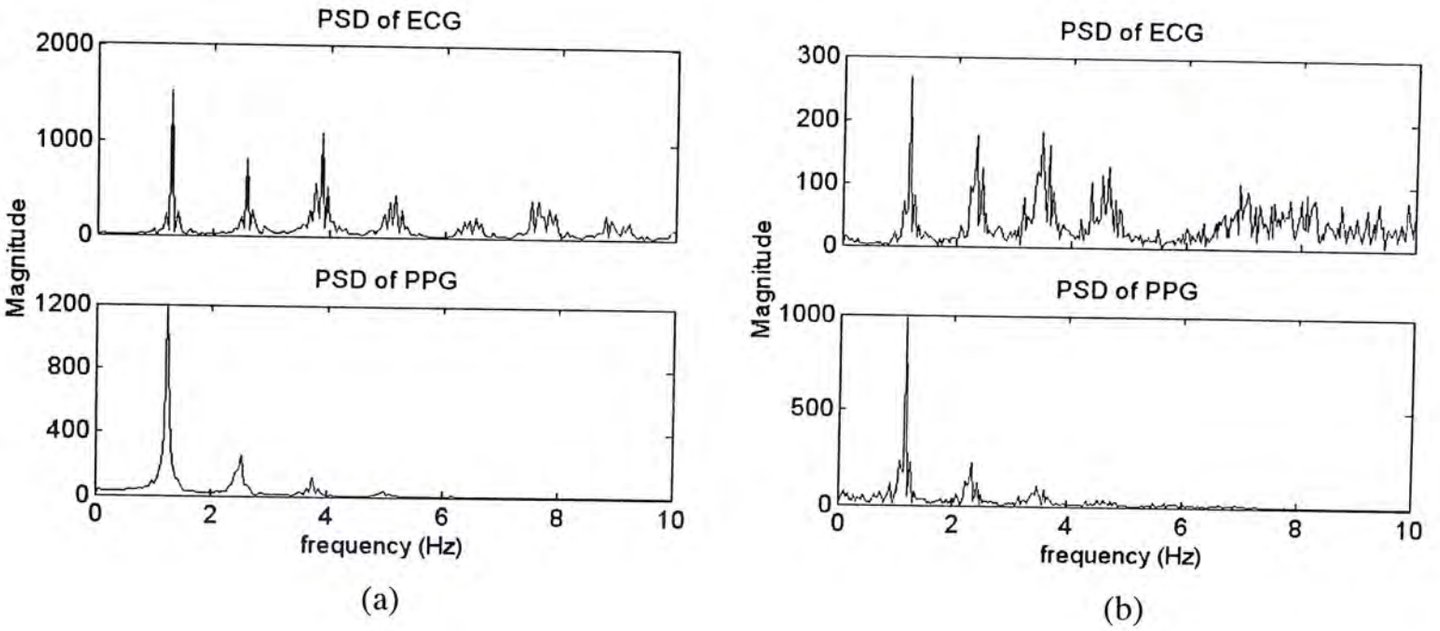

Fig. 3-15: PSD of the ECG and PPG signals (a) simulation results; and (b) experimental from a healthy subject.

Furthermore, it can be observed that the amplitude of the harmonics decays much faster in the PSD of PPG signals than that in the PSD of ECG signal. This feature is also appropriately captured by the new model, which is closely associated with the dynamics of the signal. The percentage of the harmonics over the first peak in the PSD of ECG and PPG signals are calculated, respectively. Fig. 3-16 (a) gives the results of the simulation results. Fig. 3-16 (b) shows the averaged experimental data ($mean \pm SD$) of 10 healthy resting subjects. Both results indicate clearly that

the dynamics of the ECG signal contain a frequency range which is higher than that of PPG pulse dynamics. This result suggests that the details in the contour of the waveform may have little influence on either the spectra of ECG and PPG signals. Therefore, the simplification in the new model is further validated to be reasonable.

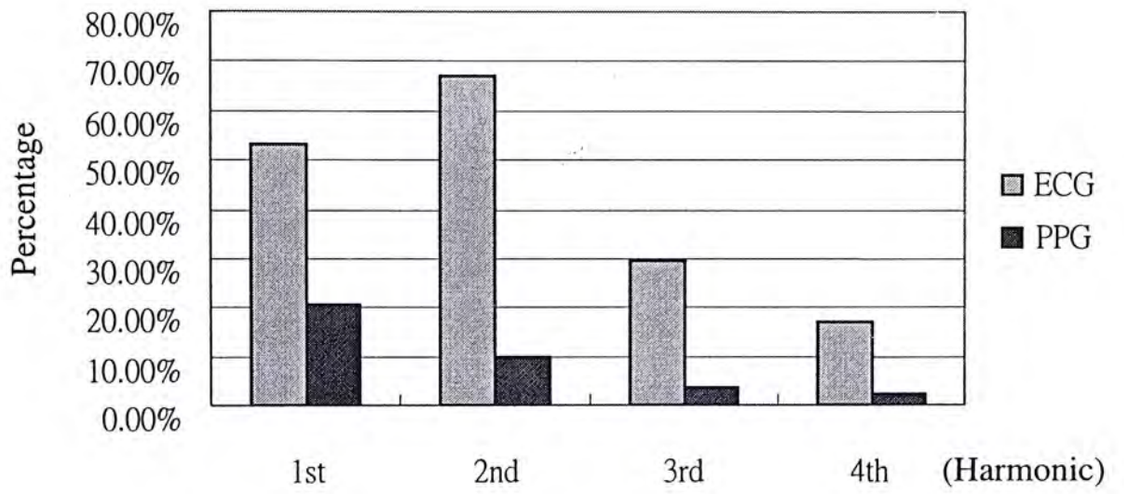

(a)

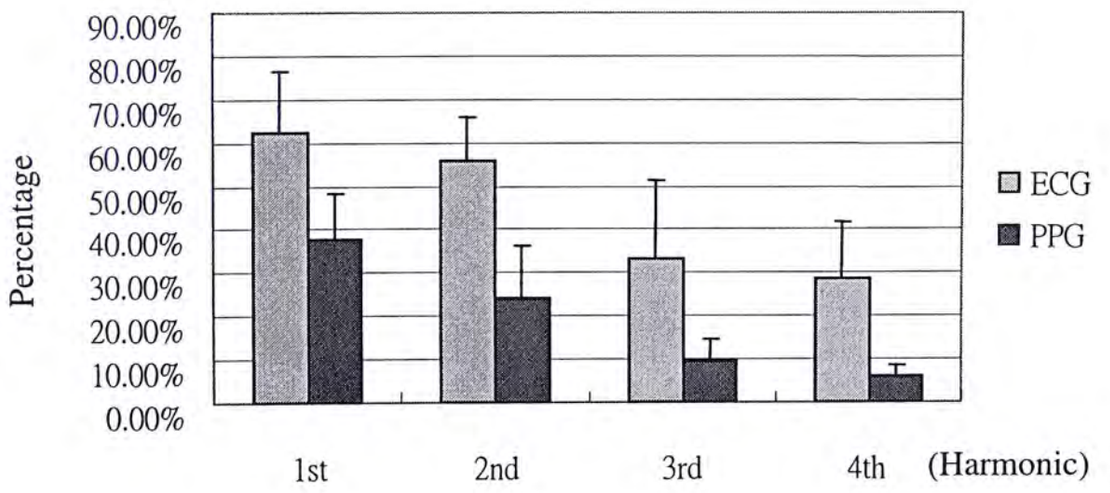

(b)

Fig. 3-16: The percentage of the first four harmonics over the first peak in the PSD of ECG and PPG signals from (a) simulation results and (b) experimental data of healthy subjects ($mean \pm SD$, n=10).

According to Eqs. (3-11) and (3-9), phase difference certainly exists between ECG and PPG signals. Both the impulse response of the WK3 model, $h(t)$, and the constant time delay, Δt, may contribute to this phase difference. The individual phase spectra of ECG and PPG signals from both simulation and experimental data are illustrated in Fig. 3-17. The only major discrepancy between the simulation results and the experimental data is that the simulated phase spectrum of PPG signals seems to be far less variable, which is nearly constant in high frequency range from 0.1-0.5Hz. It is likely due to the constant time delay in the new model, which might play a major role in the phase spectrum. The plots of the phase difference further illustrate such phenomena, as shown in Fig. 3-18. The phase difference between PPG and ECG signals from simulation does not vary significantly as that from experimental data, especially in the high frequency range.

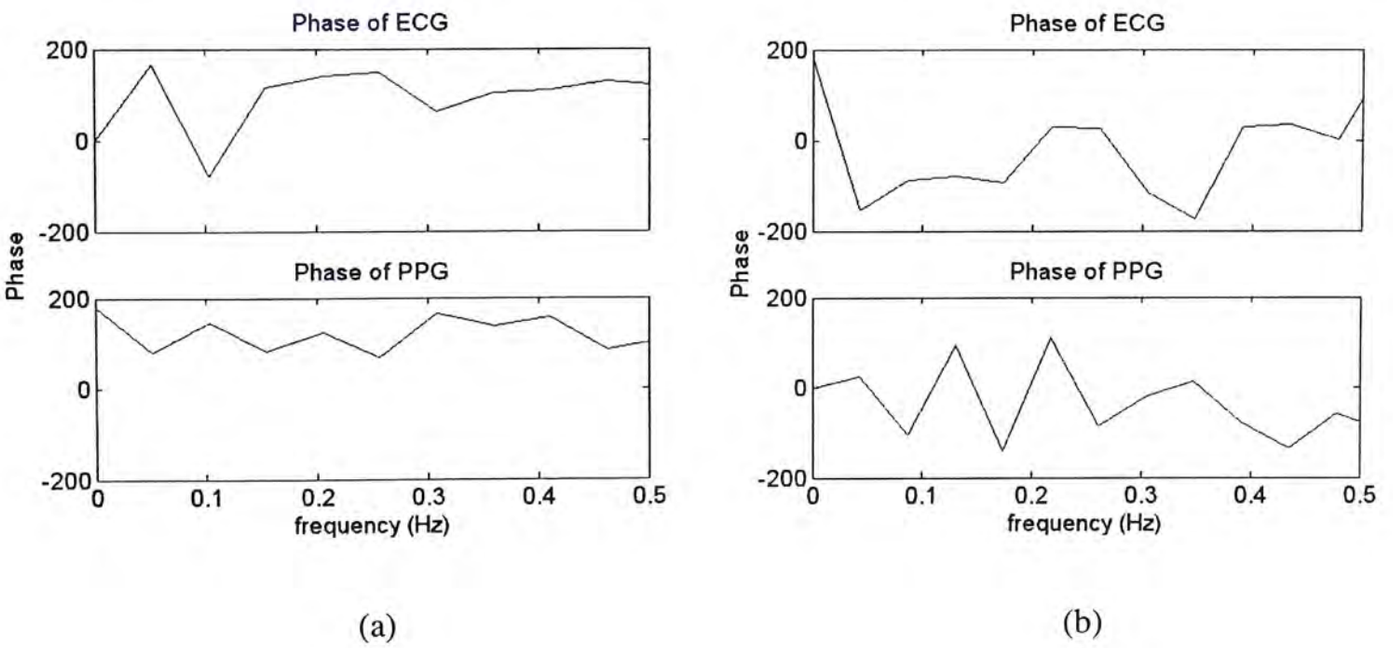

Fig. 3-17: Phase spectra of ECG and PPG signals (a) Simulation results; and (b) experimental results from a normal subject.

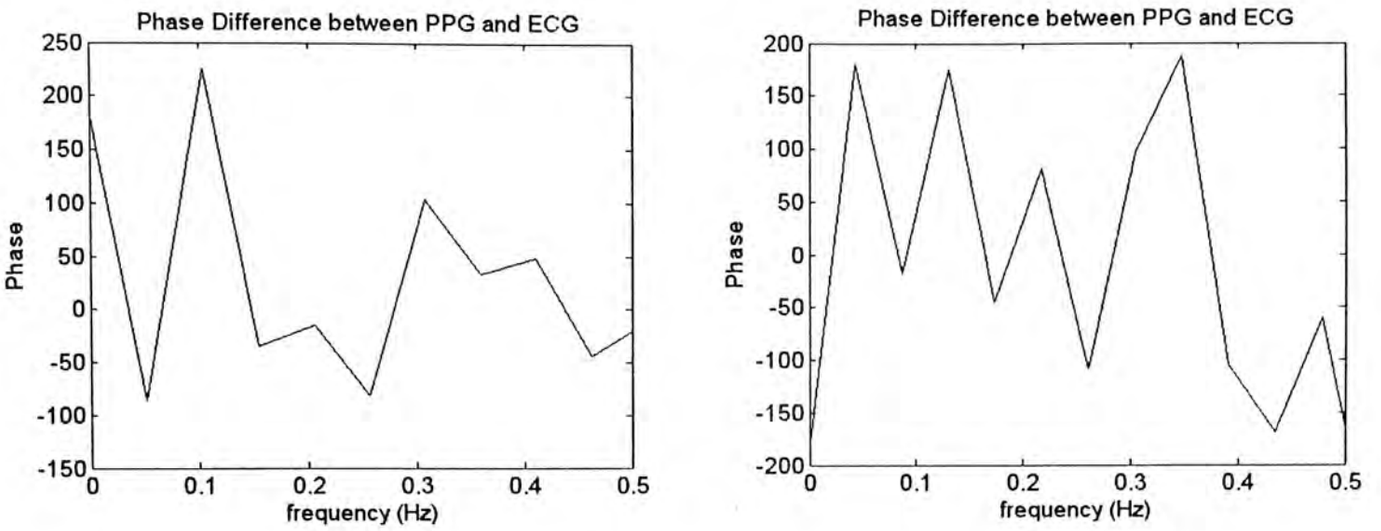

(a) (b)

Fig. 3-18: Phase difference of ECG and PPG signals (a) Simulation results; and (b) experimental data from a normal subject.

3.4.3 Effects of the Modulation Depth on the Output

The strength of the modulation is called the modulation depth or percentage of modulation. It is defined as $100\% \times (A-B)/(A+B)$ where A and B are the maximum and minimum peak-to-peak amplitudes of the modulated signal respectively. In this study, the responses to the different depths of the input modulation are revealed by changing the oscillation amplitude (the maximum peak-to-peak difference) of the sympathetic, parasympathetic, and respiratory signals, respectively (see Table 3-3). The responses of the model in terms of mean and SD of heartbeat intervals are also given in Table 3-3.

The results of all three patterns suggest that changes in the modulation depth of the input signals have little influence on the mean heartbeat intervals, while the SD of RR intervals (HRV) apparently goes up with the increase in modulation depths. The magnitudes of variations in HRV are different in Pattern A, B, and C, which is mainly due to the difference in the weight of each individual signals in $m(t)$ (refer to Table 3-1).

Table 3-3: Different patterns of input signals with different modulation depths (MD stands for modulation depth and OA stands for the oscillation amplitude).

Pattern A (OAs of parasympathetic and respiratory signals are fixed):			
OA of sympathetic signal	MD of the input signal (%)	Mean RR interval (ms)	SD of RR intervals (ms)
0.0086	4.5034	803	11.4
0.017252	5.8074	803	15.9
0.025877	7.1796	804	21.5
0.034503	8.565	805	27.9
0.043129	9.9843	805	34.5
Pattern B (OAs of sympathetic and respiratory signals are fixed):			
OA of parasympathetic signal	MD of the input signal (%)	Mean RR interval (ms)	SD of RR intervals (ms)
0.053206	5.3499	803	15.6
0.10641	5.8074	803	15.9
0.15962	6.2613	804	16.6
0.21282	7.1447	805	17.9
0.26603	8.195	806	19.5
Pattern C (OAs of sympathetic and parasympathetic signals are fixed):			
OA of respiratory signal	MD of the input signal (%)	Mean RR interval (ms)	SD of RR intervals (ms)
0.012273	4.7979	803	14.3

0.024545	5.8074	803	15.9
0.036818	6.8614	804	18.4
0.049091	7.954	804	21.5
0.061364	9.0548	804	25

Fig. 3-19 shows the relationship between the SD of the heartbeat intervals and the modulation depths of the input signal. An almost linear relationship is observed in Pattern A, B, and C, indicating that a larger modulation depth induces a lager variation in RR intervals. It is also found that the slope of Pattern A is the greatest, and the slope of Pattern B is the smallest. This result probably implies that the sympathetic nervous activities play a major role in modulating the oscillation amplitude of the heartbeat intervals, while the parasympathetic nervous activities could only have relatively minor influence on HRV.

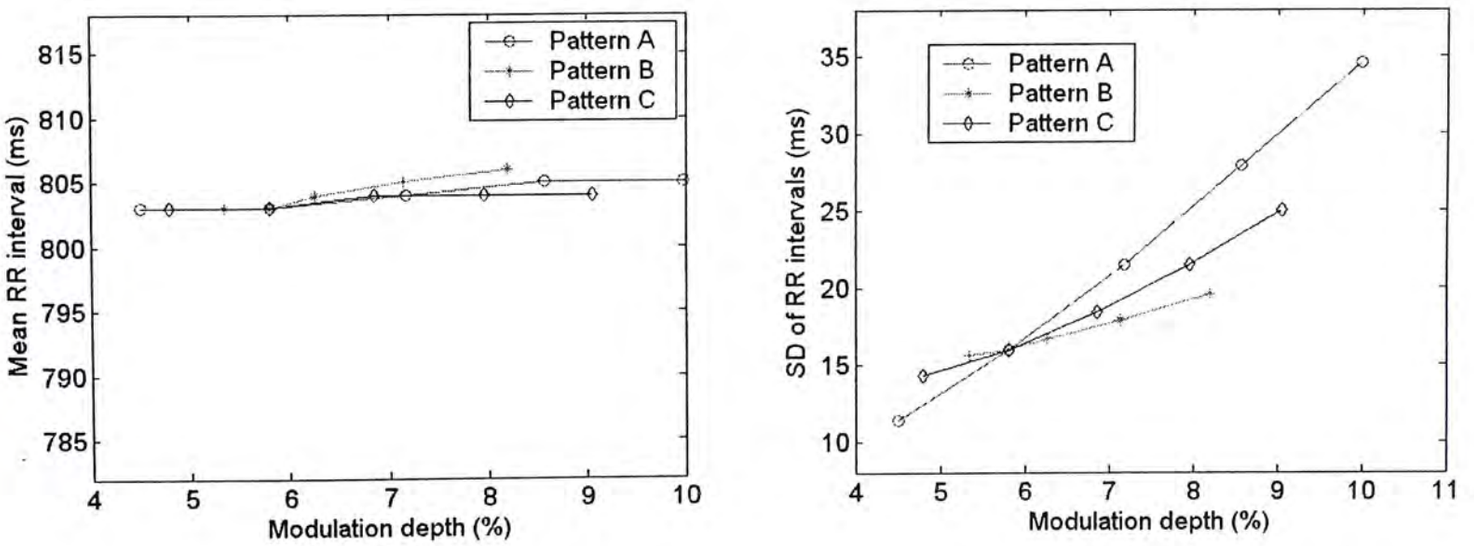

(a) (b)

Fig 3-19: The relationship between (a) mean heart beat interval and (b) the SD of the heartbeat intervals and the modulation depths of the input.

Changes in the modulation depth of the input signals could also be reflected in the PSD of the ECG and PPG trains. Fig. 3-20 shows the output spectra from the new model when the MD is increased to 20.0% by changing the OA of the parasympathetic input. As the parasympathetic signal contains frequency components that are in the range of 0.1-0.5Hz, the power of each frequency band (LF and HF) in the spectra of the heart beat interval is increased compared with Fig. 3-11 (a). This phenomenon can also be observed by the variations in the sidebands of the mean heart rate and its multiples in the spectra of the ECG and PPG trains. The power of the sidebands that are corresponding to the parasympathetic signal is increased. Because of the lower frequency component (0.1Hz) in the parasympathetic input, the increased peaks of sidebands are not apparently isolated from the mean heart rate and its multiples.

The sympathetic input is found to have a more distinct effect on the spectra of the ECG and PPG trains, although the MD is increased to the same level, as shown in Fig. 3-21. Obviously, the LF component that is corresponding to this signal becomes more predominant in the spectra of the heart beat interval. Meanwhile, the sidebands in the PSD of both ECG and PPG signals are greatly increased, which could even exceed the first peak and its multiples. Though they are not isolated ideally from the mean heart rate and its multiples, due to the low frequency of the sympathetic signal, the increased sharp peaks of the sidebands are still detectable.

By changing the OA of the respiratory signal to achieve the same level of the MD, as shown in Fig. 3-22, there is an increase in the power of the sidebands that are corresponding to the respiratory signal. It is more interested to note that in this case, the increased peaks of sidebands are clearly isolated from the mean heart rate, which is attributed to the relatively separable frequency (0.3Hz) of the respiratory signal. In other words, the increased sidebands representing an increase in the OA of

respiratory signal can probably be distinguished from that representing an increase in the OA of the neural activities. Therefore, through the analysis of the sidebands, the PSD of the ECG and PPG trains can also be used as a measure of the HRV to identify certain variations in neural control or the respiratory effect.

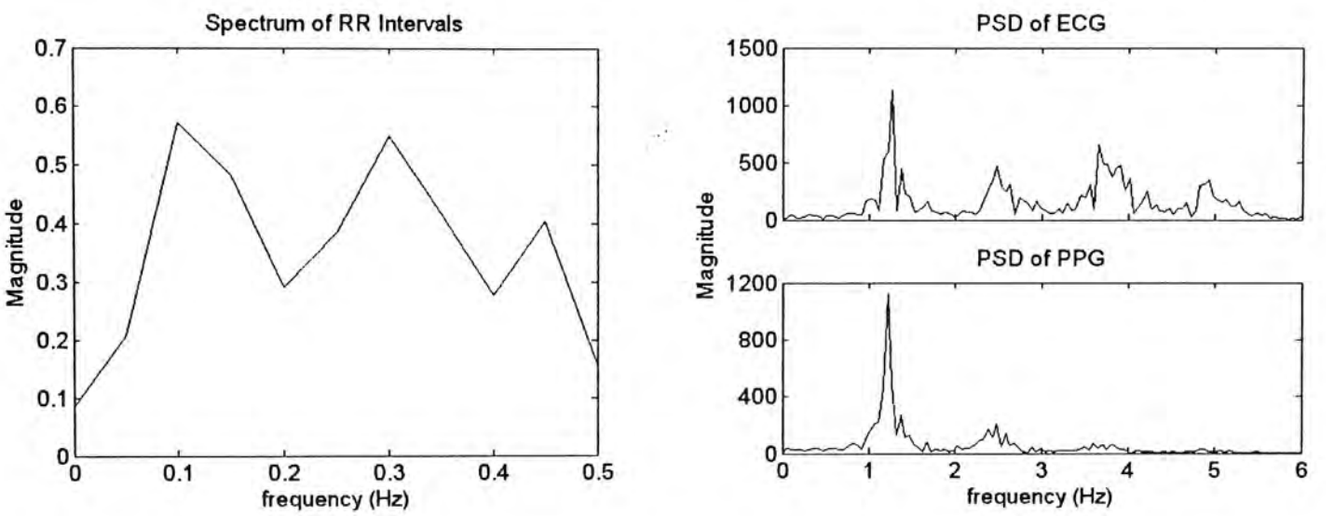

(a) (b)

Fig. 3-20: PSD of a) Heart beat intervals and b) ECG and PPG trains when the MD is increased ($MD = 20.0\%$) by changing the OA of the parasympathetic signal.

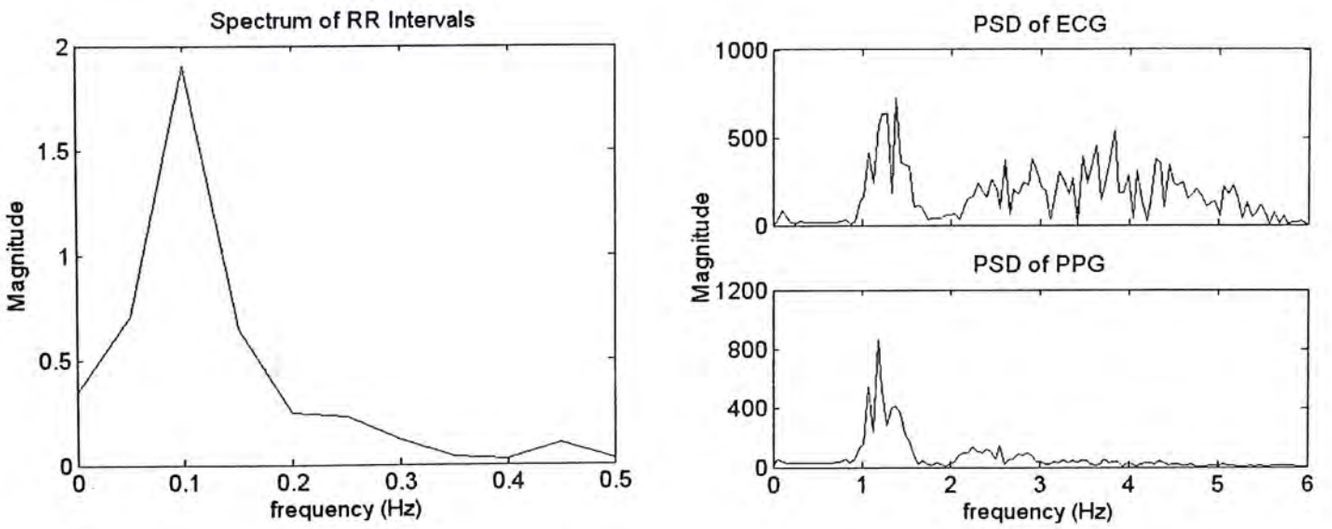

(a) (b)

Fig. 3-21: PSD of a) Heart beat intervals and b) ECG and PPG trains when the MD is increased ($MD = 20.0\%$) by changing the OA of the sympathetic signal.

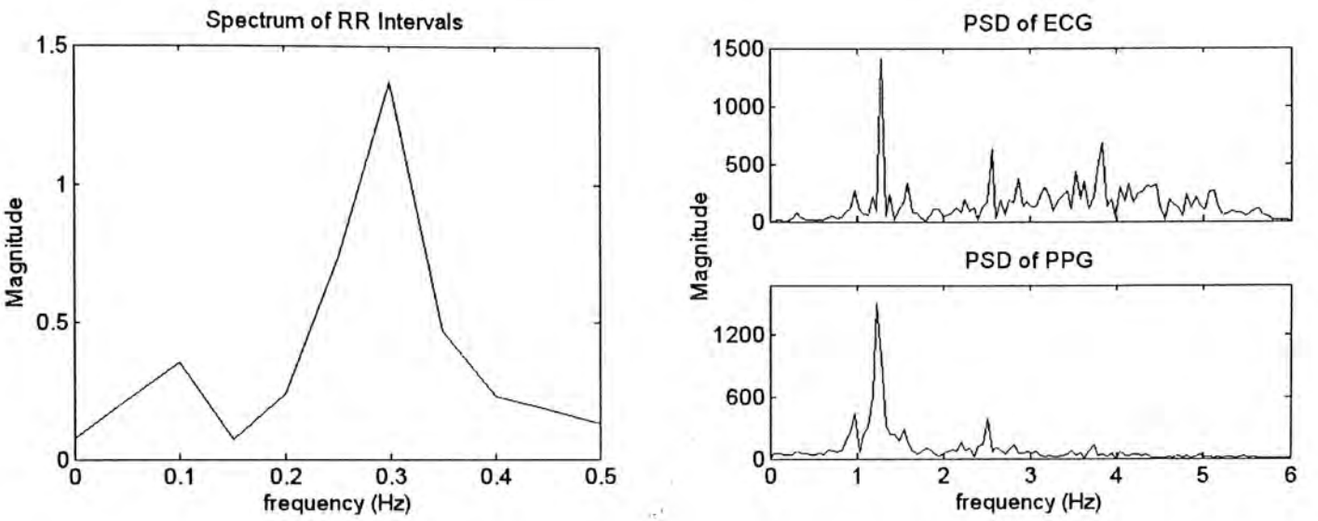

(a) (b)

Fig. 3-22: PSD of a) Heart beat intervals and b) ECG and PPG trains when the MD is increased ($MD = 20.0\%$) by changing the OA of the respiratory signal.

The above results from the simulation using the new model are found to be realistic. Fig. 3-23 illustrates the experimental data recorded at different periods with different magnitudes of the LF component from the same subject. It is clear that when there is a significant increase in the magnitude of the LF component, the power of sidebands in the spectra of both ECG and PPG signals increases substantially, while these sidebands are almost indiscernible as shown in Fig. 3-23 (b). The sharp peaks of the sidebands, though not isolated ideally from the mean heart rate and its multiples, can still be identified clearly. Therefore, these peaks are likely to be used as an indicator of the increase in the LF neural activities.

This can be further demonstrated by the data from a second healthy resting subject In Fig. 3-24(a) and (b), both the LF and HF components are strong, thus the sidebands corresponding to these two components can be identified. In Fig. 3-24 (c) and (d), the HF component becomes dominant. As a result, the sidebands corresponding to the LF component becomes almost indiscernible, while that

corresponding to the HF component can be identified more easily. Hence, the spectra of the ECG and PPG trains can be useful to some extent in reflecting the relationship between the LF and HF components of the HRV, or even in determining the levels of autonomic neural activities and the strength of respiration.

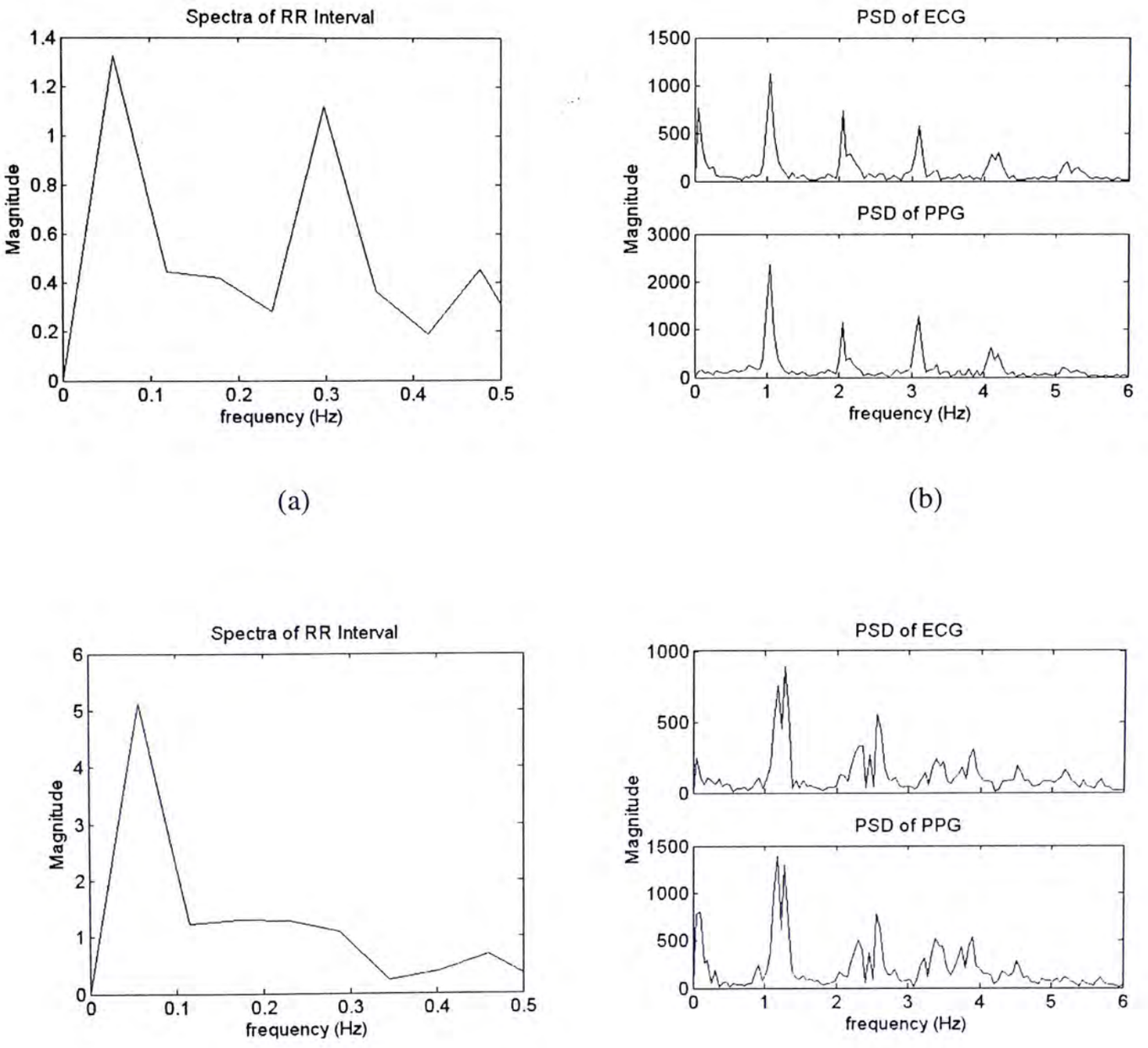

Fig. 3-23: The spectra of the RR interval, ECG and PPG trains from a healthy resting subject (a) and b) the LF component is not strong; c) and d) the LF component is dominant.

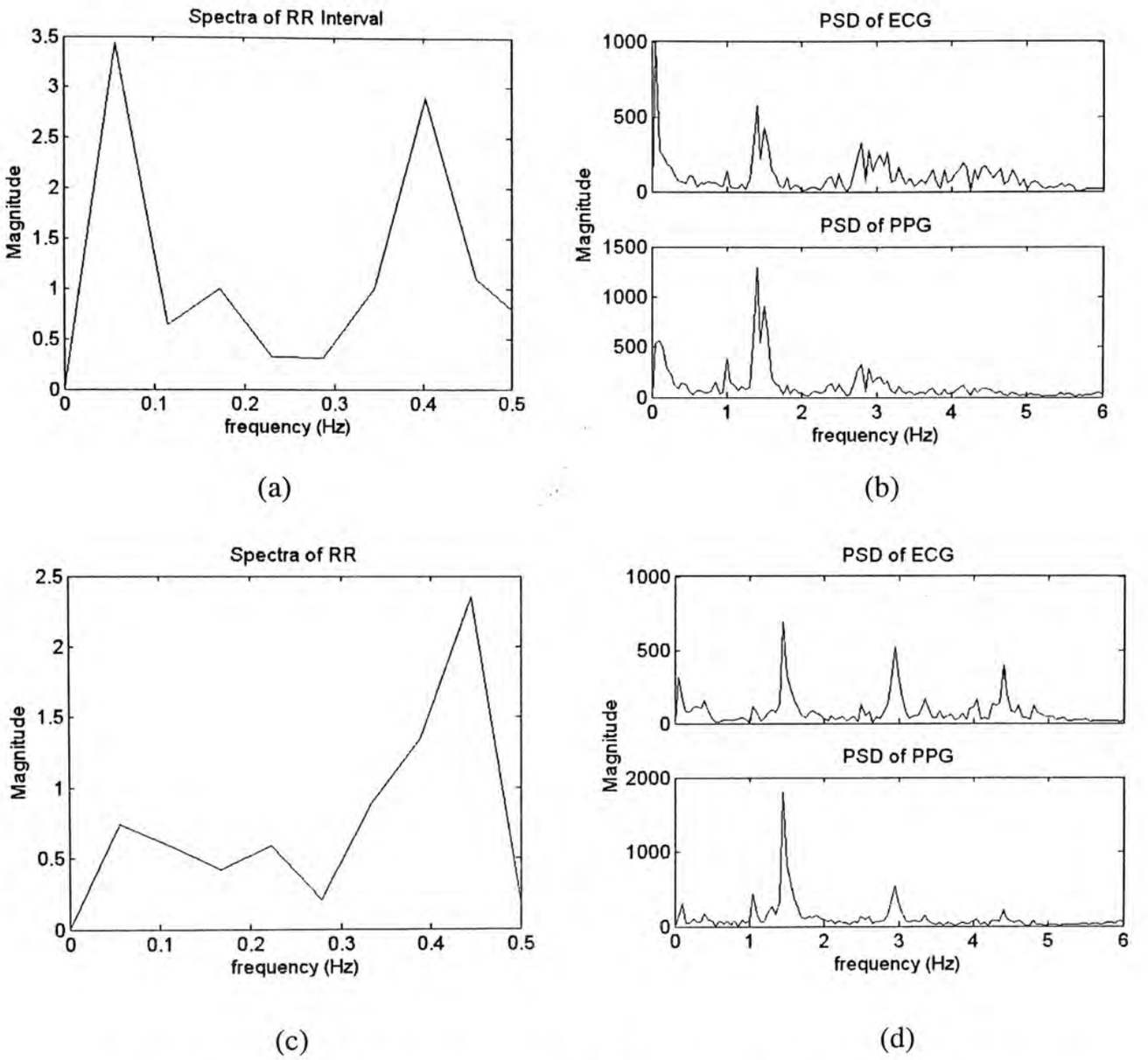

Fig. 3-24: The spectra of the RR interval, ECG and PPG trains from another healthy resting subject (a) and b) both the LF and HF components are strong; c) and d) the HF component is dominant.

3.4.4 Effects of the Mean Autonomic Tone on the HRV

The variation in RR intervals is not only caused by the fluctuation in the modulation depth of the input autonomic and respiratory signals, but is also influenced by the mean autonomic tone [56], [57]. In this study, different mean autonomic tones were applied by changing the parameter k_0, the intrinsic rate of the rise of the SA node cell potential, to investigate the responses of the proposed model. Table 3-4 shows simulation results of the mean and standard deviation of RR intervals under different

mean autonomic tones, while the threshold and other parameters are fixed. The mean heartbeat intervals are within the range that is physiologically plausible. The results indicate that an increase in the mean autonomic tone causes a remarkable decrease in both the mean and SD of heartbeat intervals. It can be observed that the relationship between either the mean autonomic tone and mean RR interval or the mean autonomic tone and the SD of RR intervals is almost exponential, as illustrated in Fig. 3-25 (a) and (b) respectively. For different thresholds, similar relationships are observed. The decreases in both the mean and SD of heartbeat intervals are more abrupt at smaller mean autonomic tones.

Table 3-4: Mean and SD of RR intervals for different mean autonomic tones.

k_0 (spikes/s)	Mean RR interval (ms)	SD of RR intervals (ms)	V_{th}
0.6	1007	33.0	0.6
0.8	753	18.8	
1	602	12.9	
1.2	502	8.5	
1.4	430	6.4	
1.6	376	5.1	
0.6	1342	44.2	0.8
0.8	1005	24.9	
1	803	15.9	
1.2	669	11	
1.4	573	8.2	
1.6	501	6.3	

0.6	1678	49.6	1.0
0.8	1256	31.0	
1	1004	19.9	
1.2	836	13.7	
1.4	717	10.3	
1.6	627	7.8	

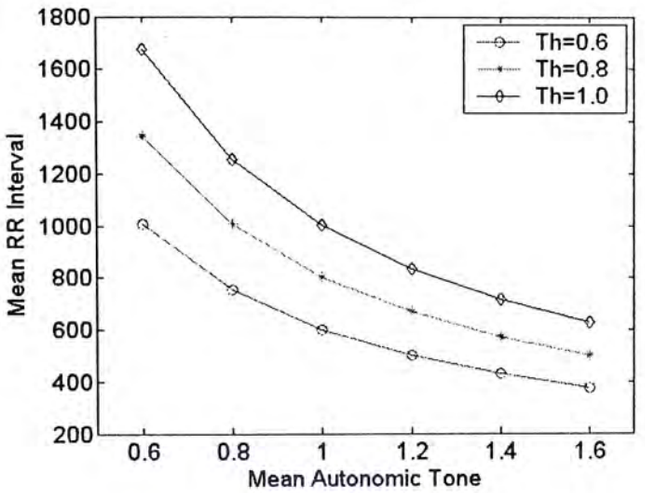

(a)

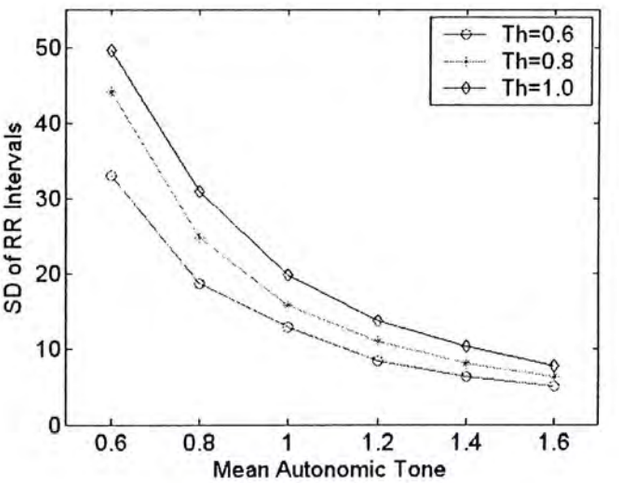

(b)

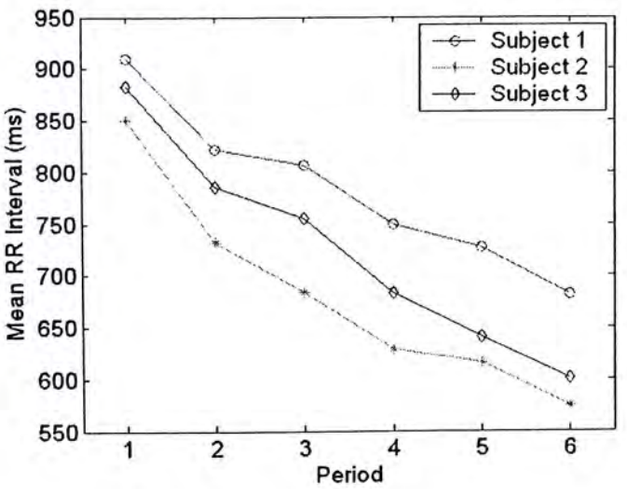

(c)

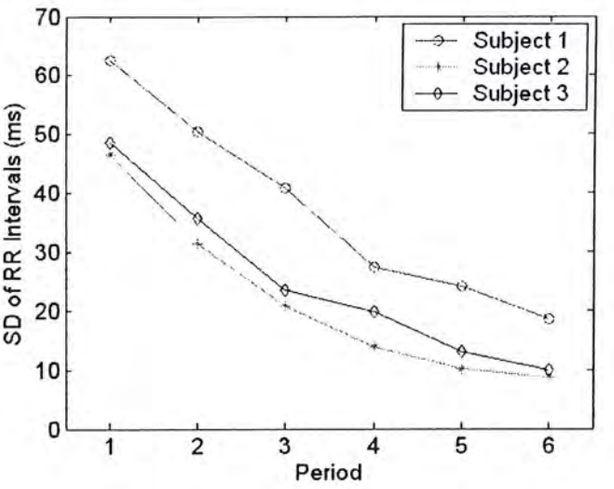

(d)

Fig. 3-25: a) and b) The simulated data from the proposed model; and c) and d) The experimental data from healthy subjects during the recovery period after exercise.

Fig. 3-25 (c) and (d) illustrate the experimental data from three healthy subjects. The data were recorded sequentially from stage 6 to stage 1 during the recovery period after running exercise. Each recording lasted for about 20 seconds, and the interval between each two consecutive recordings was within 5 minutes. The mean and SD of RR intervals were calculated for each recording to represent the physiological status at different stages with different mean autonomic tones. Though the knowledge of the threshold within each subject is not available, it is physiologically plausible to assume that different subjects have different thresholds. In this sense, these experimental data can be used as references to validate the simulation results from the proposed model. It is clear that similar relationships can be observed in the experimental data, therefore validating the results of the model.

3.5 Discussion & Conclusions

The PPG signal has attracted great interest in recent years. This is not only attributed to the remarkable convenience of the PPG technique, but also the abundance in useful information the signal contains for various clinical applications. Few literatures, however, have made it clear about the underlying principle of the PPG technique. To better understand this signal and to make better use of it, the fundamental mechanism of PPG is clarified in the first part of this chapter using the principles of fluid mechanics with the characteristics of the cardiovascular system and the arterial system. The actual source of PPG signals could be complex, probably including scattering, reflection, absorption and movement of the vessel wall, etc. Nevertheless, the most valuable information the PPG signal carries is the pulsation of the arterial blood flow caused by pressure gradient with each pressure pulse initiated at the onset of a cardiac cycle. Such understanding could provide insight into mathematical modeling of the PPG signals, which is still a blank in

current modeling work.

With the knowledge of the relationship between the pressure wave and flow pulsation in biological systems, the elementary principle for the generation of the PPG signal can be described by the combination of a conventional IPFM model and a WK3 model, together with a pulse generator and two time delay generators (the time delay caused by PEP and the transmission of the pressure wave through arterial tree). In this way, this new model is able to capture certain characteristics of the cardiovascular system and to describe certain transmission properties of the pulse wave through arterial system. It therefore transforms a continuous input signal into event series representing ECG and PPG signals. The model is tested by comparing the spectra from the simulation results with that of the experimental data from healthy resting subjects. It is found that though under certain simplifications, the model does correctly present a number of important features of the PPG signal. First, the repetition of PPG pulses is exactly the same as that of ECG signals over the same cardiac cycles. Second, with the pulse generator and WK3 model, the new model is able to render some changes in the pulse contour which are in accordance to the reality as the pulse wave traveling down the arterial system. Furthermore, the relationship between ECG and PPG signals is also appropriately interpreted with a certain time delay between the R peak of the ECG signal and the onset of a PPG pulse.

Through spectral analysis, it is found that the new model can appropriately capture the features in the PSD of ECG and PPG signals. The first sharp peak, located at the meant heart rate in both spectra, represents the same repetition rate of the signal under the same autonomic control. The harmonics located at the multiples of the mean heart rate in both spectra, however, have amplitudes that decay much faster in the PSD of PPG signals than that in the PSD of ECG signals. This is due to

the difference in the PSD of individual pulse dynamics of ECG and PPG signals. The PSD of ECG complex contains more high frequency components, while the PSD of PPG pulse has components mainly centered at the mean heart rate. It is therefore concluded that although the generation of ECG complex and PPG pulse is to some extent simplified in the proposed model, it nevertheless maintains the most important characteristics in both spectra of ECG and PPG trains.

The relationship between the input signal and the output heartbeat intervals is also studied. The information of the heartbeat interval is carried by both the ECG signal and the PPG signal. It is found that the modulation depth and the mean value in the fluctuant input signal are two important quantities that have an effect on HRV. When there is an increase in the modulation depth induced by perturbation of sympathetic activity, the oscillation amplitude of the heartbeat interval increases, and vice versa. This can also be reflected by an increase in the spectral power of the HRV that is corresponding to the sympathetic activity. Similar results are observed by the perturbation in parasympathetic or respiratory signals. However, it is interested to note that compared with parasympathetic and respiratory signals, sympathetic activity could have a more distinguished influence on the HRV. In other words, an abrupt change in heartbeat intervals is most probably due to the increased sympathetic nervous activity. This result may therefore have considerable diagnostic value. The effect of mean autonomic tone on the HRV is also significant. The results in this study are consistent with those from other studies [10], [58] and our own experimental data, i.e., both the heartbeat interval and HRV fall with the increasing of the mean values of the input signal. This result can be useful in explaining phenomena under some physiological and pharmacological conditions.

The changes in the input modulating signals could also affect the spectra of ECG and PPG trains. The increase in the OA of each input modulating signal would cause

an increase in the corresponding sidebands of the mean heart rate and its multiples. With the same level of the MD, the increase in the power of the sidebands caused by the sympathetic input is much more significant than the increase due to the parasympathetic or respiratory input. This is consistent with the results that the sympathetic signal plays a more dominant role in controlling the time domain HRV. It is more interested to note that the increase in sidebands corresponding to an increase in the OA of the respiratory signal can possibly be isolated from the increase in both mean heart rate and sidebands caused by neural (sympathetic or parasympathetic) activity. These results are found to be in accordance with the experimental data from healthy resting subjects. It is therefore concluded that the spectra of ECG and PPG trains may serve as an alternative to evaluate the HRV by analyzing the power of the sidebands.

Based on the structure of the proposed new model, it is necessary to further explore the details of the pressure waveform that are associated with the beat-to-beat hemo-dynamic information. It is generally asserted that the pressure contour is a valuable indicator of the information on arterial BP. Considering the relationship between the heart rate and BP, the pulse generator in the current model could possibly be improved more realistically to carry dynamic information of BP and some timing intervals. It should also be pointed out that in fact, the time delay between the occurrences of the proximal and peripheral pressure waves, the PTT, varies with each cardiac cycle rather than being a constant. This is reflected by the discrepancy in phase between the simulated spectra and the spectra of experimental data from a normal subject. Though the variation in PTT is quite small ($\frac{s\tan dard\ deviation}{mean} \approx 2 \sim 3\%$), it is indeed an index of the properties of the arterial elasticity [37]. It is also of great potential for non-invasive estimation of the

arterial BP, as reported by several recent studies [36] [38]. A number of factors could affect PTT, or the pulse transmission velocity, such as the elastic modulus of the arterial wall, the thickness of the wall, the lumen radius, and the density of blood, etc. Further investigations on the interactions between these factors together with the characteristics of the arterial system may eventually clarify the mathematical derivation of pulse transmission velocity, and therefore PTT. Therefore, the time delay generator in the current model could also be better modified to generate of the time varying PTT.

Chapter 4

A Correlation Study on the Beat-to-Beat Features of Photoplethysmographic Signals

4.1 Introduction

Based on the principle of the PPG technique, it is found that fluctuations in the value of the PPG signal are similar to that in some of the physiologic parameters of cardiovascular systems. It is believed that the PPG can provide useful information on the beats of the aortic origin, the characteristics of the vascular system, the properties of the peripheral vessels, the state of the blood flow, etc. [35]. It has also been reported in several literatures that the PTT assessed by the time delay between the characteristic points on ECG and PPG signals could be used for non-invasive estimation of arterial BP [36] [38] .

Undoubtedly, it is worthwhile to investigate systematically certain characteristics on the PPG waveform for the evaluation of clinically useful physiologic parameters. In spite of its simple waveform, the timing intervals, such as those reflecting the rising or falling phases, of the PPG signal could contain important information that is corresponding respectively to the periods of systole and diastole [23] [26]. The variations in the systolic or diastolic portions of the pressure wave, as well as that in PTT, may be to some extent correlated with the time-varying properties of the vascular and peripheral systems, as suggested by the Windkessel model.

In this chapter, we investigate whether the beat-to-beat parameters extracted from the waveform of PPG are correlated with each other, and how these parameters are associated with the properties of cardiovascular or arterial systems. Specifically,

the correlation coefficient was calculated as an indicator of to what extent one parameter is associated with another from the statistical point of view.

4.2 Methodology

In order to study comprehensively the relationship between PPG related parameters and their association with the parameters from ECG signals such as RR interval, different experimental conditions were taken into account. These conditions might induce certain variations in the properties of cardiovascular or arterial systems, or in the physiological status of the subjects.

4.2.1 Experimental Conditions

Data used in this study were obtained from experiments previously carried out in our laboratory [59] [60]. All the subjects participated in this study were healthy, aged 22-30, and were asked to rest for 5 min before the measurement (except for the dynamic situation), and sat still on a comfortable chair throughout the whole period of data recording [59] [60].

The PPG sensor used in the experiment was of reflective type, consisting of a LED and a photo-detector. This PPG sensor also included a thin film force sensor (Flexiforce pressure sensor PS-01, American) and a temperature sensor (LM35CAH, National semiconductor, Japan), which were used to monitor continuously the contacting force signal and the local skin finger temperature. The ECG signal was recorded by the Model 7400 - Physiological Recorder with three electrodes on the left arm, right arm and right leg, respectively. A treadmill (model C956, Precor) was also used in the study of the dynamic state. The PPG signal at the right index finger tip and the ECG signal as well as the contacting force and the finger temperature were recorded simultaneously under the following different experimental conditions:

1) At Normal Relaxed State: Data were obtained from 10 subjects. Subjects were under normal relaxed state, with normal strength of contacting force applied on the sensor. Subjects remained relaxed throughout the whole period of data recording, which lasted for about 5 minutes.

2) *At Different Levels of Contacting Force:* Data were obtained from 30 subjects, and were recorded over a range of different contacting forces applied on the sensor. To start with, each subject was asked to put their fingertip naturally on the PPG sensor without consciously exerting contacting force, and signals were recorded for about 15 seconds. In the successive recordings, subjects were instructed to exert different levels of contacting force on the PPG sensor with the index finger tip. The signal recordings were obtained over a range of contacting force varying from 0.1N to 1.2N, and each of the recordings lasted for about 15 seconds [59].

3) *At Different Levels of Local Skin Finger Temperatures:* Data were obtained from 15 subjects, and were recorded over a range of different local skin finger temperatures. Before data recording, a cold pressor test was preformed by asking the subject to immerse his/her right index finger into water of 18°C for 1 minute. Immediately after the finger was taken out, data were continuously recorded until the finger temperature recovered to the natural state. Each of the recordings lasted for about 10 minutes [60].

4) *At Dynamic State:* Data were obtained from 15 subjects. Each subject took part in a 4-minute's running exercise with a uniform speed of 8kph. The slope of the treadmill was set to zero. Immediately after exercise, three trials of data recording were conducted on each subject, and each of the recordings lasted for about 1 minute. The time period between each two successive recordings was within one minute.

4.2.2 Definition of the Parameters

A set of parameters were defined on the PPG waveform as shown in Fig. 4-1 (a).

Point F is defined as the foot of PPG waveform, corresponding to the onset of the systolic phase or the end of the diastole phase [26]. Point Y is defined as the peak of PPG waveform. Point W is the first turning point encountered during the descending phase of PPG waveform if such a point exists; otherwise it is regarded as the point with amplitude 50% of the FY amplitude. Point G can be the last turning point after which the slope (absolute value) remains below 0.1 until the next F point of consecutive PPG pulse (or it can be the point with amplitude 5% of the FY amplitude).

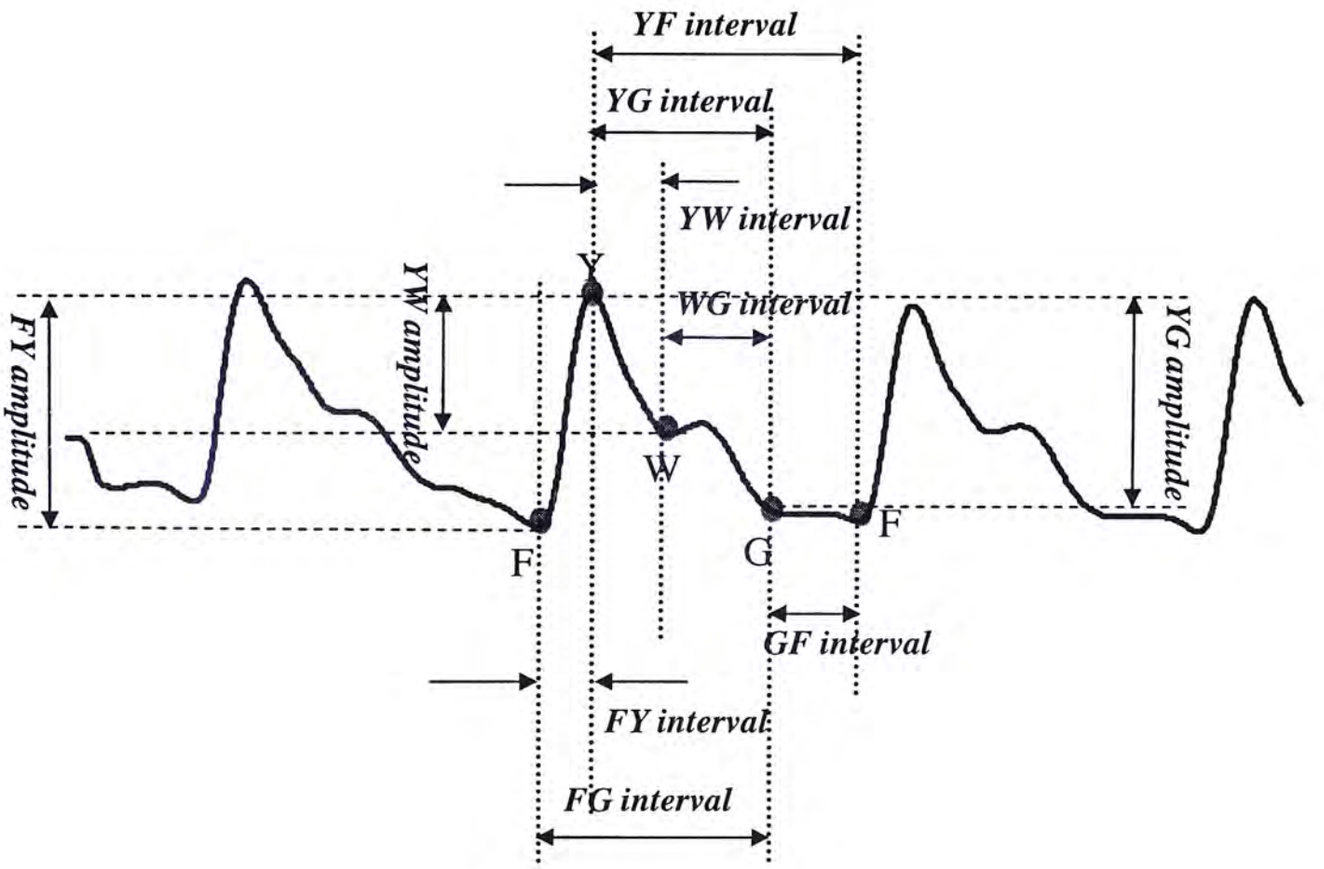

(a)

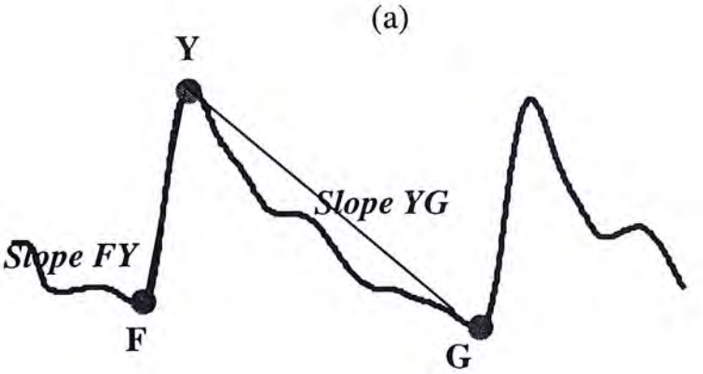

(b)

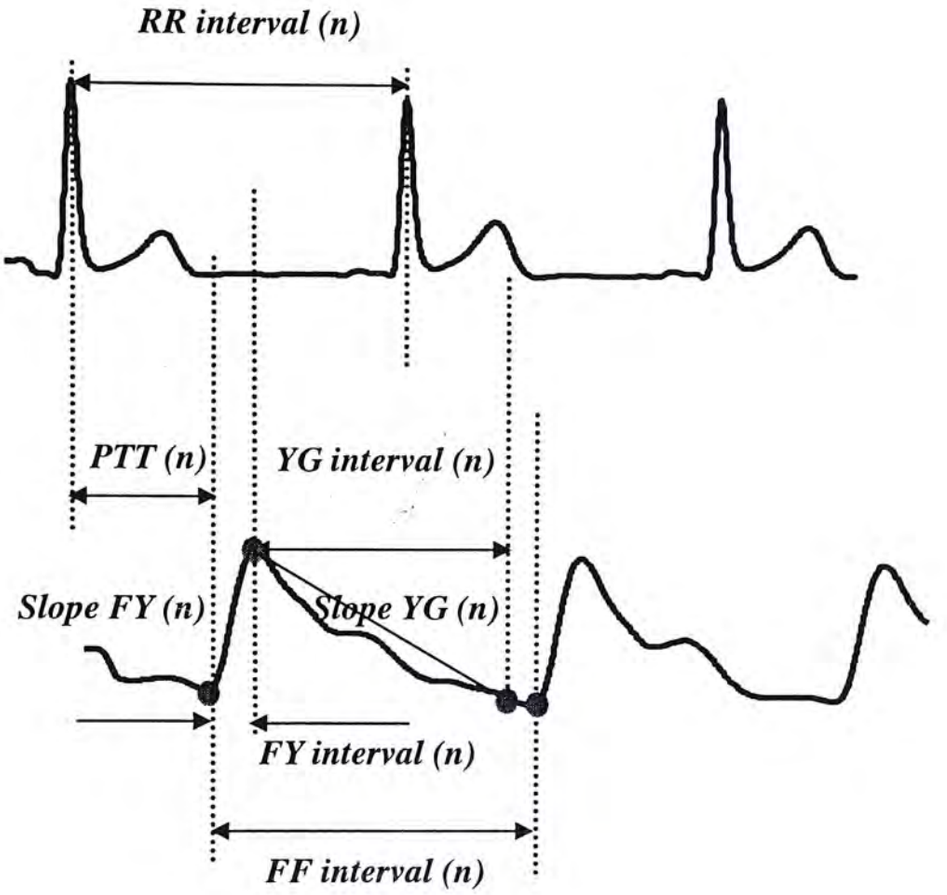

(c)

Fig. 4-1: Definitions of the PPG related parameters.

In this way, a number of parameters can be generated from the PPG waveform, such as FY interval, YG interval, FF interval, etc. Particularly, as shown the Fig. 4-1 (b) slope FY is defined as FY amplitude/FY interval, and slope YG is defined as YG amplitude/YG interval. This study was focused mainly on the FY interval, the YG interval, the FF interval, the slope FY and the slope YG. The PTT was assessed by the time delay between the R-peak of ECG and the F point of PPG. The RR interval is calculated from the time interval between two consecutive R peaks of ECG signal.

A set of seven parameters as indicated in Fig. 4-1(c) were obtained from 15-second segments for different experimental conditions. A correlation analysis was carried out to investigate the relationship between these beat-to-beat parameters. The

correlation coefficients between FY and RR intervals, YG and RR intervals, RR interval and PTT, FF and RR intervals, FY and YG intervals, FY interval and PTT, and YG interval and PTT were calculated for each level of contacting force, each level of finger temperature, the normal relaxed state and the dynamic state. Meanwhile, the correlation between slope FY and RR interval, slope YG and RR interval, slope FY and PTT, slope YG and PTT and slope FY and slope YG were also determined.

4.3 Data Analysis

In this section, the correlation coefficients between those PPG and ECG related parameters are calculated under different experimental conditions.

4.3.1 At Normal Relaxed State

Table 4-1 presents the correlation coefficients between the five timing intervals, FY interval, YG interval, FF interval, PTT and RR interval, under the normal relaxed state. As expected, the correlation coefficient between the FF interval of PPG and the RR interval of ECG is fairly high (0.981 ± 0.0146, $p<0.0001$) since the repetition of PPG pulses should be the same as that of ECG signals over the same cardiac cycles. Besides, a significantly high correlation was also found between the YG interval and the RR interval, of which the correlation coefficients range from 0.90 to 0.98 ($p<0.0001$). Meanwhile, PTT exhibits a moderate correlation with FY interval in some subjects. This table also indicates that some parameters may have no correlation with each other (see Table 4-1). If the absolute value of the correlation coefficient is less than 0.3, the correlation is considered negligible [26]. For example, there seems to be little correlation between RR and FY intervals, PTT and RR interval, PTT and YG interval, and FY and YG intervals.

Table 4-1: The correlation coefficients among the five timing intervals under normal relaxed state (SD represents for standard deviation).

Sub.	RR & YG	RR & FY	RR & FF	PTT & RR	PTT & FY	PTT & YG	FY & YG
1	0.912	0.493	0.987	-0.442	-0.422	-0.422	-0.484
2	0.904	0.454	0.980	-0.537	-0.698	-0.353	-0.087
3	0.981	0.430	0.996	-0.363	-0.365	-0.416	0.457
4	0.982	0.107	0.995	-0.226	-0.466	-0.682	0.702
5	0.983	0.233	0.990	-0.423	-0.831	-0.665	0.401
6	0.970	-0.039	0.981	-0.153	-0.543	-0.194	-0.317
7	0.967	0.106	0.966	-0.214	-0.650	-0.318	0.229
8	0.961	-0.027	0.947	0.235	-0.409	0.309	0.415
9	0.975	0.470	0.982	0.112	-0.498	0.002	-0.211
10	0.966	0.100	0.988	-0.054	-0.326	0.131	0.435
Mean	***0.960***	***0.233***	***0.981***	***-0.206***	***-0.521***	***-0.261***	***0.154***
SD	***0.028***	***0.211***	***0.015***	***0.249***	***0.161***	***0.326***	***0.398***

Table 4-2 gives the correlation coefficients between the timing intervals and the slope information. Slope FY seems to be highly inversely proportional to slope YG in most subjects. However, there is hardly any statistical relationship between PTT and slope FY, PTT and slope YG, RR interval and slope FY, and RR interval and slope YG.

Table 4-2: The correlation coefficients between the timing intervals and the slope information.

Sub.	PTT & Slope FY	PTT & Slope YG	RR & Slope FY	RR & Slope YG	Slope FY & Slope YG
1	-0.107	0.034	-0.268	0.202	-0.927

2	0.049	0.516	-0.095	-0.462	-0.607
3	-0.092	0.238	0.041	-0.092	-0.874
4	-0.186	-0.471	0.084	0.675	-0.522
5	-0.214	0.484	-0.138	-0.071	-0.860
6	-0.266	0.028	-0.248	0.206	-0.554
7	0.0353	0.081	-0.137	0.23	-0.890
8	-0.453	0.627	-0.489	0.486	-0.607
9	-0.317	0.387	-0.227	0.212	-0.520
10	0.345	0.014	-0.283	0.435	-0.724
Mean	***-0.121***	***0.194***	***-0.176***	***0.182***	***-0.708***
SD	***0.225***	***0.326***	***0.167***	***0.326***	***0.165***

4.3.2 At Different Levels of Contacting Force

Seven levels of contacting forces were recorded during the experiment. Table 4-3 gives the recorded forces with F1-F7 representing the seven different levels. As some subjects were not able to achieve all the seven force levels, the number of subjects at each force level is also given in Table 4-3.

It is generally know that the contacting force may affect the amplitude or other features on the pulse contour. The PPG signals of one subject at different levels of contacting force are illustrated in Fig. 4-2. Similarly to that under normal relaxed state, high correlations also exist between RR and YG intervals, and the values of those correlation coefficients do not have much variation with different force levels. Meanwhile, the overall correlations between RR and FY intervals, RR interval and PTT, PTT and YG interval, and FY and YG intervals are still insignificant at whatever force levels. The mean and SD of the correlation coefficients for the timing intervals

at each force level are given in Fig. 4-3.

Table 4-3: Mean and standard deviation of the seven force levels, and the number of subjects at each level.

	F1	F2	F3	F4	F5	F6	F7
Force (N) (Mean)	0.11	0.21	0.40	0.60	0.80	1.01	1.19
Force (N) (SD)	0.03	0.03	0.02	0.02	0.02	0.04	0.03
No. of Subjects	16	29	30	30	29	20	10

Unlike that under normal relaxed state, however, the correlation between PTT and FY interval becomes much more remarkable under relatively higher levels of contacting force, though the ranges of higher force to obtain the higher correlations may vary a little bit from person to person. It is clearly indicated by Fig. 4-3 that the correlation coefficient between PTT and FY interval goes up with the increasing of force levels, which can be as high as $r = -0.8384 \pm 0.0912$ ($p < 0.0001$) at the F7 level. The negative correlation coefficients between the PTT and the FY interval of PPG appears to imply that the transit time of PPG pulse along the peripheral system will decrease with the increase of FY interval which might be associated with cardiac dynamics or arterial BP.

Fig. 4-4 shows the mean and SD of correlation coefficients between the timing intervals and the slopes at different force levels. Similar to that between PTT and FY interval, the correlations between PTT and slope FY, PTT and slope YG, and slope FY and slope YG go up with the increasing of force levels. Therefore, at relatively higher levels of contacting force, there is a moderate correlation between PTT and slope FY, and PTT and slope YG; while slope FY and slope YG exhibit an even higher correlation (r reaches up to -0.76 at F7 level). On the contrary, there is still little correlation between RR and slope FY, and RR and slope YG at whatever force levels.

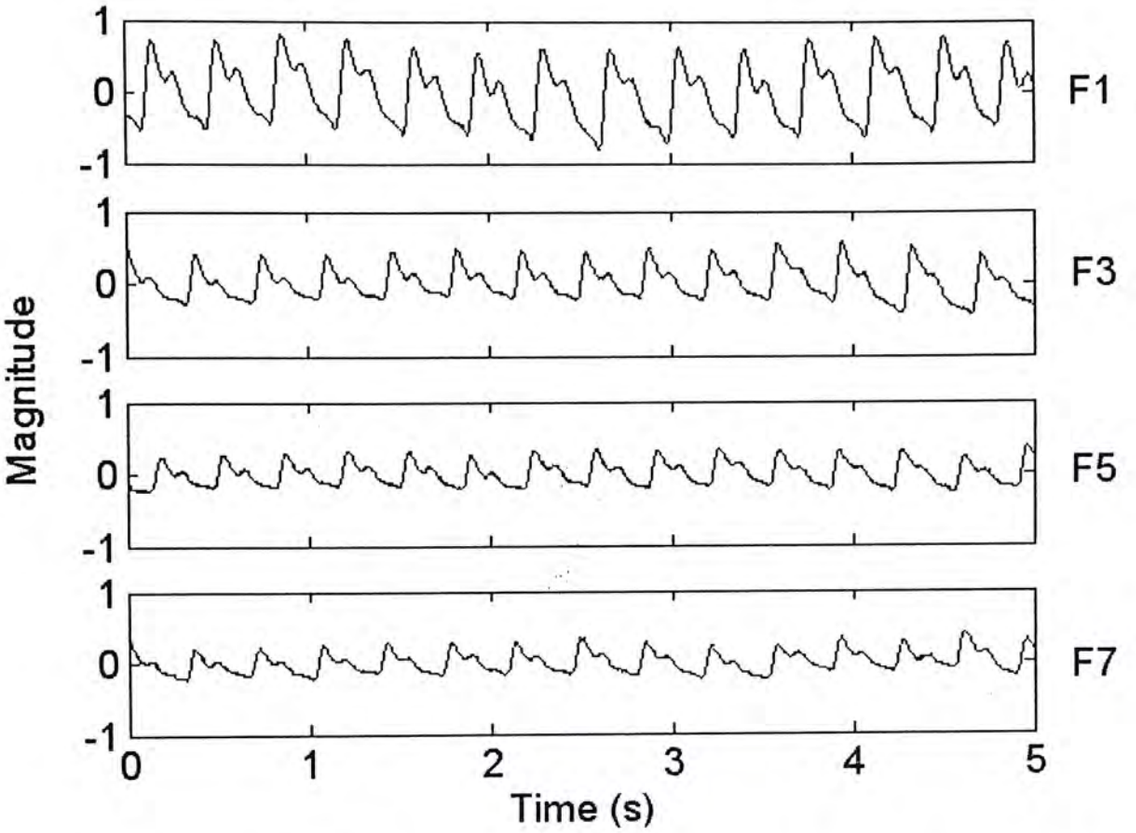

Fig. 4-2: PPG signals at different levels of contacting force from one subject.

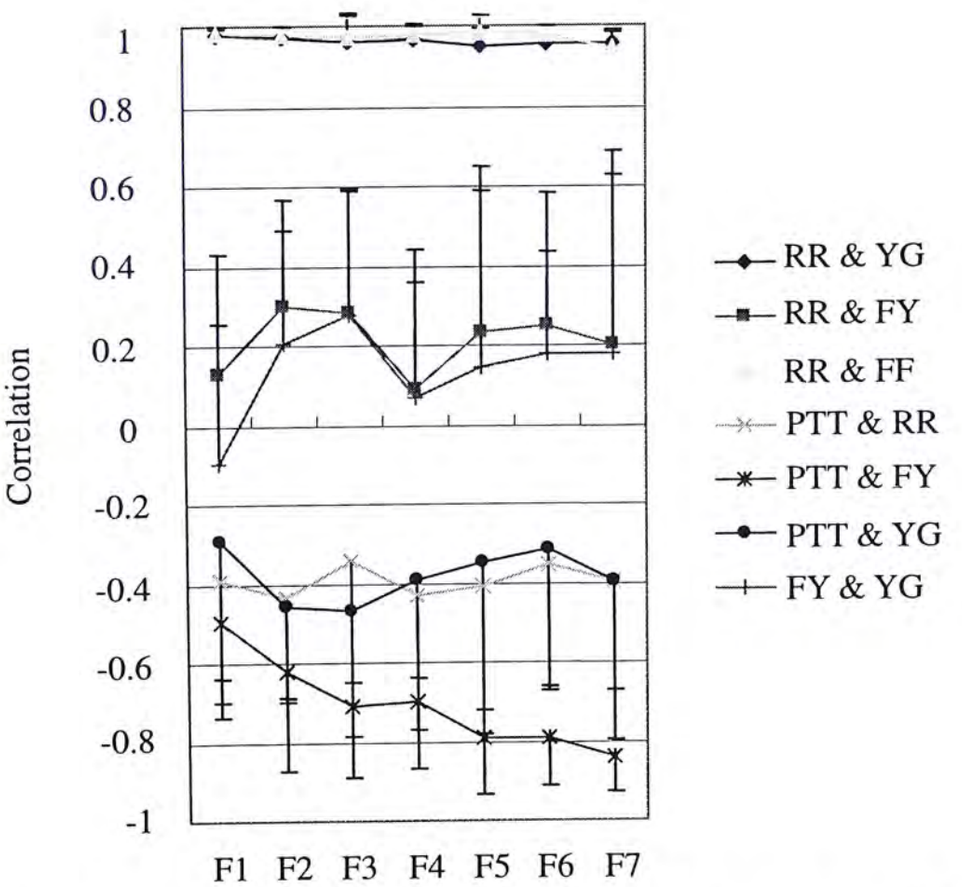

Fig. 4-3: The mean and SD of correlation coefficients for the timing intervals at different force levels.

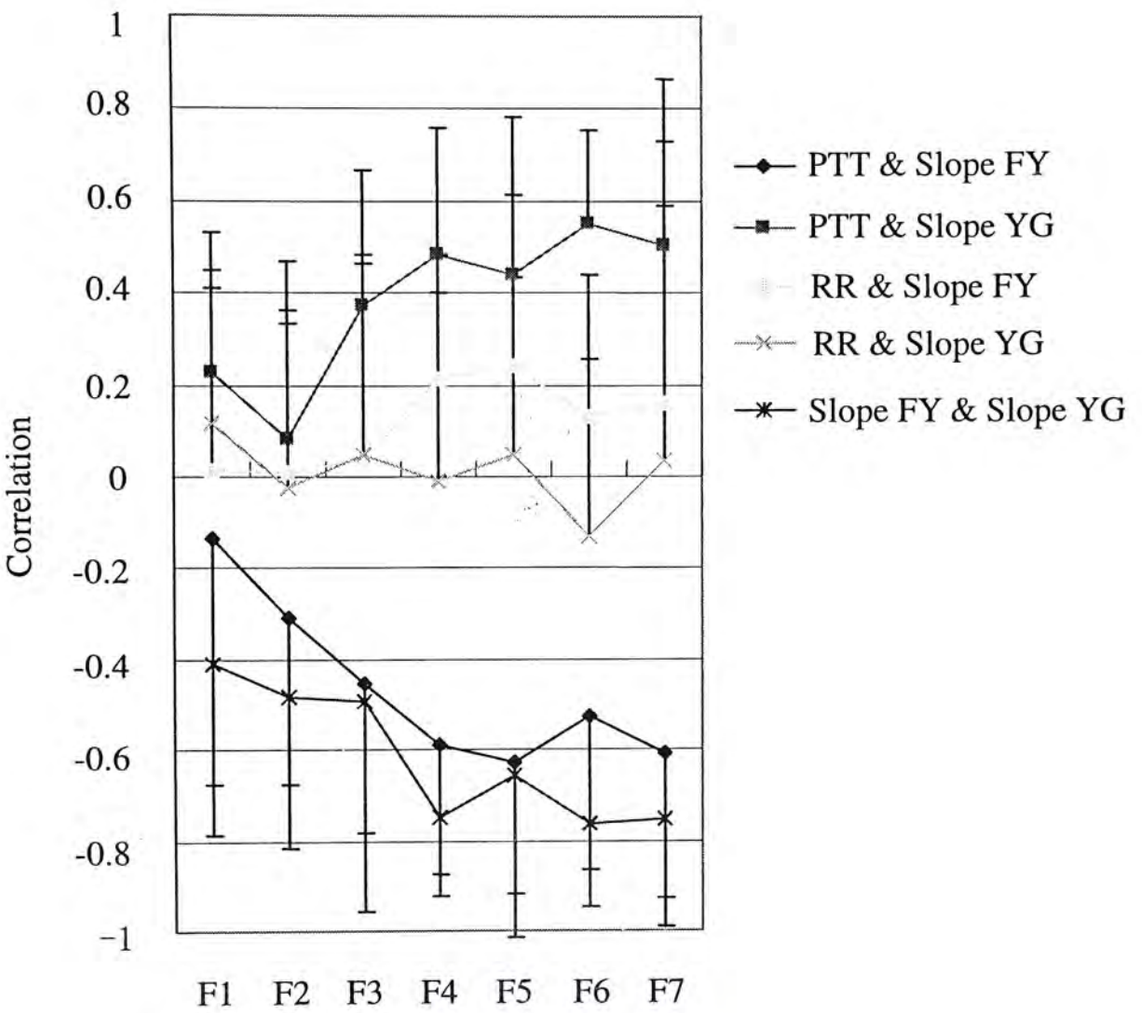

Fig. 4-4: The mean and SD of correlation coefficients between the timing intervals and the slopes at different force levels.

4.3.3 At Different Levels of Local Skin Finger Temperature

By performing the cold pressor test, a range of different local skin finger temperatures was achieved. Seven different temperatures were studied. Table 4-4 gives the detailed temperature values with T1-T7 representing the seven different levels, and the number of subjects at each temperature level as well. The temperature range (24-30°C) used in our study also have a effect on the amplitude of PPG signals, but is not so significant as the force effect, as illustrated in Fig. 4-5.

Table 4-4: Values of the seven temperature levels and the number of subjects at each level.

	T1	T2	T3	T4	T5	T6	T7
Temperature (± 0.5 °C)	24	25	26	27	28	29	30
No. of Subjects	11	12	15	14	14	14	13

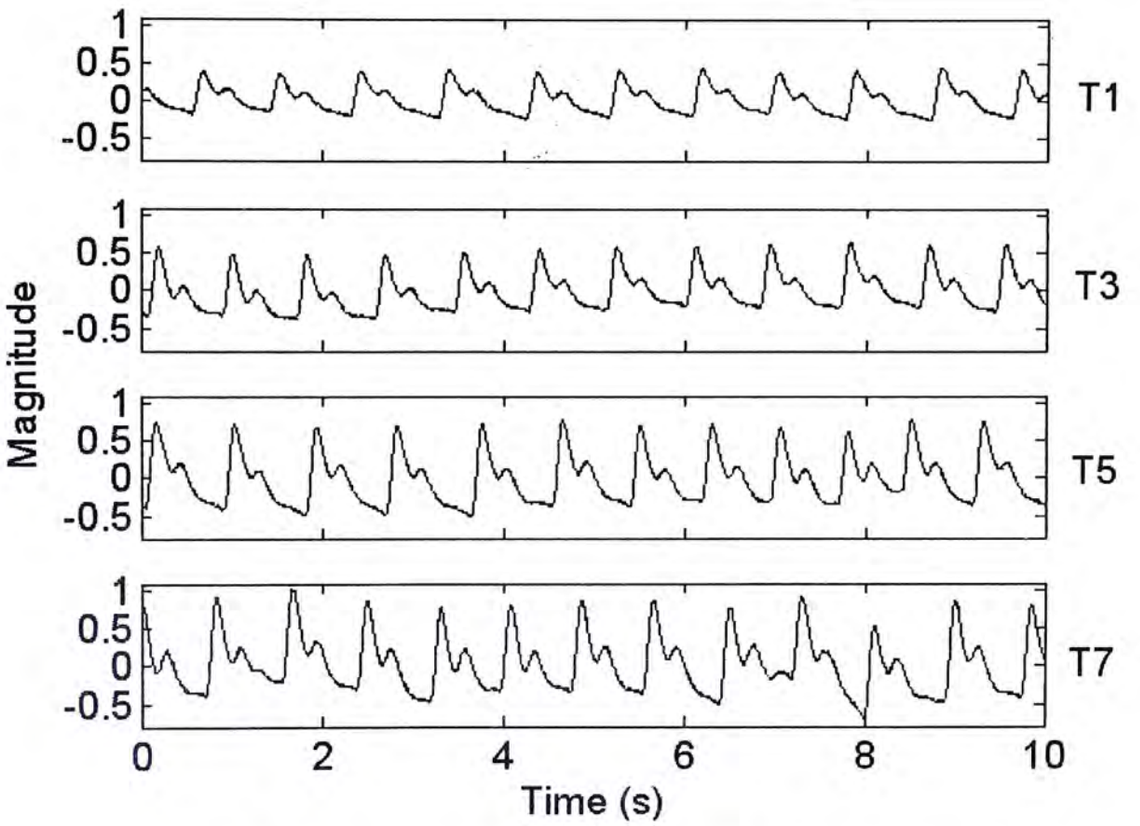

Fig. 4-5: PPG signals at different temperatures from one subject.

Fig. 4-6 shows the mean and SD of the correlation coefficients for the timing intervals at different temperature levels. There is consistently high correlation between RR and YG intervals, as well as that between RR and FF intervals at whatever temperature levels. PTT also exhibits a moderate correlation with FY interval, especially in levels from T3 to T6 ($|r| > 0.6$, $p < 0.0001$). On the other hand, the overall correlation between RR and FY intervals, RR interval and PTT, PTT and YG interval, and FY and YG intervals are still not significant, which also seem to be

independent of the temperature level. The mean and SD of correlation coefficients between the timing intervals and the slopes are given in Fig. 4-7. It seems that there is little correlation between these parameters at whatever temperature levels, except that slope FY exhibits moderate correlation with slope YG at certain temperatures.

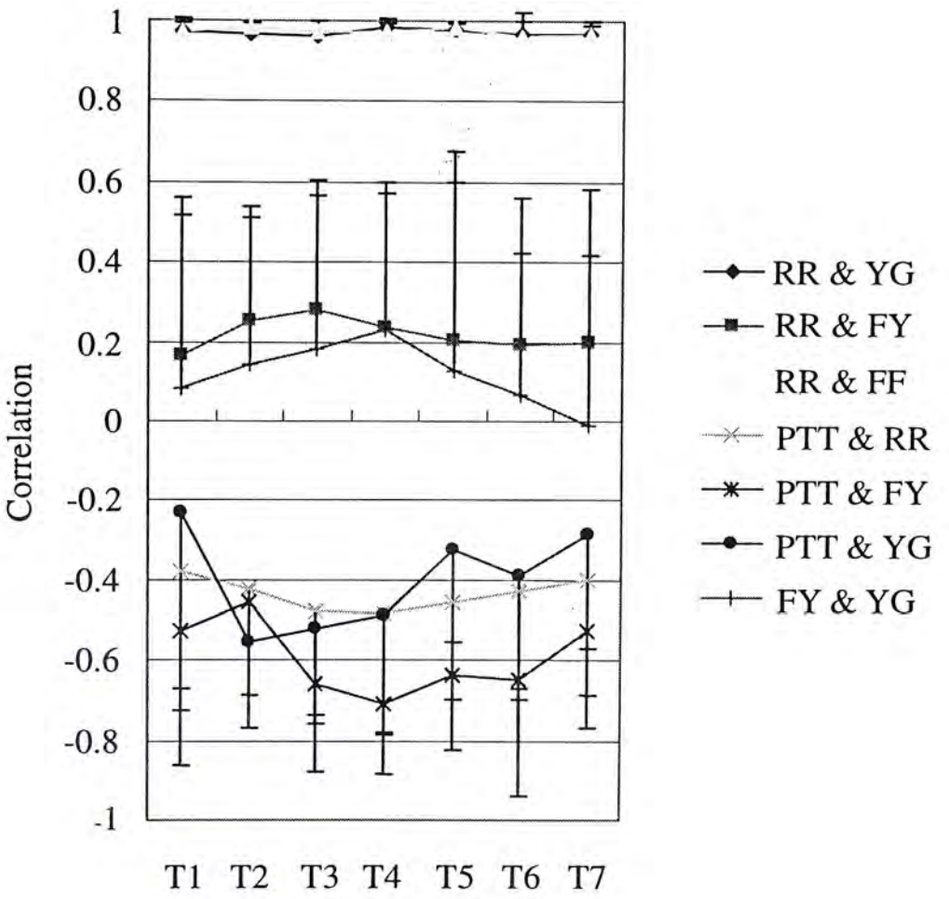

Fig. 4-6: The mean and SD of correlation coefficients for the timing intervals at different temperature levels.

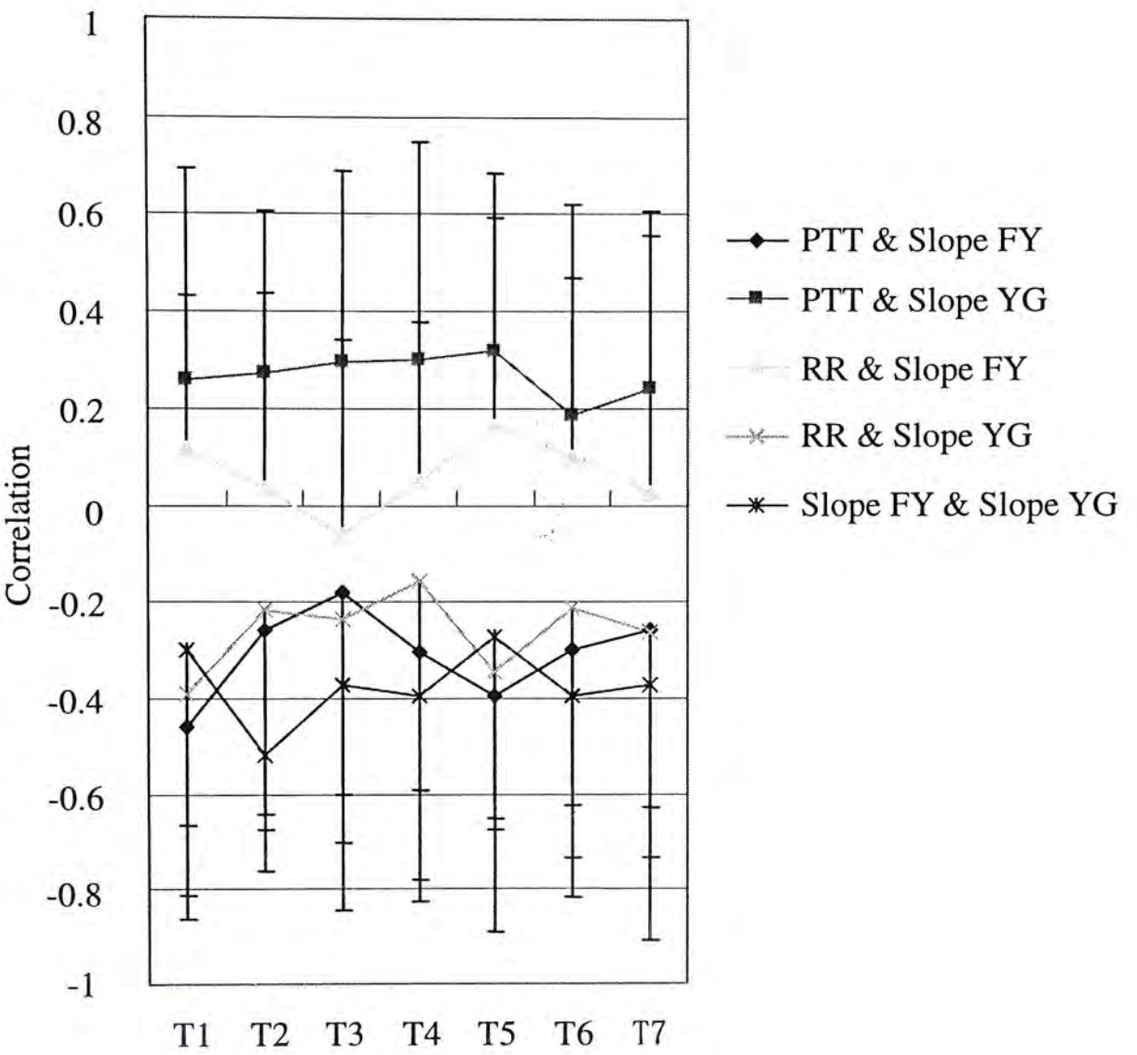

Fig. 4-7: The mean and SD of correlation coefficients between the timing intervals and the slopes at different temperature levels.

4.3.4 At Dynamic State

Three successive data recordings were obtained from each subject immediately after running exercise. As generally known, heart rate and some other physiological parameters, such as BP, etc., may have large fluctuations due to exercise. Thus, the three independent data recordings could be associated with quite different physiological statuses during the recovery period. As shown in Fig. 4-8, Period 1, Period 2 and Period 3 are corresponding to the three different trials of data recording, respectively. The mean and SD of the correlation coefficients for the timing intervals

at each period is also given.

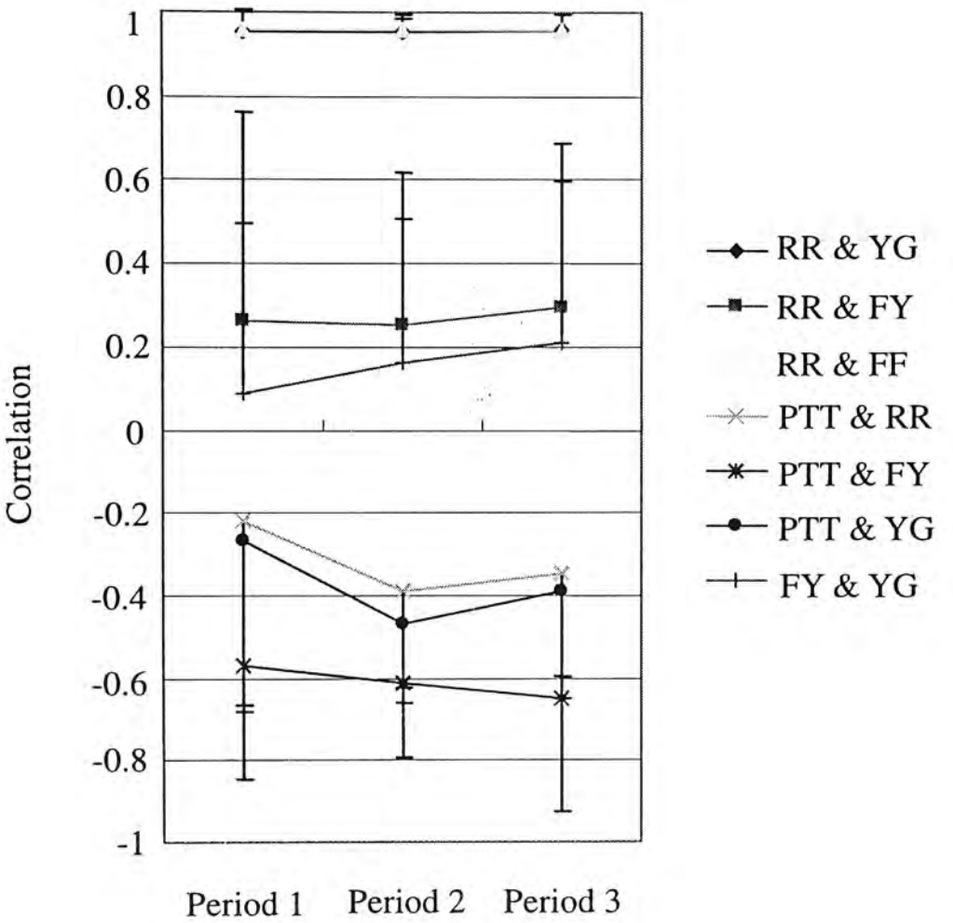

Fig. 4-8: The mean and SD of correlation coefficients for the timing intervals at different periods during the recovery period of exercise.

Besides the remarkable correlation between RR and YG intervals, PTT again exhibits a high correlation with FY interval, which is around $r = -0.6$, $p < 0.0001$. Meanwhile, the correlation between RR and FY intervals, RR interval and PTT, PTT and YG interval, and FY and YG intervals do not show much difference from that under other conditions.

As shown in Fig. 4-9, a relatively high correlation is still found between slope FY and slope YG in period 2 and period 3. These two periods were the latter stage during the recovery after exercise. In other words, this result is consistent with that at normal relaxed state.

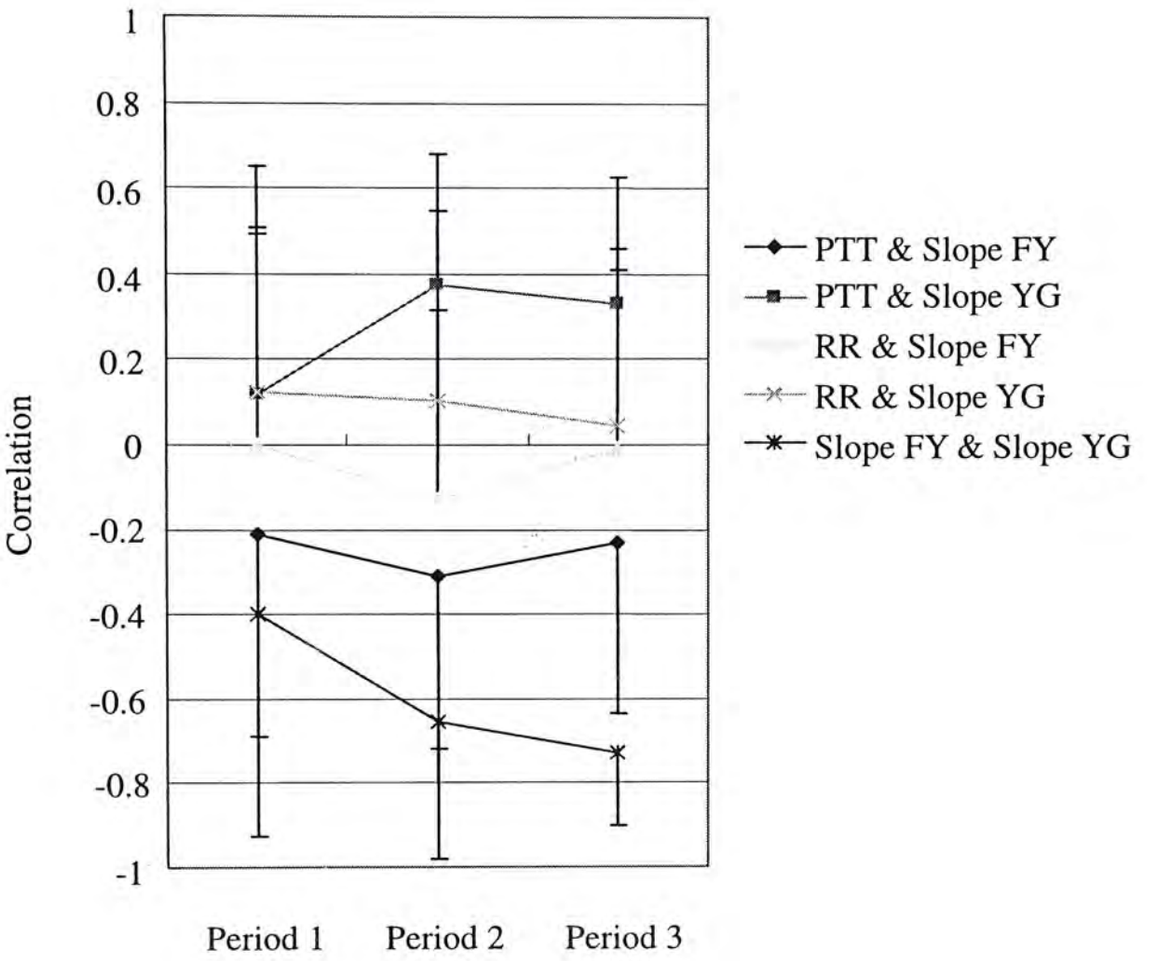

Fig. 4-9: The mean and SD of correlation coefficients between the timing intervals and the slopes at different periods during the recovery of exercise.

4.3.5 Repeatability Study

According to the results above, it is interesting to note that there is a statistical significant correlation between PTT and FY interval under certain conditions, especially at higher levels of contacting force. In order to further demonstrate this phenomenon, a repeatability test was conducted on 10 of the 30 subjects studied in section 4.3.2. This test was carried out several days after the first experiment and was under exactly the same experimental protocol, as described in section 4.2.1 (2). The number of subjects at each force level is given in Table 4-5.

Table 4-5: Mean and standard deviation of the seven force levels, and the number of subjects at each level in the repeatability test.

	F1	F2	F3	F4	F5	F6	F7
Force (N) (Mean)	0.10	0.21	0.39	0.60	0.80	1.01	1.19
Force (N) (SD)	0.02	0.01	0.02	0.01	0.02	0.02	0.03
No. of Subjects	10	10	10	9	7	6	3

The mean and SD of the correlation coefficients between PTT and FY interval at each force level are given in Fig. 4-10. The result is consistent with that in section 4.3.2: the correlation coefficient between PTT and FY interval goes up with the increasing of force levels. Thus, this phenomenon is further demonstrated to be true.

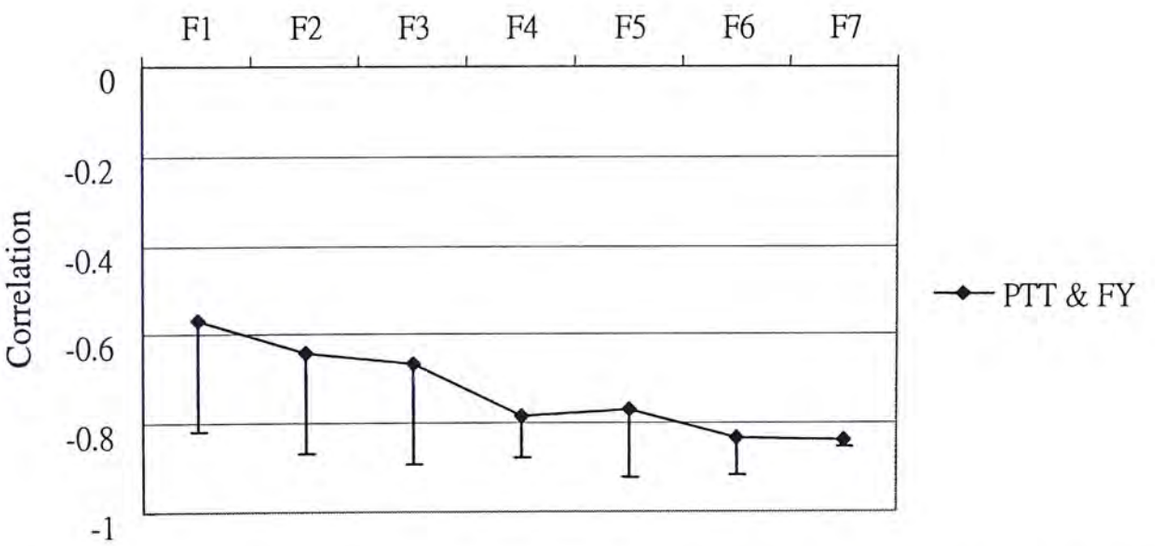

Fig. 4-10 Mean and SD of the correlation coefficients between PTT and FY interval at each force level in the repeatability test.

4.3.6 Spectral Analysis

To further understand the relationship between PTT and FY interval, it is also worthwhile to look into the individual spectra of PTT and FY interval.

Fig. 4-11 shows the spectra of PTT and FY interval from two different subjects

(a) and (b) at normal relaxed state. The spectra were calculated from 15-second data segments using FFT. The correlations between PTT and FY interval corresponding to (a) and (b) are almost negligible (for (a): $r = -0.148$, $p = 0.5215$; for (b): $r = -0.403$, $p = 0.1241$). It is clearly indicated by Fig. (5) that the dominant frequency components of PTT and FY interval appear at quite different frequency bands. For both (a) and (b), a remarkable component around 0.3Hz can be observed in the spectra of PTT; while in the spectra of FY interval, the main component is in the lower frequency range, between 0.04-0.15Hz. This may consequently lead to the insignificant correlation between PTT and FY interval.

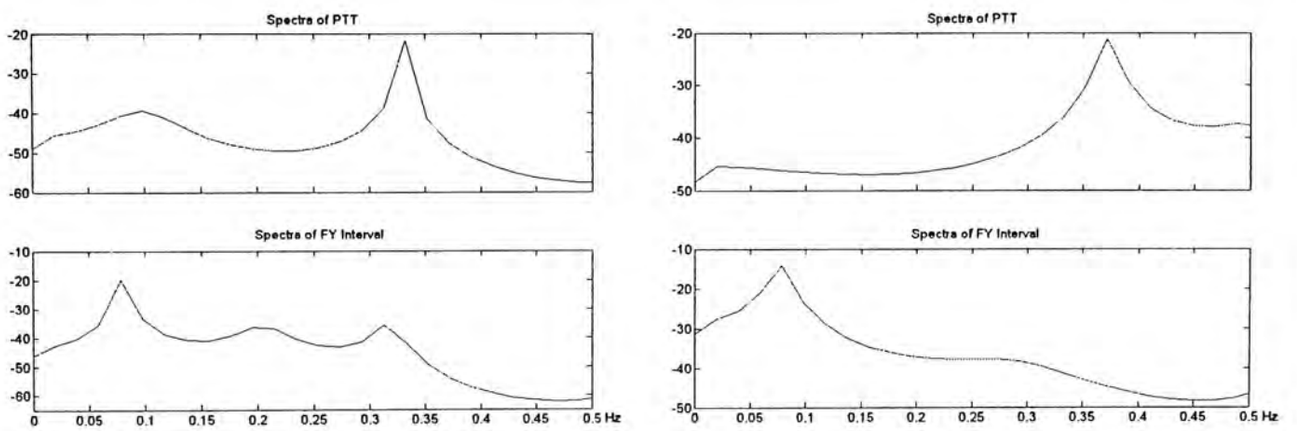

(a) (b)

Fig. 4-11: Spectra of PTT (upper panel) and FY interval (lower panel) from two subjects (a) and (b) at normal relaxed state.

Fig. 4-12 shows the spectra of PTT and FY interval from another two different subjects under relatively higher levels of contacting force. Under such a condition, as reported above, significant correlations exist between PTT and FY interval. For (a): $r = -0.930$, $p < 0.0001$; for (b): $r = -0.908$, $p < 0.0001$. Unlike that under normal relaxed state, the spectra of PTT exhibit a considerable increase in the low-frequency power, between 0.04-0.15Hz. The spectra of FY interval maintain the dominant

low-frequency component as that at normal relaxed state. As a result, the similarity between these two spectra can be observed in both (a) and (b). The significant correlation between these two time series indicates that the low-frequency component could be the key factor in determining the correlation between the time series.

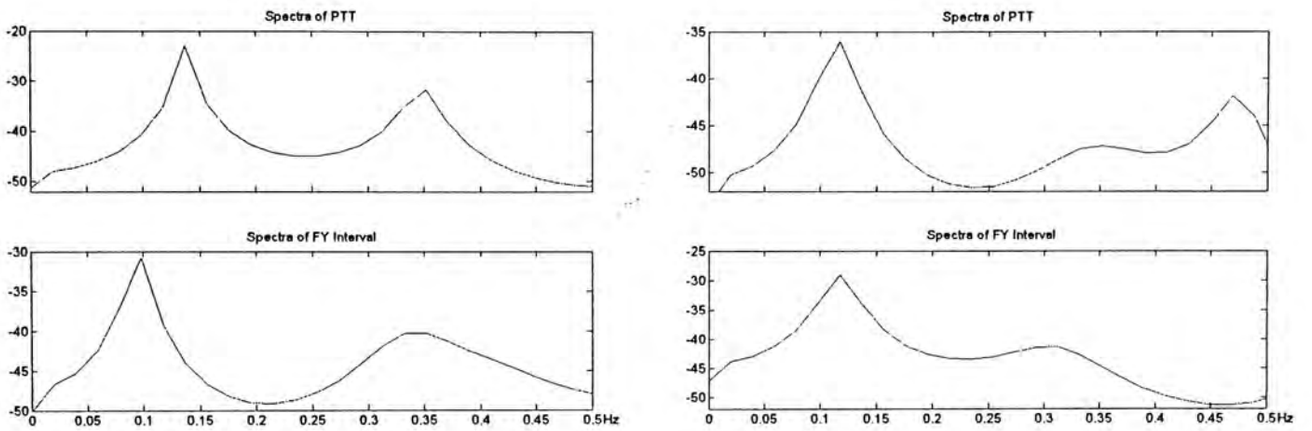

(a) (b)

Fig. 4-12: Spectra of PTT (upper panel) and FY interval (lower panel) from two subjects (a) and (b) under relatively higher levels of contacting force.

4.4 Discussion

As reported in several literatures [38] [39] [61], the intensity variations of the PPG signals mainly arise from blood volumetric changes in the peripheral micro-vascular bed with each pressure pulse initiated by the heart. Specifically, the signal of the photo-detector decreases when tissue blood volume increases, as during heart systole – the heart contraction, when blood is ejected from the heart to the tissue; while the PPG signal increases with the decrease in the volume of red blood cells, as during heart diastole. Thus, the FY interval and the YG interval of the PPG signal could to some extent reflect the periods of systole and diastole respectively.

It is often stated that the systolic and diastolic pressure, as well as PTT are affected by the changes in elastic properties of arteries [21]. Such changes could also

be associated with the variations in durations of systole, diastole, and the heart cycle. However, it is not yet fully established the complex interactions among these important parameters. A study on the characteristics of PPG signal as described by a set of its parameters can be useful for further understanding the underlying mechanisms of these cardiovascular processes. This preliminary work therefore was focused on the correlation study from statistical point of view to investigate the relationship between PPG related parameters and their association with the parameters from ECG signals such as RR interval.

Aside from the control under neural activities, the changes in the arterial elasticity may also be attributed to some other factors, such as the temperature fluctuations [62], or a large contacting force that results in the flattening of the arterial wall [21]. Also, the dynamic state that is immediately after exercise is taken into account, which could cause some variations in the physiological status in association with the changes in certain physiological parameters, such as heart rate, BP, etc. Therefore, the relationships of the PPG parameters under different experimental conditions were studied in this work.

Significantly high correlation is found consistently between the YG interval and the RR interval under all the different conditions. As mentioned before, YG interval of PPG could probably represent the period of heart diastole, during which elastic recoil of the arterial walls propels blood to perfuse the smaller peripheral resistance vessels. In fact, the end of diastole, or more precisely the onset of the ventricular contraction coincides with the R peak of ECG [21]. Thus, this result suggests that diastolic period is rather determined by the duration of a heart cycle than other factors, such as total peripheral resistance, or arterial compliance, etc. However, there is still a need to further investigate how closely the YG interval is related to the actual period of heart diastole.

It is interesting to note that the correlation between PTT and FY interval becomes substantially higher at larger contacting force levels. As reported in several literatures, PTT estimated from ECG and PPG agreed well with that obtained from some established methods [37], therefore it could be an index of the elasticity of the arterial wall. According to the early elaboration, the FY interval of PPG may be closely associated with the heart systole. As the pressure wave propagates down the aorta and its braches, the systolic portions of the wave become narrowed and elevated due to the changes in vascular compliance [21]. In other words, the systolic portions of the pressure wave could also provide value information about the elastic characteristics of the arterial tree. This leads to the possible conclusion that when under a large external pressure and the arterial wall is flattened, the changes in the local vascular compliance could be remarkable. Such changes will consequently influence PTT as well as the systolic portions of the pulse wave. Therefore, there could be highly correlated information in both PTT and FY interval. On the contrary, when under relaxed situation, there might be little variation in vascular compliance, which results in the independence of PTT and FY intervals. Similarly, as the temperature fluctuations may also induce variations in the arterial elasticity, the moderate correlation between PTT and FY interval at certain lower temperatures (26-29°C) can be understood. The slightly lower correlations at levels T1 (24 ± 0.5 °C) and T2 (25 ± 0.5 °C) might be attributed to the poor quality of the PPG signals at such low levels of finger temperature, which could probably disturb the peripheral blood microcirculation to certain extent. The correlation between PTT and FY interval at dynamic state is comparable to the results at resting state.

The spectral analysis plays an important role in interpreting the correlation between the PTT and FY interval. When at normal relaxed state, for some cases that have lower correlation between PTT and FY interval, the spectra of PTT and FY

interval contain dominant components at quite different frequency ranges. In the high-frequency range, generally around 0.3Hz, a remarkable component can be identified in the spectra of PTT. Such a rhythm, synchronous with the respiration rate, is probably due to the intra-thoracic pressure change and mechanical variations caused by the breathing activity [63]. In the low frequency range, between 0.04-0.15Hz, there is a rhythm, generally centered around 0.1 Hz, in the spectra of FY interval. Both sympathetic and parasympathetic contributions can be involved in this low frequency activity. However, an increase in its power has always been observed as a consequence of the sympathetic activation. Thus, an increase in the low-frequency power is regarded by many researchers as a marker of the sympathetic activity [63]. The distinctive difference in the main frequency components therefore results in an insignificant correlation between these two time series of PTT and FY interval. However, on the other hand, it is interesting to note that there is an apparent increase in the low-frequency power of the PTT spectra when PTT exhibits higher correlation with FY interval at relatively higher levels of contacting force. Such an increase is mainly attributed to the sympathetic activation, as mentioned before, which provides the major neural control of the peripheral vessels. In other words, variations in the properties of the peripheral system, such as the peripheral resistance and compliance, etc. [21], though induced by some external factors, may eventually be associated closely with the sympathetic nervous activity. Consequently, the spectral analysis leads to the same conclusion that with large changes in the characteristics of the peripheral vessels, it is possible to identify a certain increase in the frequency power corresponding to the sympathetic activation. Hence, PTT and FY interval could contain highly correlated information in the low-frequency range.

The correlation between PTT and RR varies considerably from person to person. In some subjects, the correlation coefficient can be as high as r=-0.8, while in some

others there is little correlation. Meanwhile, the results do not show much difference under different experimental conditions. This result demonstrates that the duration of the heart cycle as measured by RR interval is not so significantly associated with the arterial elasticity as PTT does. During recent years, several studies have employed PTT as an indicator of the arterial BP with reasonable accuracy, while in some other work a combination of PTT and RR was used for arterial BP estimation [64]. However, the relationship between PTT, RR and the beat-to-beat BP has not yet been fully explored. Further study based on the simultaneous recording of beat-to-beat BP, ECG, and PPG could be helpful in clarifying the matter. Based on these findings, the improvement of the non-invasive BP estimation only using PPG technique is just under way.

Chapter 5

The Estimation of the Beat-to-Beat Blood Pressure Variability

5.1 Introduction

The systemic arterial BP fluctuates with each heart cycle between a diastolic value and a higher systolic value. Obtaining estimates of an individual's systolic and diastolic pressures is one of the most routine diagnostic techniques available to physician for assessing the cardiovascular status. More importantly, the analysis of the beat-to-beat oscillations in BP plays a fundamental role for a better comprehension of the patho-physiological properties of the complex mechanisms which act through neural, mechanical, vascular, humoral factors and others [40].

Essential to the analysis on BP is the availability of the BP measurements. Two methods are commonly employed currently in the non-invasive arterial pressure measurement: 1) sampling of arterial pulse pressure, including the occlusive cuff-based approaches of Korotkoff and oscillometry; and 2) continuous recording of the pulse waveform. The sampling methods typically provide systolic and diastolic pressures, and sometimes mean pressure. These values are normally obtained from different heart beats within a minute. These methods are neither comfortable or convenient for frequent use nor capable of continuous BP monitoring. Alternatively, continuous recording methods provide resolution of the single beat pulse waveform and beat-to-beat pressure as well additional hemo-dynamic information [68]. However, these approaches still employ an occlusive cuff with the cuff pressure continuously altered to equal to the arterial pressure, such as the FINAPRES device. In other words,

they do not improve much the ease of positioning and manipulating or the patient comfort.

The BP estimation based on PTT or other beat-to-beat physiological parameters could provide an alternative to existing approaches for the non-invasive continuous BP monitoring. It has been reported in several literatures that PTT determined by the time delay between the characteristic points on ECG and PPG signals can be used for non-invasive estimation of arterial BP with reasonable accuracy [26][36][38]. Such an approach is much easier to use with much lower cost of development. Furthermore, it may also provide the information on the beat-to-beat variation of BP as well.

Undoubtedly, it is necessary to explore further the estimation of BP and BPV using PTT and other related parameters. Based on the correlation study in last chapter, a new parameter, the FY interval of PPG signals, which has a significant correlation with PTT at relatively large contacting forces, could possibly be of great potential for the non-invasive BP estimation, using only PPG technique. This will provide a substitute that is even simpler and more comfortable for continuously monitoring of BP and BPV. In this chapter, the feasibility of BP estimation using FY interval is first investigated. In the second part, FY interval as well as PTT is employed for the analysis of the beat-to-beat BPV.

5.2 BP Estimation using FY Interval

In this section, BP estimation using the FY interval of PPG signals is introduced. Different estimation scenarios were applied to investigate the feasibility of this new approach for either non-continuous BP measurement or the beat-to-beat BP estimation.

5.2.1 Multi-Beat BP Estimation under Different Levels of Contacting Force

Based on the results that the correlation between PTT and FY interval becomes substantially higher at larger contacting force levels, the BP estimation using FY interval is carried out on the same experimental data as that used in last chapter at different levels of contacting force. Seven levels of contacting forces were recorded during the experiment, and each was followed by a BP measurement using standard oscillometric BP meter (Model BP-8800, COLIN) at the left upper arm. Some of the standard BP recordings were used for calibration, while the others were used as reference values to evaluate the accuracy of the BP estimations. (The mean and standard deviation of the seven force levels, as well as the number of subjects at each level can be referred to Table 4-3.)

The mean values of FY interval at each level of contacting force were calculated for each subject, so as to be used for the estimation of BP corresponding to that certain period. Fig. 5-1 shows the mean and standard deviation of FY intervals over the 30 subjects at different force levels. There is an apparent decreasing trend in the value of FY interval with the increasing of force levels. In other words, the rising phase of the PPG signal becomes narrowed when under a large external pressure.

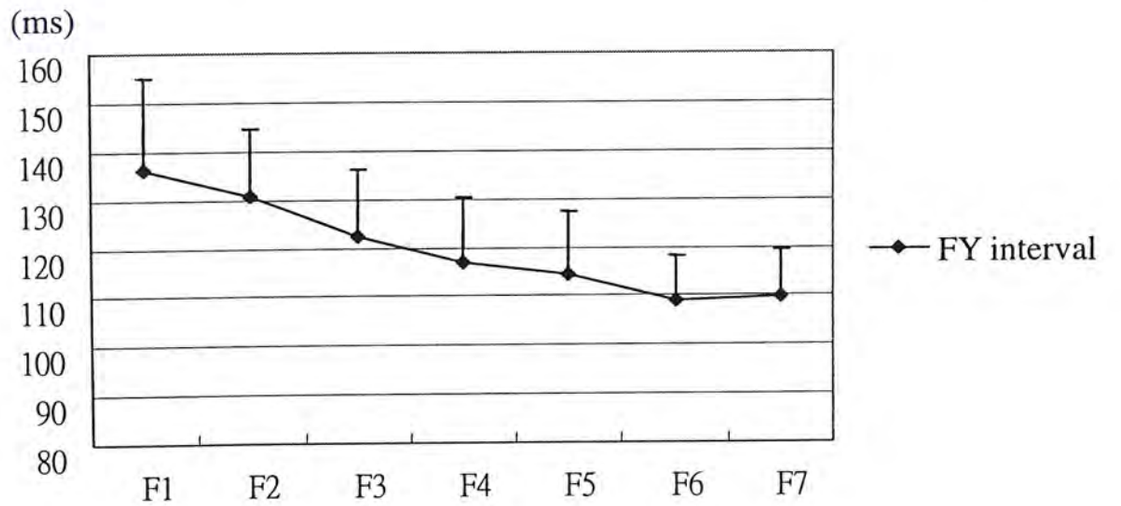

Fig. 5-1: Mean and standard deviation of FY intervals over the 30 subjects at different force levels.

Since FY interval is inversely correlated with PTT (see 4.3.2), while PTT is inversely correlated with BP [36], a simple equation for BP estimation is proposed as:

$$BP = a \cdot FY^n + b \tag{5-1}$$

where BP can be either the SBP or DBP, FY represents the FY interval, a and b are two constants determined by calibrations on each individual, and $n > 0$ (n=2 is used in this study). Taking into account the decrease in FY intervals with the increase in contacting force, a two-point calibration is necessary to obtain the values of a and b, using the mean FY interval of the lowest and highest force levels of each subject, respectively, so as to include the full range of FY intervals. Once a and b are determined after calibration, the estimation of BP at all other force levels can be carried out according to Eq. (5-1). Meanwhile, the same calibration approach is applied to the estimation equation for BP using PTT:

$$BP = c / PTT^2 + d \tag{5-2}$$

to obtain the values of c and d. The PTT-based BP estimation was carried out as well for comparison.

For a force level besides the lowest and highest force levels, only one BP value was estimated using the mean FY interval or mean PTT at that force level. The mean and standard deviation of the estimation error were calculated by comparing the estimated BP values with that from the standard BP measurement taken immediately after the data recording. The overall results for 30 subjects using both estimation approaches, FY interval approach and PTT approach, are given in Fig. 5-2 (SBP stands for systolic BP and DBP stands for diastolic BP). It is observed that though the mean errors in the estimation of SBP and DBP using PTT are slightly smaller than that using FY interval, either approach provides satisfactory results in terms of mean error (the AAMI standard: $|mean| \leq 5mmHg$). On the other hand, the standard

deviations of the estimation error using FY interval ($SD = 5.7mmHg$ for SBP and $SD = 6.1mmHg$ for DBP) are obviously smaller than that using PTT ($SD = 8.8mmHg$ for SBP and $SD = 9.6mmHg$ for DBP), which still meet the AAMI standard ($SD \leq 8mmHg$). In this sense, based on the two-point calibration approach under different levels of contacting force, the overall performance ($mean \pm SD$) of BP estimation using FY interval so far are within the AAMI standard for these 30 subjects, and the errors of both approaches are not significantly different from zero ($p < 0.05$).

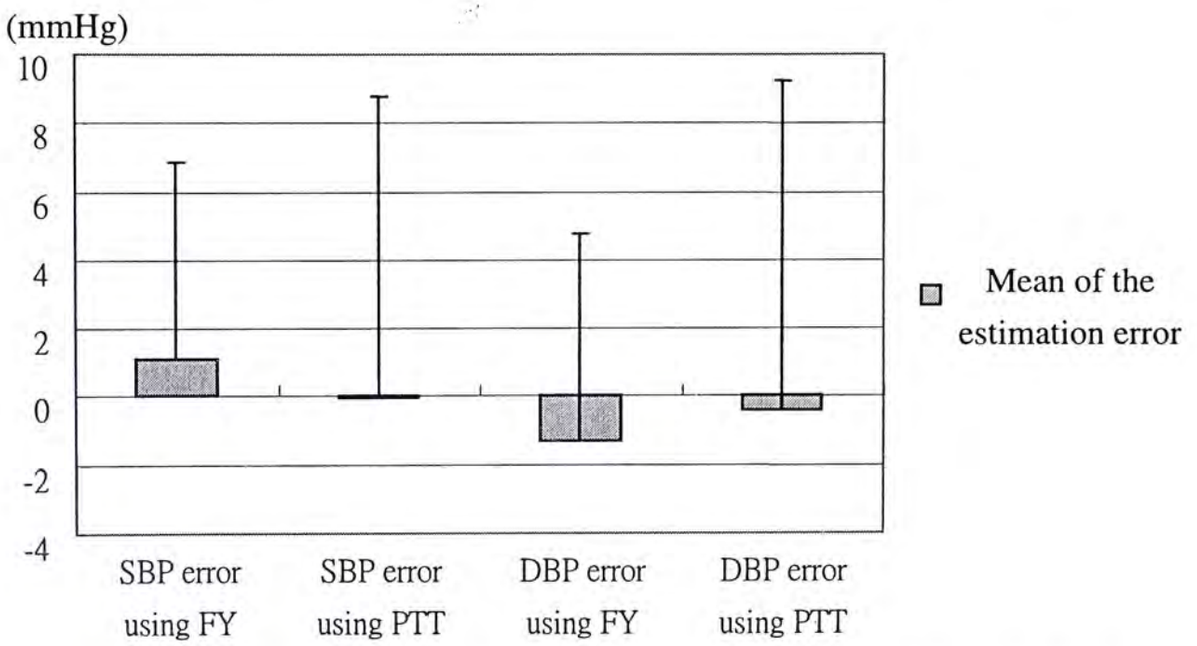

Fig. 5-2: Overall mean and standard deviation of the estimation errors using FY interval and PTT at different levels of contacting force.

Fig. 5-3 shows the estimation results at different contacting forces (level F1 and F7 are not included because of the two-point calibration approach). It is interesting to note that though the correlation between FY interval and PTT goes up with the increasing of force levels, the estimation results are not improved much or become even worse at relatively higher levels of contacting force, especially for the estimation of DBP. This is most likely due to the distortion of the PPG signals at higher levels of contacting force, which might influence to a large extent the relationship between BP

and PTT that is estimated by ECG and PPG signals. Hence, though there is a high correlation between FY interval and PTT at higher contacting force, the correlation between FY interval and BP may not be significant enough.

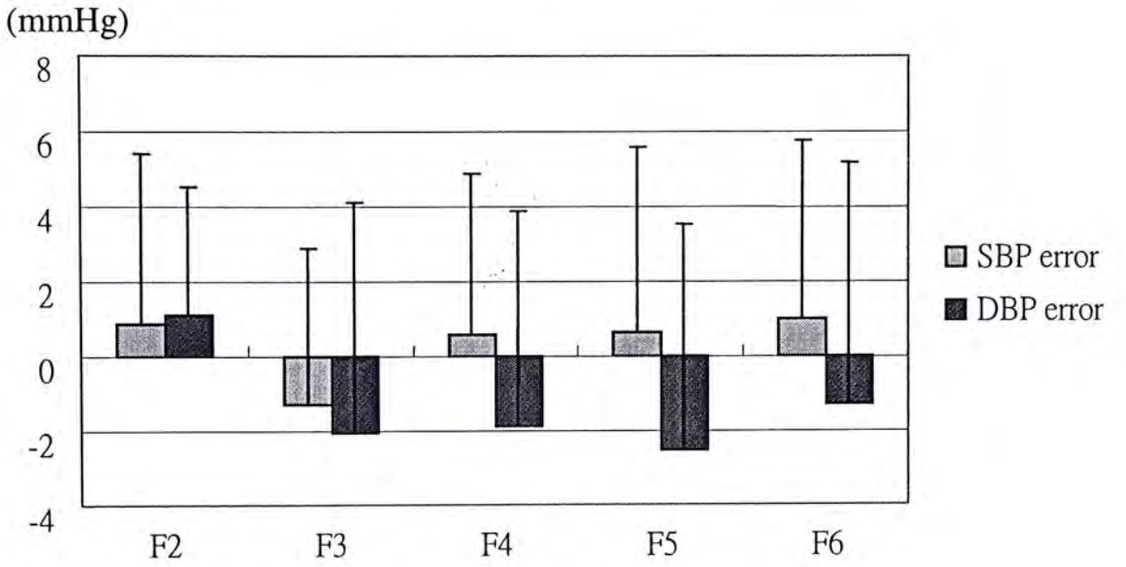

Fig. 5-3: Mean and standard deviation of the estimation errors using FY interval at each level of contacting force.

5.2.2 Beat-to-Beat BP Estimation

The knowledge of the continuous beat-to-beat BP could be of significant clinical value for better understanding the oscillatory behavior of BP. It can be particularly useful for monitoring continuously the patho-physiological statuses, and therefore providing valuable information about the neural and mechanical activities. As FY interval is a beat-to-beat parameter, it is also worthwhile to investigate the feasibility of using this new parameter for the estimation of the beat-to-beat BP.

Data used in this study are from another experiment conducted on 12 subjects at normal relaxed state. The subjects participated in this experiment were healthy, aged 22-30, and were asked to rest for 5 min before the measurement, and sat still on a comfortable chair throughout the whole period of data recording.

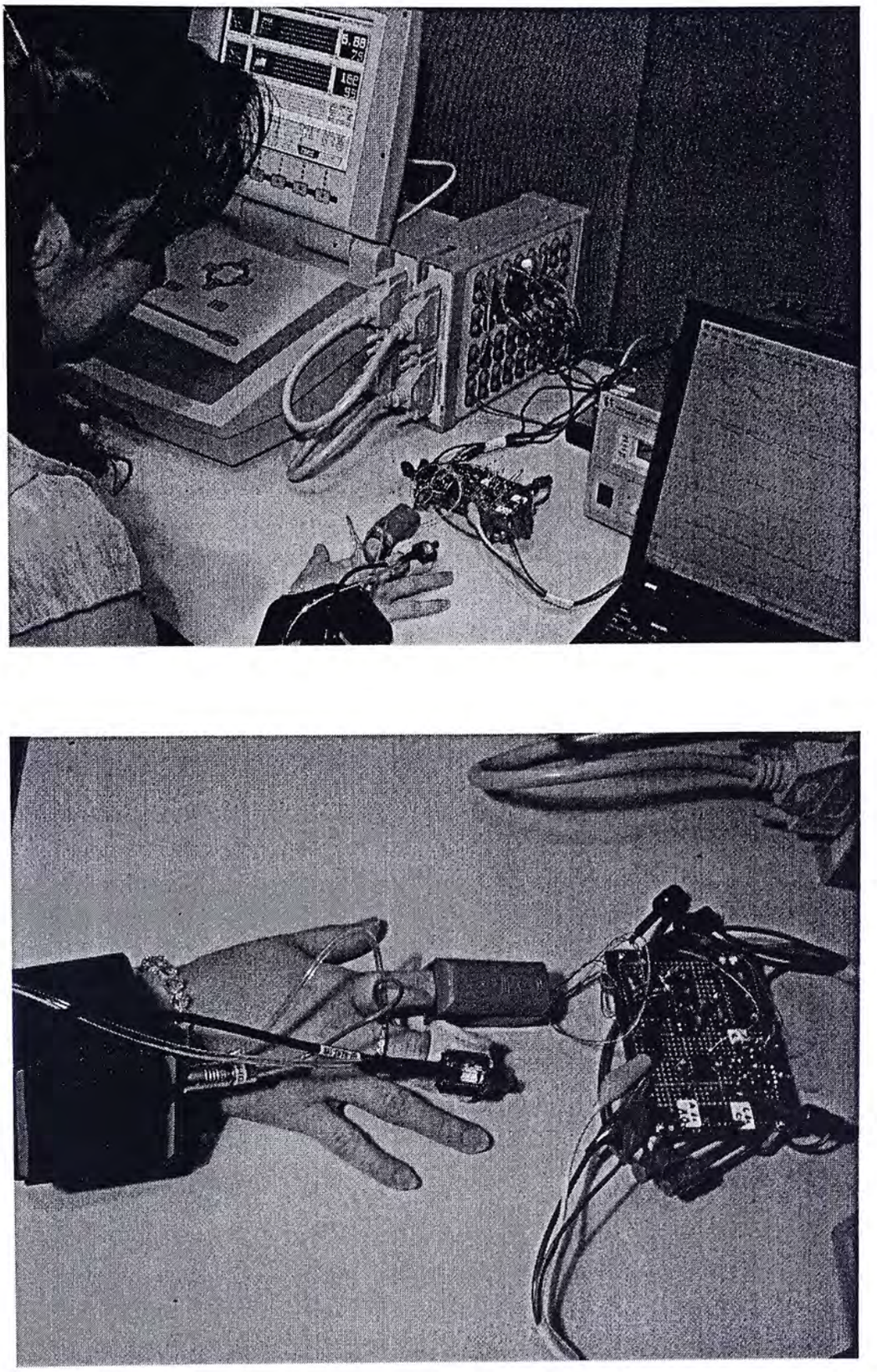

Fig. 5-4: The experimental setup for simultaneous recording of PPG signals, finger arterial pressure and ECG signals.

The PPG sensor used in the experiment was of reflective type, consisting of a LED and a photo-detector. The ECG signal was recorded by the Model 7400 -

Physiological Recorder with three electrodes on the left arm, right arm and right leg, respectively. Meanwhile, the FINAPRES monitor (FMS, Finapres Medical Systems BV, Netherland) was used for the continuous recording of the arterial pressure, the cuff of which was wrapped on the right middle finger. The PPG signal at the right index finger tip, the arterial pressure wave at the right middle finger, and the ECG signal as well were recorded simultaneously for about two minutes for each subject (see Fig. 5-4). During the whole period of recording, the subjects were asked to exert natural strength of contacting force on the sensor that they felt comfortable with.

Due to the interruptions by the inflation of the FINAPRES monitor from time to time during the period of data recording, the arterial BP waves were not absolutely continuous. Therefore, a data segment of 20 seconds was selected from each recording, which contains continuous recordings of ECG, PPG and BP waveforms. For each data segment, the beat-to-beat SBP and DBP were obtained from the BP wave; the beat-to-beat FY interval was extracted from the PPG signal; and the beat-to-beat PTT was estimated by the time delay between the R-peak of the ECG signal and the F point of the PPG signal.

Unlike that under different levels of contacting force, the FY interval does not vary significantly during the whole period of data recording at the normal relaxed state. As a result, the two-point calibration approach becomes unnecessary for the BP estimation. Alternatively, a one-point calibration method is used, and the equation for the estimation is expresses as:

$$\begin{cases} SBP = a \cdot FY^2 + 70 \\ DBP = b \cdot FY^2 + 50, \end{cases} \tag{5-3}$$

where SBP and DBP represents the systolic and diastolic BP, respectively, a and b are the constants determined by the one-point calibration on each subject. In other words, once the value of SBP, DBP and FY interval corresponding to one

particular heart cycle is known, a and b can be calculated, and the beat-to-beat BP estimation using FY interval is just under way. Similarly, the same one-point calibration approach is applied to the estimation equation using PTT:

$$\begin{cases} SBP = c / PTT^2 + 70 \\ DBP = d / PTT^2 + 50, \end{cases} \quad (5\text{-}4)$$

to obtain the values of c and d. The PTT-based beat-to-beat BP estimation was carried out as well for comparison.

For each data segment, the values of SBP, DBP, FY interval and PTT corresponding to the first heart cycle of the segment were used for the calibration. The beat-to-beat BP values of the subsequent heart cycles of that data segment were then calculated. The mean and standard deviation of the estimation error were obtained by comparing the estimated BP value with that from the BP wave corresponding to the same heart cycle. The overall results for 12 subjects as a whole using both estimation approaches, FY interval approach and PTT approach are given in Fig. 5-5. The errors of both approaches are not significantly different from zero ($p < 0.05$).

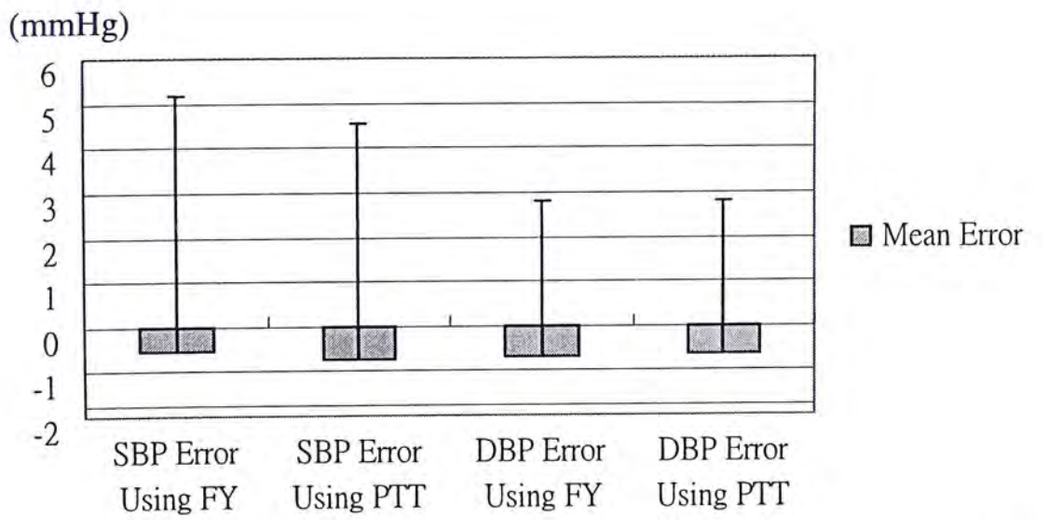

Fig. 5-5: Mean and standard deviation of the beat-to-beat BP estimation errors using the FY interval and PTT at the normal relaxed state.

It is clearly observed that the two approaches for the beat-to-beat BP estimation provide quite comparable results in terms of either mean error or standard deviation. The mean estimation errors of SBP and DBP using FY interval are $-0.54mmHg$ and $-0.7mmHg$, respectively; while those using PTT are $-0.73mmHg$ and $-0.64mmHg$. The standard deviations of the estimation errors using FY interval are $5.7mmHg$ and $3.5mmHg$ for SBP and DBP, respectively; while those using PTT are $5.3mmHg$ and $3.4mmHg$. The results of both methods are satisfactory compared with the AAMI standard.

5.2.3 Repeatability Study

In order to further validate the feasibility of the beat-to-beat BP estimation using FY interval for long-term BP monitoring, the repeatability study was carried out as well. In this test, calibration is no longer needed. The constants in the estimation equations were determined by previous calibrations and the estimation equations were applied to data segments that are different from what used in Section 5.2.2 for each subject. In other words, the aim of this repeatability test is to investigate that whether the estimation equation determined by a randomly chosen point can be applicable to the subject for a long time without new calibrations.

The new data were obtained from that same 12 subjects several days after the first experiment and was under exactly the same experimental protocol. The overall results for 12 subjects as a whole both estimation approaches are given in Fig. 5-6. For the SBP estimation, the PTT based approach provides better results that the FY based method; while for the DBP estimation, the two approaches provide quite comparable results in terms of either mean error or standard deviation. Overall, the repeatability results of the FY based method for the beat-to-beat BP estimation ($SBP\ error = 1.34 \pm 7.13mmHg$, $DBP\ error = -1.50 \pm 4.95mmHg$) are still

acceptable compared with the AAMI standard.

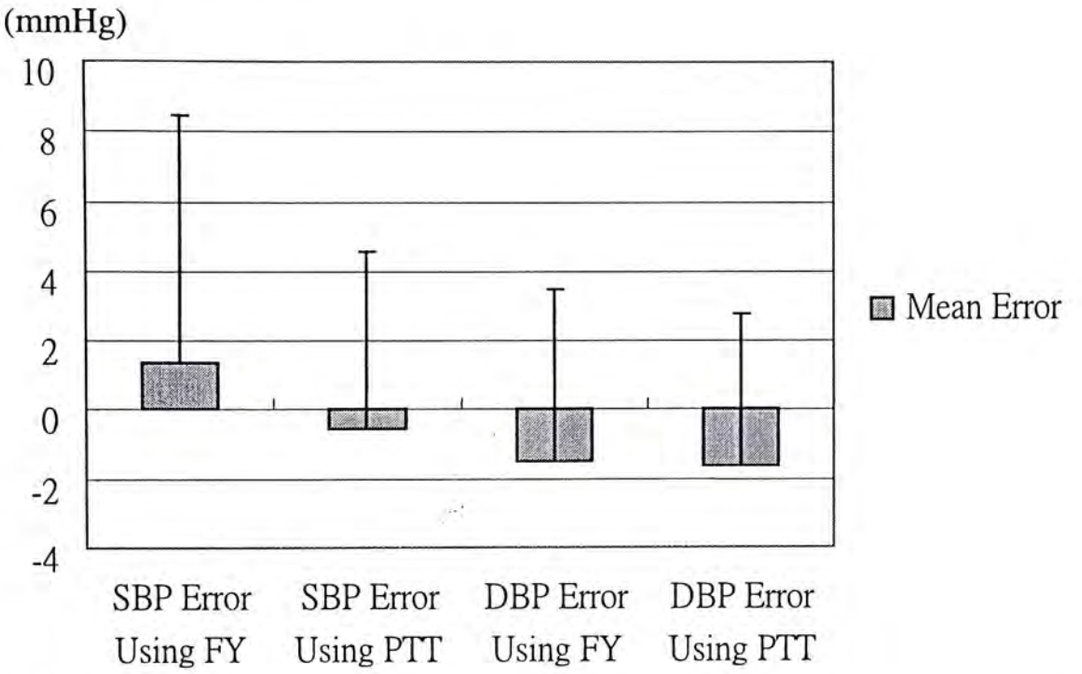

Fig. 5-6 Mean and standard deviation of the beat-to-beat BP estimation errors using the FY interval and PTT in the repeatability test.

5.3 A Study on the Beat-to-Beat BPV

The analysis of the beat-to-beat oscillations in BP plays a fundamental role for a better comprehension of the patho-physiological properties of the complex mechanisms which act through neural, mechanical, vascular, humoral factors and others [40]. However, due to the technical limitations in the non-invasive continuous BP measurement, the BPV has not yet been studied extensively.

Based on the promising results of the beat-to-beat BP estimation using either FY interval or PTT, it is of great importance to further extend these simple approaches for the study of the beat-to-beat BPV. In this section, the feasibility of using the FY interval and PTT for the analysis of the beat-to-beat BPV is investigated.

5.3.1 Background of the Beat-to-Beat BPV

The beat-to-beat analysis on arterial BP has been possible by using invasive

techniques which employ either an external or an internal transducer. Recently, non-invasive plethysmographic techniques have raised great interest in the study of the beat-to-beat BPV and also become commercially available (FINAPRES) in clinical applications.

Through proper detection algorithm, a few beat-to-beat parameters like systolic /diastolic/mean/pulse pressure values can be recognized on arterial BP waveforms. In this way, systograms, diastograms and so on, intended as discrete series synchronous to the corresponding cardiac cycles, may be obtained, which reflect the beat-to-beat fluctuations of arterial BP with time. An example of the systogram and diastogram is given in Fig. 5-7.

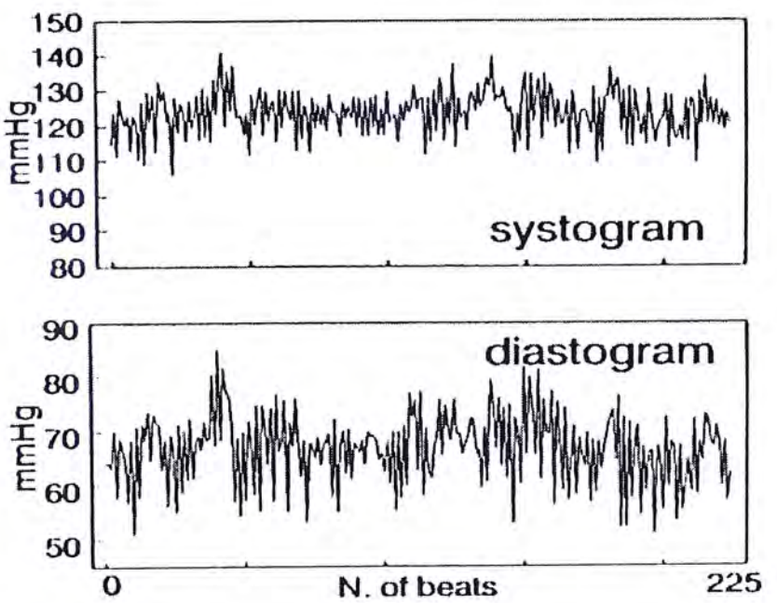

Fig. 5-7: An example of systogram and diastogram obtained from continuously BP recording of a normal subject [40].

Spectral analysis was first used in 1978 to obtain the beat-to-beat BPV [65], [66]. It has been used more extensively in the last few years to provide useful information on neural control of the cardiovascular system [40]. Particularly, considerable attention has been focused on fluctuations occurring at frequencies in the range of

approximately 0.04-0.45 Hz, which are believed to reflect intrinsic vascular activity and neural modulation of the vascular tone.

Fig. 5-8 shows an example of the autospectra for systogram series detected in a healthy subject. It is easy to identify the three main components: 1) a very low frequency (VLF) component located around 0.01-0.04Hz; 2) a low frequency (LF) component at around 0.1Hz; and 3) a high frequency (HF) component synchronous with the respiration rate, generally from 0.15Hz to 0.45 Hz. The power spectral densities of these three frequency bands are closely associated with baroreflex control, sympathetic and parasympathetic nervous activities, and the respiratory activity. Therefore, the spectral analysis of the beat-to-beat BPV could definitely provide more information that is of great physiological importance.

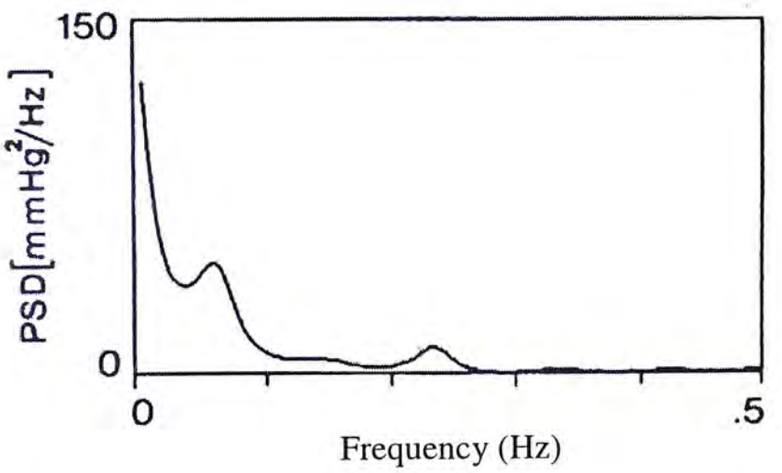

Fig. 5-8: An example of the autospectrum of SBP from a healthy subject [40].

5.3.2 Analysis of the Beat-to-Beat BPV

The beat-to-beat BP estimations using FY interval and PTT have already been carried out on 12 subjects in Section 5.2.2 (Estimations were carried out on a 20-second period for each subject.). The further analysis on the beat-to-beat BPV in both time domain and frequency domain is based on these estimation results; and its reliability is verified by comparing with the analysis based on the data from the FINAPRES.

Figs. 5-9, 5-10, and 5-11 give the systograms and diastograms from three of the twelve subjects over 20-second periods. The solid lines represent BP obtained from the FINAPRES, which is used as the reference value. The results of the BP estimations using FY interval and PTT are plotted as dotted lines and dashed lines, respectively. In all three subjects, the estimations of BP using either FY interval or PTT agree well with the data from FINAPRES. (The mean and standard deviation of the errors for the 12 subjects are given in Section 5.2.2.)

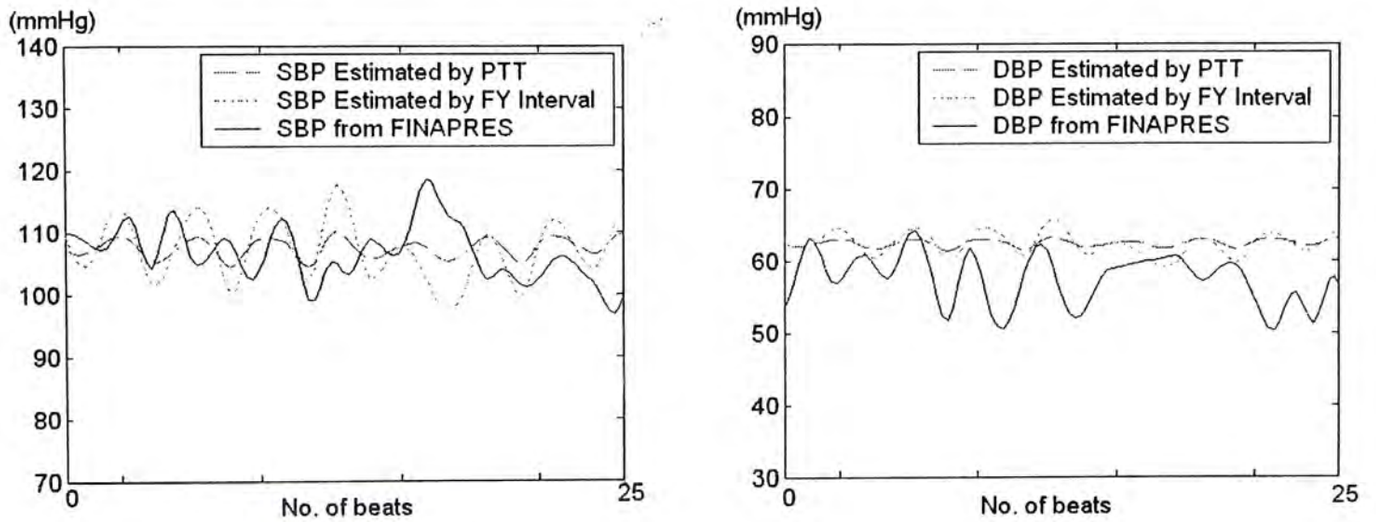

(a) (b)

Fig. 5-9: (a) Systogram; and (b) diastogram from subject 1, healthy and aged 40.

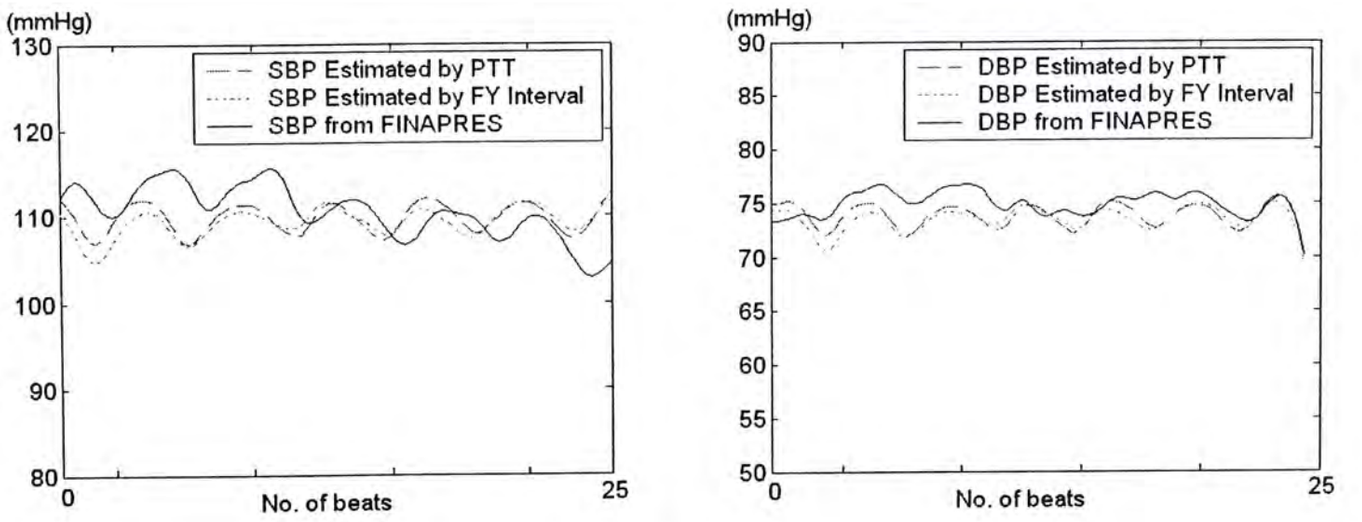

(a) (b)

Fig. 5-10: (a) Systogram; and (b) diastogram from subject 2, healthy and aged 26.

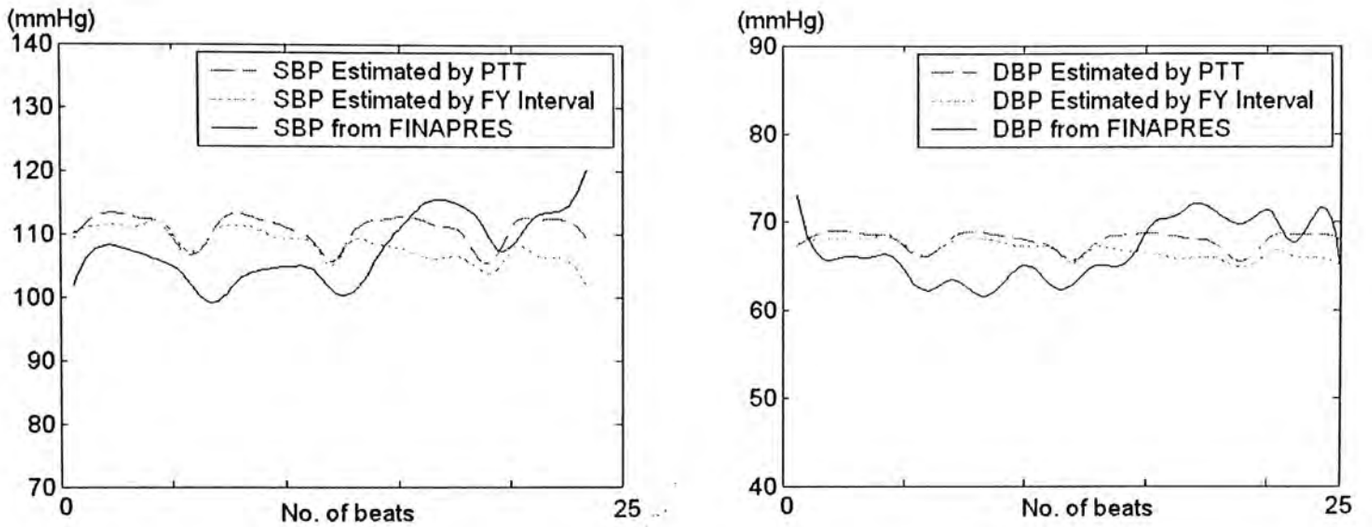

(a) (b)

Fig. 5-11: (a) Systogram; and (b) diastogram from subject 3, healthy and aged 23.

To evaluate the accuracy of the beat-to-beat BPV estimations in the frequency domain, the spectral characteristics of each estimation segment and each recording from FINAPRES were calculated using Fast Fourier Transform (FFT). Cumulative powers were computed over two main frequency bands, the LF band between 0.04-0.15Hz and the HF band between 0.15Hz and 0.45Hz. Since each segment lasted for only 20 seconds, the VLF component located around 0.01-0.04Hz is not considered in this study.

For each subject, LF and HF powers were calculated in absolute values integrating the density curves over the corresponding frequency ranges, and then over the total absolute power from 0 to 0.5Hz. The mean and standard deviation of the LF and HF power percentages were obtained for the group of twelve subjects.

Fig. 5-12 gives the spectra of Subject 2, the same one used in Fig. 5-10, calculated from both the estimated SBP and the SBP from FINAPRES. Obviously, the LF component, centered around 0.05Hz, and the HF components, centered around 0.3Hz, can be identified in the power spectra of the SBP obtained from FINAPRES

recordings. The power spectral density (PSD) of the SBP estimated from FY interval shown in Fig. 5-12 (b) is quite similar to that in Fig. 5-12 (a). The locations of the LF band and HF band in Fig. 5-12 (b) are found in correspondence with those in Fig. 5-12 (a). The LF component shown in Fig 5-12 (c)is hardly observed, while the HF component is as strong as that in Fig. 5-12 (a) and (b).

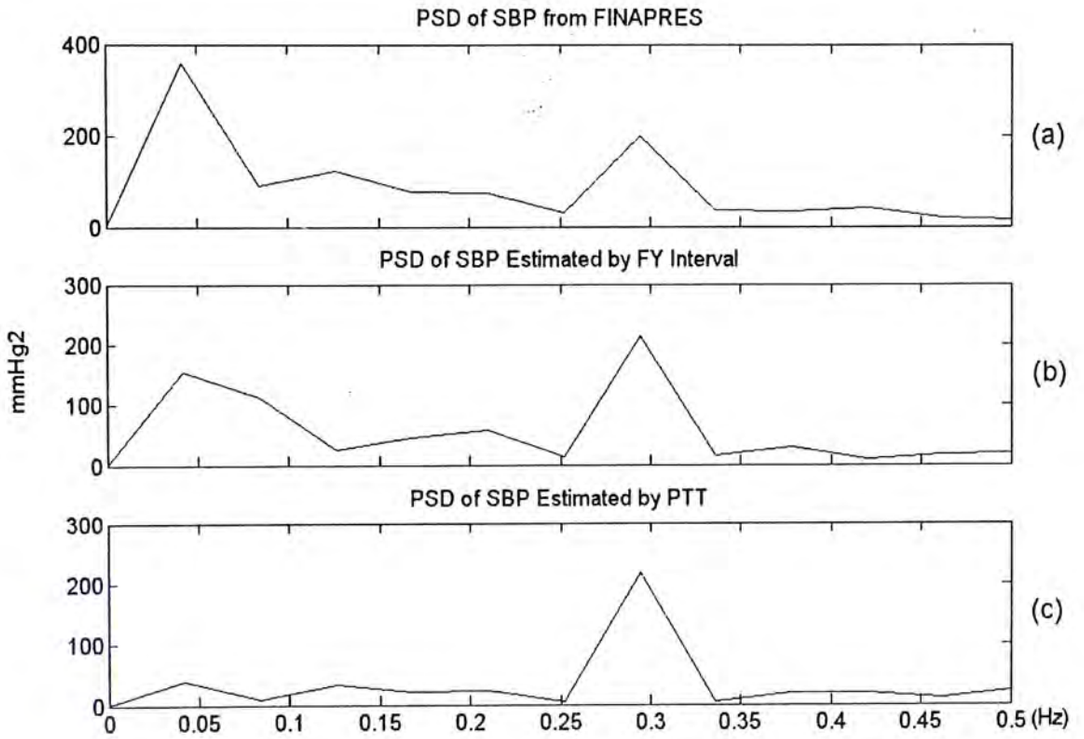

Fig 5-12: (a) Power spectral density (PSD) of SBP obtained from FINAPRES; (b) PSD of SBP estimated by the FY interval;, and (c) PSD of SBP estimated by PTT from the same subject of Fig. 5-10.

To illustrate more clearly the relationship between the spectral characteristics of the three SBP series shown in Fig. 5-12, the respective coherence functions are also computed. Fig. 5-13 shows the magnitude square coherence (MSC) functions between the estimated BP and that from FINAPRES. The result is consistent with that manually observed. The coherence is quite high between the SBP of FINAPRES and the SBP estimated by FY interval in both the LF and HF bands. The coherence function between the SBP of FINAPRES and the SBP estimated by PTT has a sharp

decrease in the LF range, but is still as high as the one in HF range.

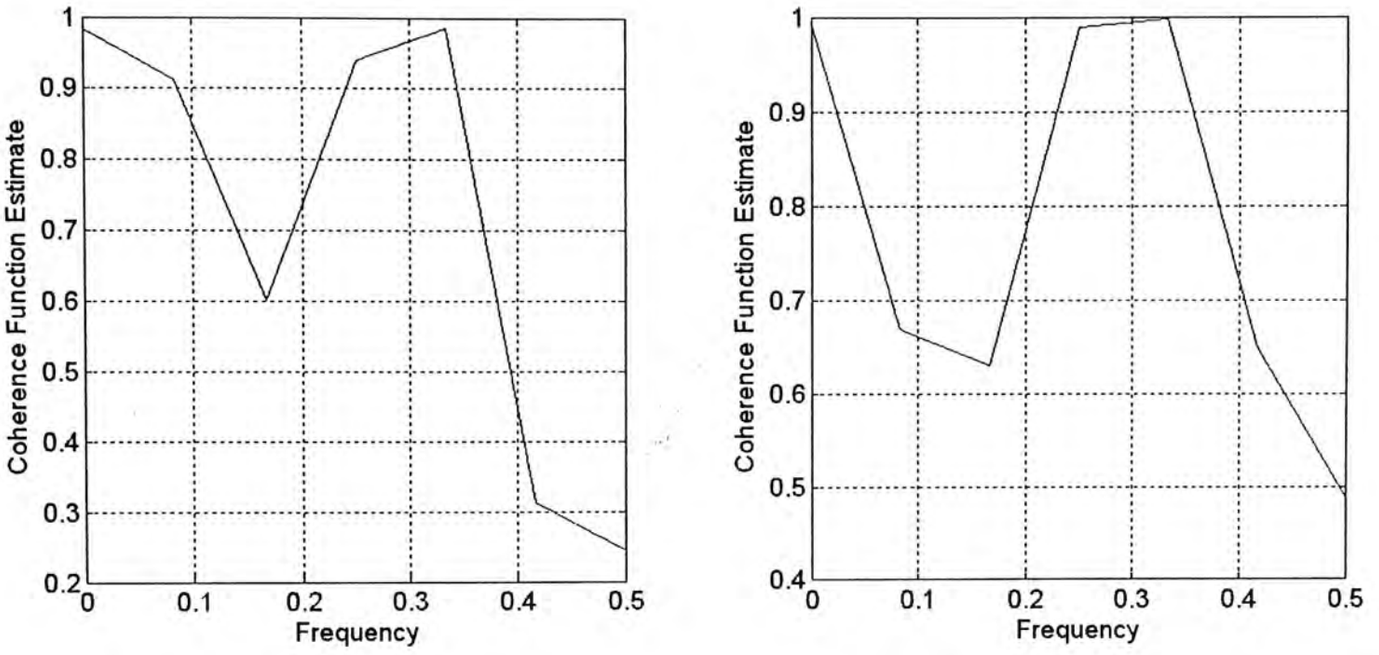

(a) (b)

Fig. 5-13: (a) Magnitude square coherence (MSC) functions between BP series estimated by FY interval and that from FINAPRES; and (b) Magnitude square coherence (MSC) functions between BP series estimated by PTT and that from FINAPRES.

Fig. 5-14 illustrates the average of the cumulative power percentages of BP spectral components obtained from FINAPRES and estimated BP values for the 12 subjects. The LF and HF power percentages ($mean \pm SD$) are given in Fig. 5-14(a) and (b), respectively. For the LF power percentage, the BPs using both FY interval and PTT are underestimated. On the contrary, for the HF power percentage, both FY interval and PTT approaches give overestimated BPs. It is also found that the FY interval based BP estimation seems to perform better that the PTT based method. It provides less underestimated LF power percentages than those using PTT (about 25% underestimation using FY interval and about 50% underestimation using PTT), and less overestimated HF power percentages (about 25% overestimation using FY interval and 50% overestimation using PTT).

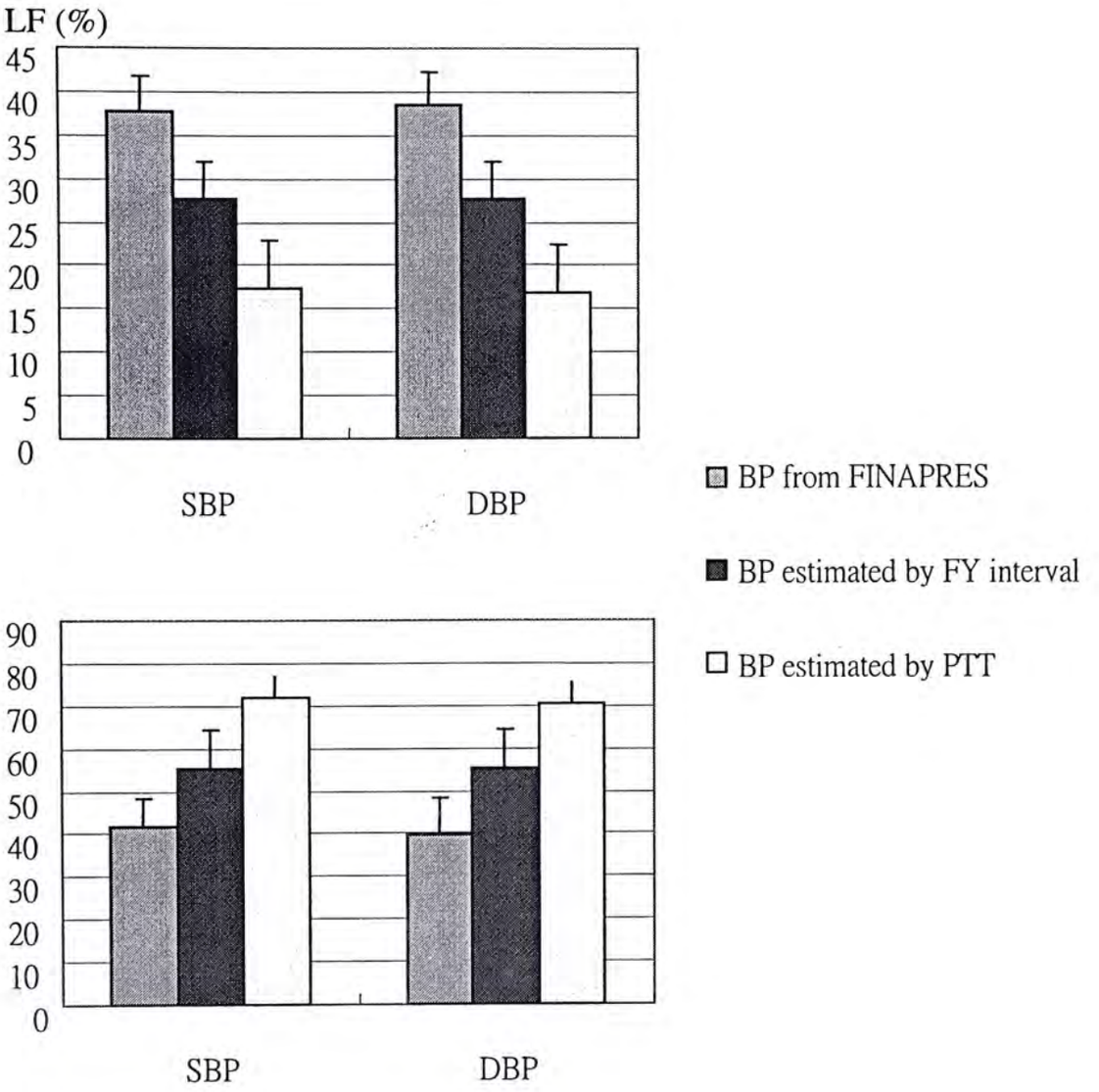

Fig 5-14: LF (upper panel) and HF (lower panel) power spectral densities of SBP and DBP. Data are shown as $mean \pm SD$ for the group as a whole.

5.4 Improving the PPG Model with the Time-Varying BP

So far, the new PPG model proposed in this study does not take into account any dynamic information related to the beat-to-beat oscillatory BP. Undoubtedly, it would be of great importance if this new model can be further extended to reflect the beat-to-beat fluctuation of arterial BP. Also, it should be noticed that the transmission time delay generated in the model has been simplified as a constant, as introduced in Chapter 3. In fact, however, the transmission delay is the time for the pressure wave

traveling down the arterial system, or actually the PTT and it varies from beat to beat. The discrepancy between the simulation results and the experimental data has already been identified in Fig. 3-17. Therefore, it is desirable that the time delay generator in the current model could be modified for generation of the time varying PTT.

5.4.1 Modification of the PPG Model

The first objective of the modification of the PPG model is to generate the beat-to-beat oscillatory arterial BP. Since the new model is able to mimic the generation of heart beats, it would be a breakthrough if there is certain relationship between the beat-to-beat heart rate and BP.

Obviously, the interaction between the heart rate and BP is not simple, which involves the baroreflex control and therefore the modulation of neural activities as well. The fundamental mechanism in the control of arterial BP and heart rate may be illustrated by the diagram in Fig. 5-15 [63].

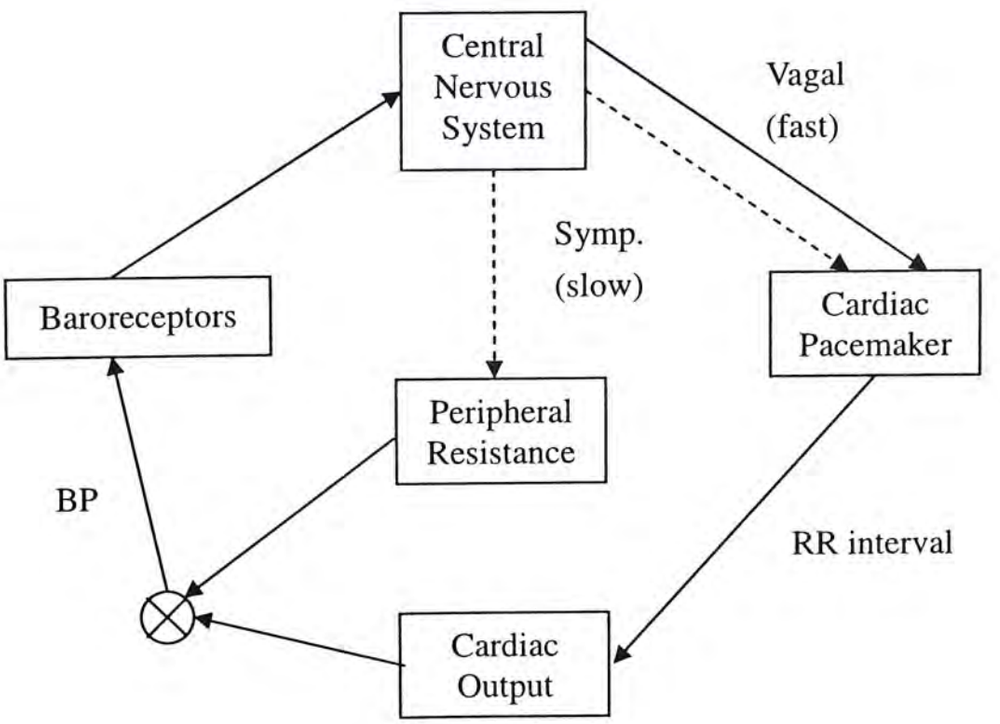

Fig. 5-15: Schematic diagram of cardiovascular system.

The value of BP is sensed by the baroreceptors, and accordingly, the central nervous system (CNS) adjusts the heart rate by both fast vagal (parasympathetic) action and slower sympathetic action (baroreflex control of HR). The baroreflex also affects the peripheral resistance but only via sympathetic efferent activity, which has already been taken into account in the new model. The heart rate (or equivalently the length of the RR interval) influences the cardiac output, which together with the peripheral resistance determines the value of the BP and thus closes the loop.

The relationship between the heart rate and BP can be considered as two branches: the forward branch (heart rate → BP) and the feedback branch (BP → heart rate). The feedback branch is actually the baroreceptor-heart rate reflex. Quantitatively, it can be evaluated by the baroreflex sensitivity (BRS), that is the ratio between the increase (or decrease) in consecutive RR intervals and the increase (or decrease) in successive SBPs [40]. The CNS processes the baroreceptor input for the adjustment of both the fast parasympathetic activity and slower sympathetic activity, and therefore modulating the next heart beats. It is this baroreflex control that provides a proper adaptation of the cardiovascular system to specific physiological conditions. The feed forward branch in which BP varies accordingly to heart rate, on the other hand, can be approximated by the empirical sigmoidal law, as shown in Fig. 5-16 [18].

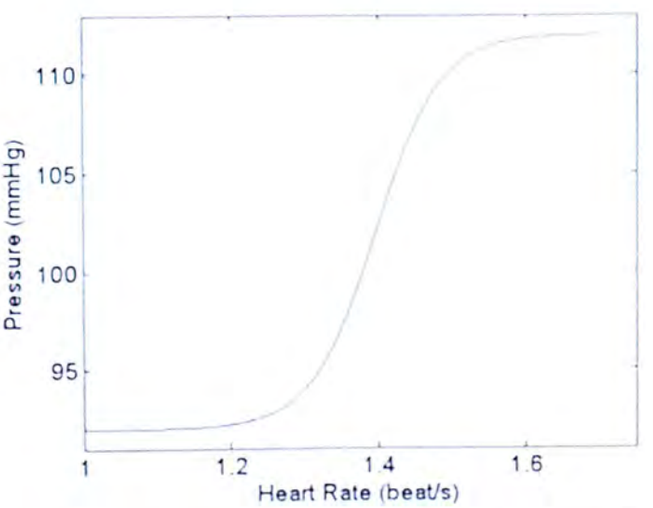

Fig. 5-16: Relationship between heart rate and mean arterial BP in steady state.

The second objective of the modification of the new model is to generate the dynamic beat-to-beat PTT. As mentioned before, the significant linear relationship between PTT (PEP plus the actual transmission time) and arterial BP has been recognized for long time [36] [38]. The feasibility of using PTT for either discrete or beat-to-beat BP estimation has also been confirmed in the above sections. Indeed, the statistical correlation between PTT and BP can be quite high. Fig. 5-17 illustrates the beat-to-beat correlation between PTT and BP from a healthy subject.

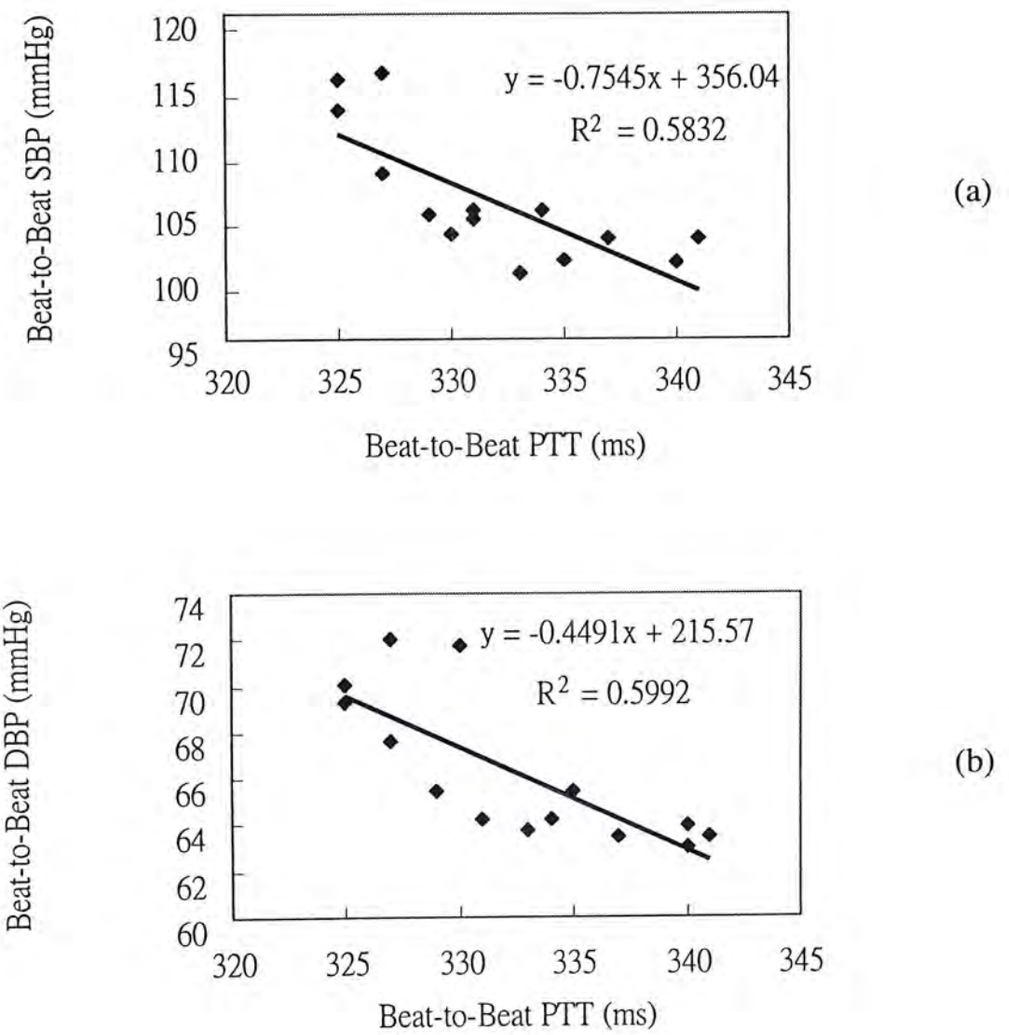

Fig. 5-17: The beat-to-beat correlation between PTT and (a) SBP; and (b) DBP obtained simultaneously with the SBP in (a).

The correlation between average PTT and BP can even be much higher. Both the

PTT and BP are calculated as the mean of the beat-to-beat values of 10-second data segments. Fig. 5-18 gives the results for the same subject used in Fig. 5-17.

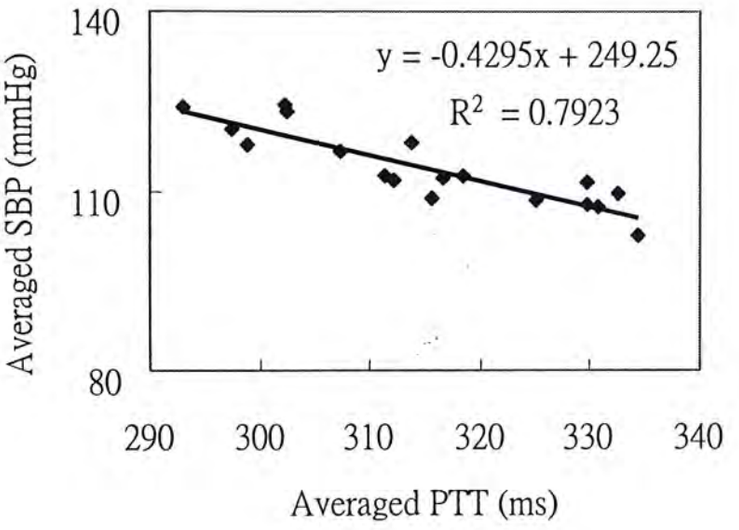

(a)

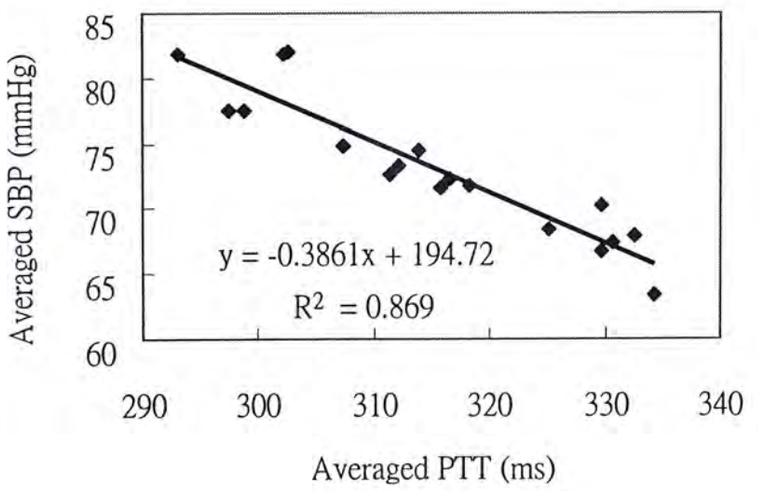

(b)

Fig. 5-18: The correlation between average PTT and (a) average SBP; and (b) the corresponding average DBP.

Based on these results, the time delay generator in the new PPG model can be modified to make it more realistical by taking into account this nearly linear relationship between BP and PTT. More specifically, using BP as an input for the time delay generator, PTT can be generated accordingly. A generalized diagram of the

modified model is shown in Fig. 5-19 (a). Fig. 5-19 (b) gives the specification that is used in our study.

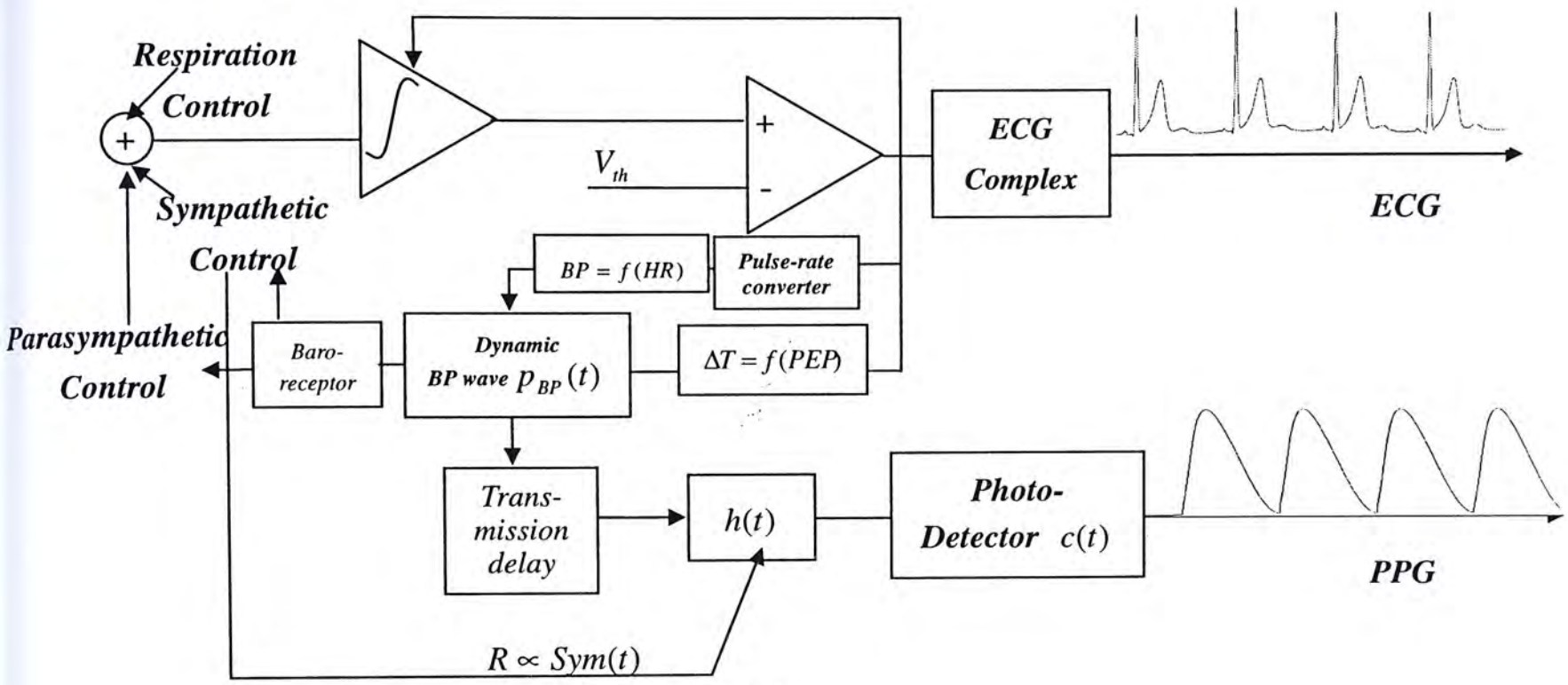

(a)

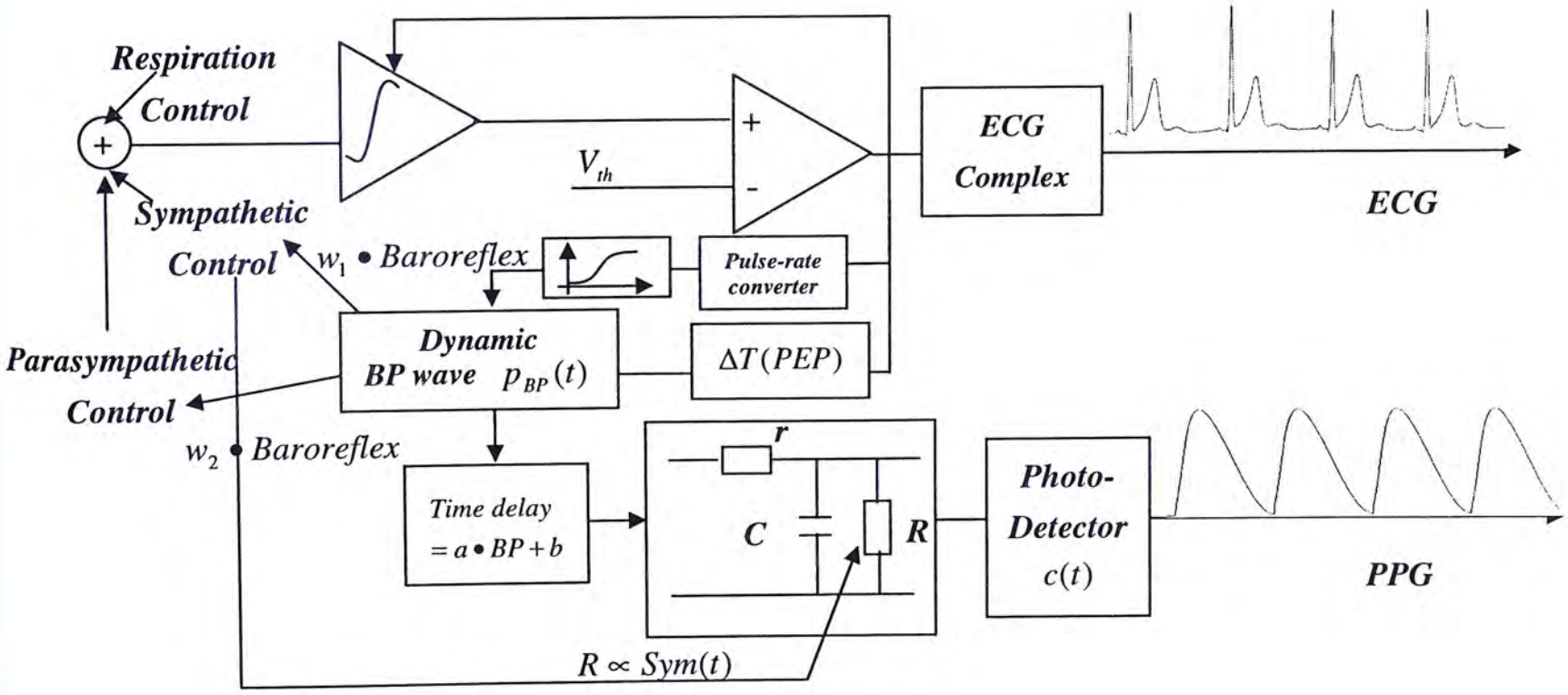

(b)

Fig. 5-19: (a) Generalized diagram of the modified model; and (b) the model specification that is used in our study.

Taking into account the time-varying BP and PTT, the output train of PPG signals in our modified model can therefore be expressed as:

$$e_{PPG}(t) = y(t - \Delta t(BP) - \Delta T(PEP)) * h(t) * p_{BP}(t) * c(t) \qquad (5\text{-}5)$$

where $y(t)$ is the neural spike train generated by IPFM model and is adjusted by the baroreflex control as well, $\Delta t(BP)$ .is the time-varying transmission delay determined by BP, $h(t)$ is the impulse response of the WK3 model, $p_{BP}(t)$ is the dynamic BP waveform determined by the sigmoidal function together with the corresponding heart rate, $c(t)$ is the impulse response of the photo-detector. Fig 5-20 gives an illustration of PPG generation according to Eq. (5-5).

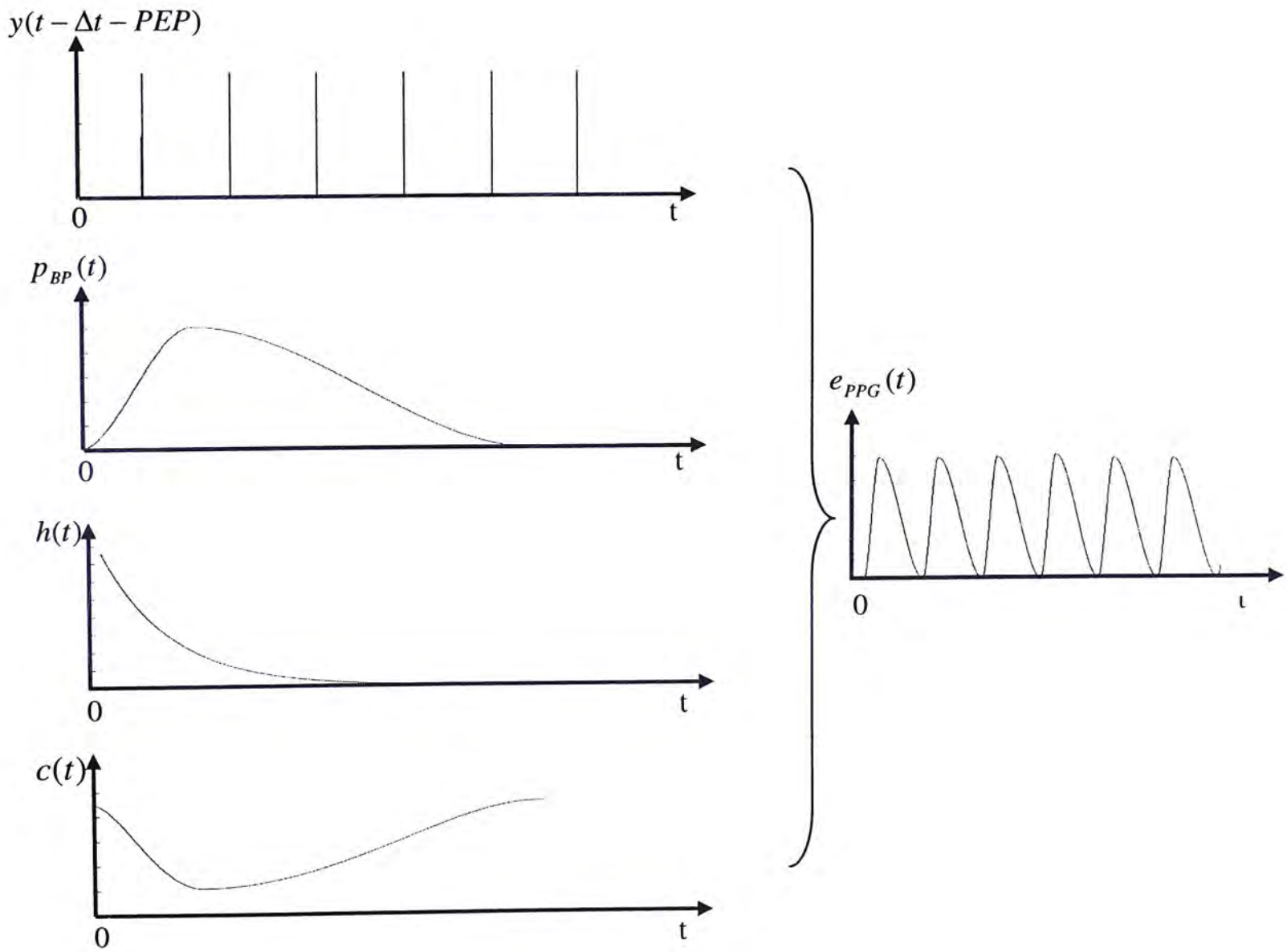

Fig. 5-20 Illustration of the generation of PPG signals.

5.4.2 Simulation

The empirical sigmoidal function was determined by best-fitting data drawn from physiological literature [18]:

$$P(HR) = 90 + \frac{20}{1 + 6.7 \times 10^{13} e^{-31 \times HR / 1.35}} \tag{5-6}$$

in which HR represents the beat-to-beat heart rate, and P is the value of BP corresponding to the same cardiac cycle. It should be pointed out that the pressure P in the Eq. (5-6) is regarded as the mean arterial BP rather than SBP or DBP. In other words, with the generation of each heart beat, the mean arterial BP corresponding to the same cardiac cycle can be estimated. The relationship between the mean BP (P_m), SBP (P_s) and DBP (P_d) can be approximated by the following empirical formula:

$$P_m = P_d + \frac{1}{3}(P_s - P_d) \tag{5-7}$$

In our simulation, DBP is fixed as a constant ($DBP = 75mmHg$), and thus SBP can be derived from Eq. (5-7). By doing so, the baroreceptor senses the change in two consecutive SBPs and sends the information ($\frac{SBP(n-1)}{SBP(n)}$) back to control the neural activities so as to counteract possible deviations of BP from the reference set point. According to the study by [68], an equal weight ($w_1 = w_2 = 1$) is used for the contribution of baroreflex control to the parasympathetic and sympathetic activities. The simulation is thus carried out by assuming a normal physiological status.

Fig. 5-21 (a) shows the simulated beat-to-beat oscillatory BP waves. DBP is assumed as constant, while SBP exhibits the beat-to-beat oscillations, as illustrated in Fig. 5-21 (b).

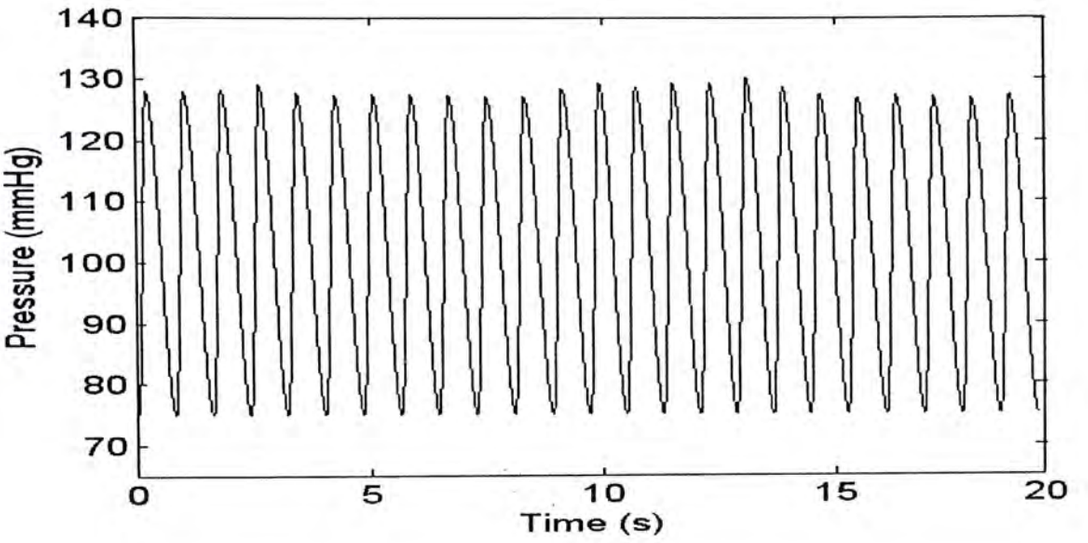

(a)

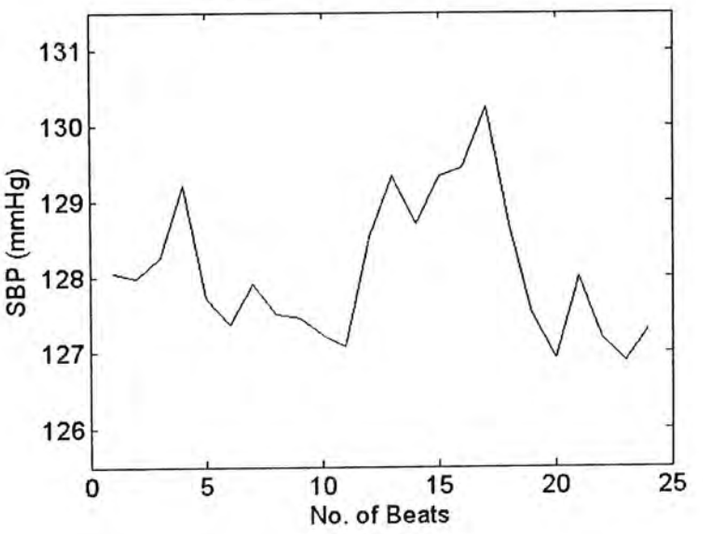

(b)

Fig. 5-21: (a) The simulated BP wave; and (b) the oscillation of simulated SBP.

The spectrum of the simulated SBP is also computed, as shown in Fig. 5-22 (a). Similar to the spectra of RR interval, the PSD of SBP also reflects clearly the frequency components associated with the input modulation signals, and it agrees with the that from experimental data as shown in Fig. 5-22 (b). Therefore, by utilizing the empirical sigmoidal relationship between heart rate and mean BP and by taking into account the baroreflex control, the new model is able to generate beat-to-beat SBP (or mean BP) that is physiologically plausible.

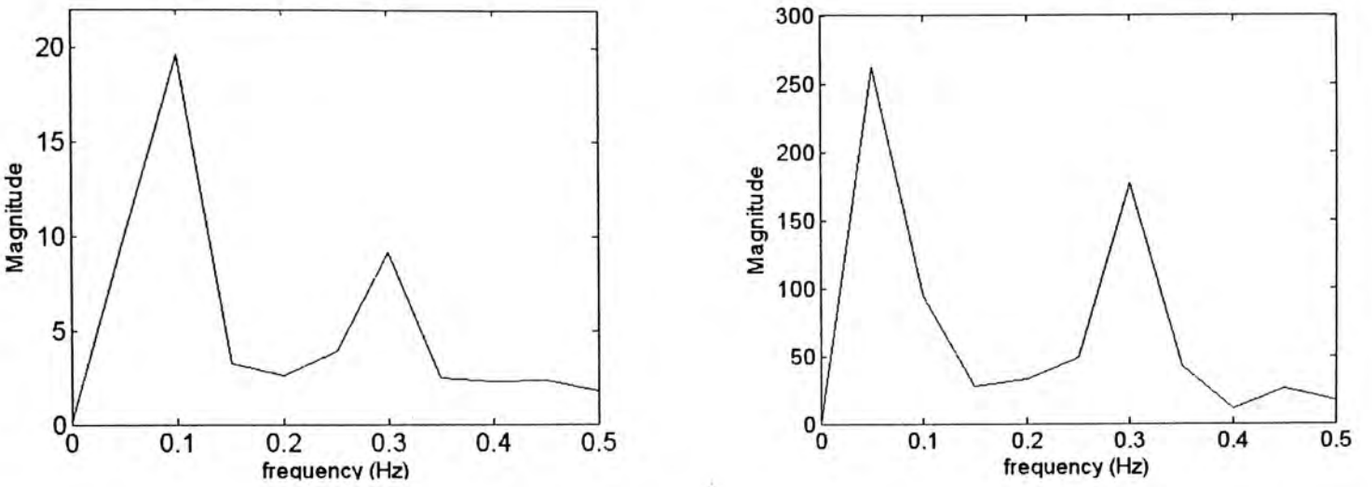

(a) (b)

Fig 5-22: Spectra of SBP from (a) simulated data and (b) experimental data.

Fig. 5-23 shows the cumulative LF and HF power percentages of the RR interval and SBP obtained from both the simulations and the experimental data for 10 healthy subjects, respectively. It can be seen that from either the simulation or the experimental data, the RR interval provides comparable results with that of SBP in terms of LF or HF power percentage. Indeed, there is prominent consistence between the spectra of RR interval and SBP [40], and they serve as alternatives to analyze the mechanisms responsible for the cardiovascular control.

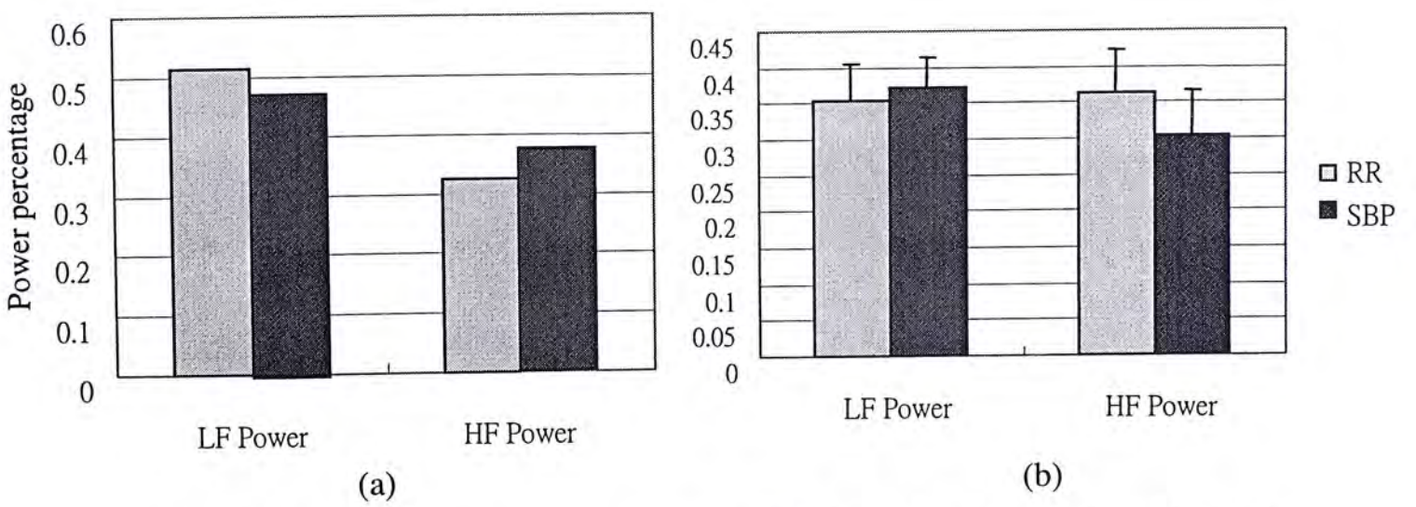

(a) (b)

Fig. 5-23 LF and HF power spectra densities of RR interval and SBP obtained from (a) simulated data and (b) experimental data ($mean \pm SD$, $n = 10$).

Besides the measure of individual LF or HF power, the ratio between LF power and HF power also carries valuable information associated with the balance of the sympatho-vagal control mechanism affecting the heart rate. Fig. 5-24 gives the comparison between the simulated LF/HF ratio and that from experimental data (the same subjects as used in Fig. 5-23). Obviously, the simulated results are within the normal physiological range.

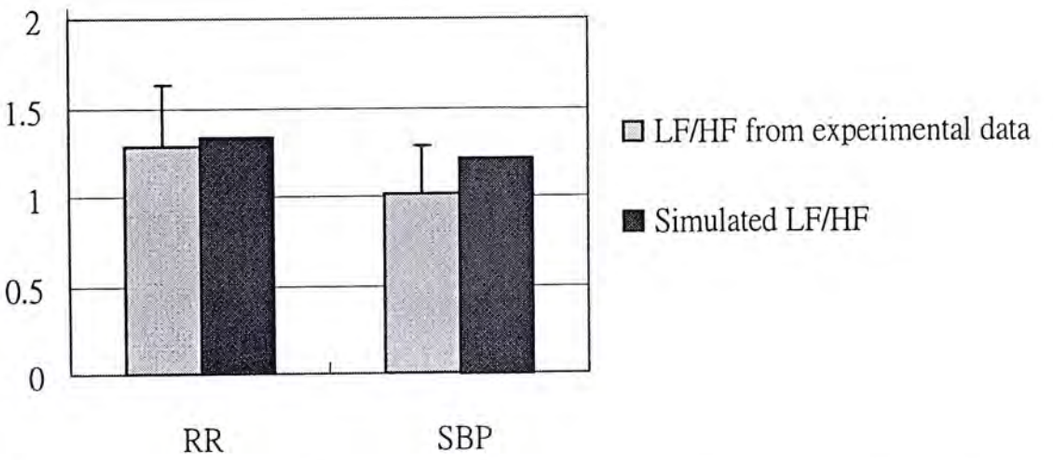

Fig. 5-24 LF/HF ratio of RR interval and SBP obtained from simulation (dark columns) and experimental data ($mean \pm SD$, $n = 10$, light columns).

Considering that DBP is fixed in the new model while SBP varies from beat to beat, we use SBP is used as the input to the transmission time delay generator. The parameters a and b can be predetermined for each individual subject through linear regression. In this simulation, the subject in Fig. 5-17 and 5-18 is used as an example to obtain a and b, and the PPG signals can therefore be generated with reasonable time-varying PTT calculated from $PTT = a \bullet SBP + b$ ($a = -1.6678$ *and* $b = 342.5584$). The results of the simulated PTT series and its spectrum are given in Fig. 5-25.

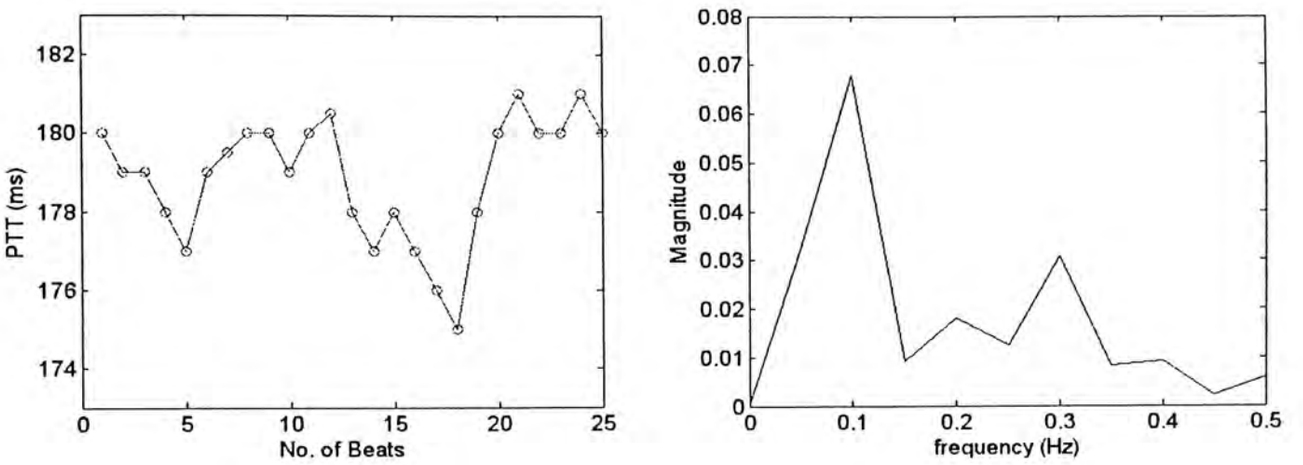

Fig. 5-25 (a) Simulated PTT series and (b) its spectra.

Fig. 5-26 gives the phase spectra of ECG signal and pressure wave, respectively. From the experimental data of simultaneously recorded ECG and figure pressure wave (see Fig. 5-26 (b)), it is clearly indicated that these two signals are almost in phase with each other. Our simulated data provide similar results, as shown in Fig 5-26 (a), which further demonstrates the feasibility of using the sigmoidal function to interpret the feed forward relationship between heart rate and BP, and therefore paving the way for the generation of beat-to-beat BP series in our model.

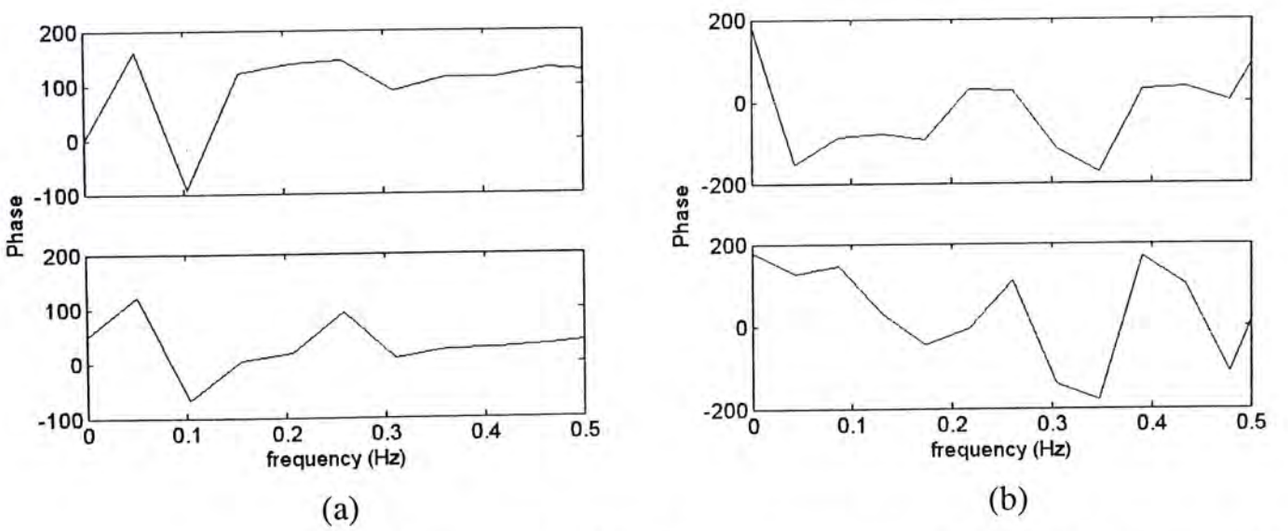

Fig. 5-26: The phase spectra of ECG (upper panel) and pressure wave (lower panel) from (a) simulated data and (b) experimental data.

The modification to include the time-varying PTT in the PPG model, as a result, could also affect the phase spectra of simulated PPG signals, as shown in Fig. 5-27. It can be noticed that the simulated phase spectrum of PPG signals with variable PTT becomes more realistic compared with that of experimental data than the results of our previous simulation with a constant PTT (see Fig. 3-17). The spectra of ECG and PPG signals, on the other hand, remain almost unchanged.

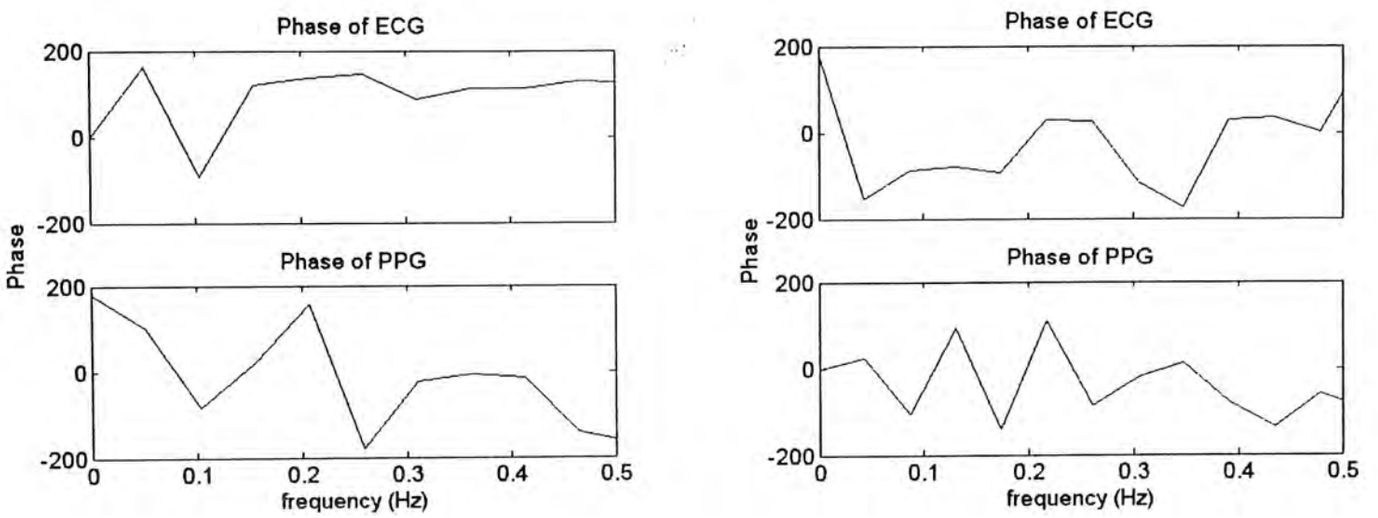

Fig. 5-27: (a) Phase spectra of PPG and ECG signals with time-varying PTT; and (b) Phase spectra of experimental PPG and ECG signals.

5.4.3 Application of the PPG Model

The above modifications have made the new model more comprehensive and physiologically plausible by including the approximated beat-to-beat BP series, and thereby mimicking the generation of PPG signals with time-varying PTT. The modified model could be a useful tool to investigate certain characteristics of PPG signals under different physiological conditions.

Take an example that is after the administration of certain vasoactive agents, such as ephedrine and phenylephrine, which could have an effect on the duration of

PEP, i.e. PEP decreases by the inotropic action after ephedrine and it increases by reflex negative inotropic action after phenylephrine. Under such conditions, the PTT assessed by the time delay between the R peak of the ECG signal and the onset of the PPG signal, which actually includes the PEP and the transmission time, could no longer exhibit a significant linear relationship with arterial BP, or at least the slope (parameter a) or the intercept (parameter b) may change. On the other hand, there is little influence on the relationship between the actual transmission time and the arterial BP. In other words, the new model is still workable under such abnormal physiological conditions. However, the PTT based BP estimation is likely to provide unsatisfactory results under such conditions.

Assume that the PEP is 10% shortened after the administration of ephedrine. A simulation is done to investigate the difference between the PTTs before and after the administration of ephedrine, as shown in Fig. 5-28. Obviously, if the same equation for the PTT based BP estimation is used, there is inevitably a biased error after the administration of ephedrine.

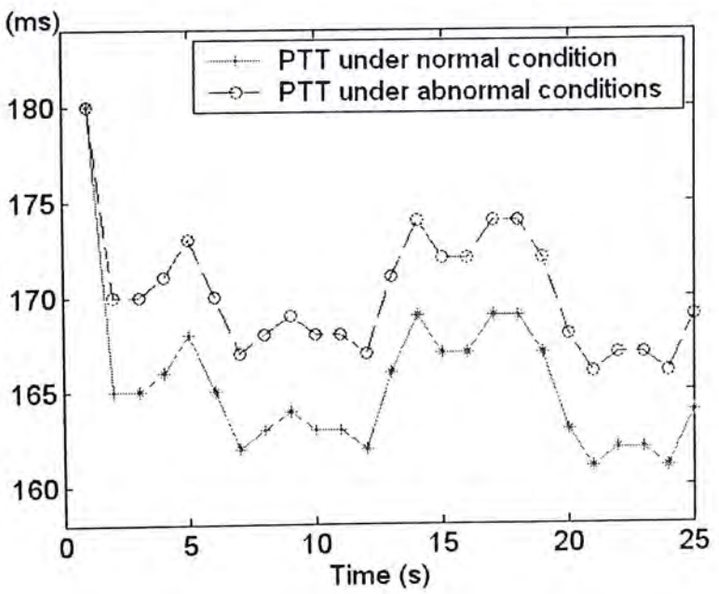

Fig. 5-28: Simulated PTT series under normal and abnormal physiological conditions.

To investigate the effect of the conditions under different physiological status on PTT, such as the dynamic state immediately after exercise, it is necessary to adjust or further modify the sigmoidal function that is derived on a steady-state basis since it may not be well applicable to an abnormal physiological status. It is therefore of great importance to understand better the relationship between the heart rate and BP under different physiological status, and thereby enabling the new model for more comprehensive studies.

5.5 Discussion & Conclusion

As one of the most important cardiovascular parameters, the arterial BP has been studied extensively. Most of the currently used approaches for the BP estimation are still based on the auscultatory measurement and the oscillation method. These cuff-based methods, however, could only provide discrete BP measurements, and therefore can hardly tell the beat-to-beat hemo-dynamic information.

The beat-to-beat oscillatory behavior of BP has been known for long time. The analysis of the oscillations in BP plays a fundamental role for a better comprehension of the patho-physiological properties of the complex mechanisms which act through neural, mechanical, vascular, humoral factors [40]. The currently available methods for beat-to-beat BP monitoring include intra-arterial (invasive) recordings and some non-invasive approaches which have already been commercialized, such as the tonometer and the Finometer (FINAPRES), etc. Certain limitations such as the lack in patients' comfort, the difficulty in manipulating or positioning the cuff, and the high cost, etc, have undoubtedly kept these methods from being extensively used.

In this chapter, the feasibility of a new approach for the beat-to-beat BP estimation is studied. It simply employs a beat-to-beat parameter extracted from PPG signals, the FY interval. The results from last chapter show that there is a significant

correlation between PTT and FY interval. Taking into account the relationship between PTT and BP, the estimation of BP using the FY interval was carried out similarly to the PTT-based BP estimations. The accuracy in both discrete and beat-to-beat BP estimation was investigated using the standard BP monitor or the FINAPRES as reference. The result from the FY interval based approach was also compared with PTT-based approach.

For either multi-beat or beat-to-beat estimation, the result of FY interval based approach is satisfactory in comparison with the AAMI standard for the group of subjects used in our study. It is comparable to or even better than the result from the PTT-based method. It is therefore a promising approach to realize the beat-to-beat BP monitoring using the PPG signal only even at natural strength of the contacting force. This is because the correlation between FY interval and PTT can also be quite high with the normal strength of contacting force for some subjects. In the future development, with a finger clip to fix a moderate level of the contacting force, the estimation of the beat-to-beat BP could possibly achieve better accuracy. There are certainly a number of distinguished advantages in this new approach, including much lower cost, the ease in the measurement, the improvement in patients' comfort, etc. Furthermore, it should be emphasized that by discarding the use of a cuff, this new approach could possibly provide beat-to-beat BP measurement that is continuous for as long as necessary with a single PPG sensor, while the person may still have the flexibility to move around.

The accuracy in the analysis of the beat-to-beat BPV using this new approach is also investigated. Particularly, the spectral analysis could provide insight into understanding the similarity in the elementary rhythms of the estimated BP and the BP obtained from FINAPRES. The spectral characteristics of each individual frequency band can be described in terms of the power percentages. All power percentages of

SBP and DBP over the frequency ranges considered in our study were evaluated by analysis on both the estimated BP and the BP obtained from FINAPRES.

For the LF band, the FY interval based method gives underestimated power percentages. On the contrary, for the HF band, it gives overestimated power percentages. Both the underestimation and overestimation are around 25%. This result indicates that there are certainly different relationships between LF and HF rhythms of BP and FY interval. Specifically, according to the individual spectra and the MSC functions, it is found that the main difference is in the absolute power of LF band, which is remarkably lower in the spectra of the estimated BP using either FY based or PTT based approach. The absolute values of the HF power are in fact almost the same in all three spectra. Therefore, it is concluded that the only significant difference between the proposed new approaches, using both FY interval and PTT, and the Finapres in the spectral estimation is the underestimation of LF power. The main factor causing this discrepancy might be associated with the sympathetic nervous control. Further studies to explore the underlying relationship between sympathetic nervous activity and FY interval and PTT could be extremely useful in improving the accracy of this new approach from physiological point of view.

Nevertheless, this new approach is still of great potential as an acceptable substitute for estimation of the beat-to-beat BP or BPV. It should be pointed out that the BP recordings from FINAPRES may not be accurate enough. In fact, several studies have investigated the reliability of the FINAPRES device. By comparing with the simultaneously obtained BP values by inter-arterial cannulation, it has been reported that the LF power of SBP is overestimated by FINAPRES [40], [67]. In this sense, the FY interval based (or PTT based) method could probably provide much better estimations of the actual arterial BP. In other words, the true accuracy of this new method might be higher than that reported in this study by using FINAPRES as

reference.

So far, the simplest equation was applied to BP estimation and the results are reasonable. It is necessary to improve these equations, as well as the calibration approaches, to enhance the accuracy for the BP estimation. It could be useful by including other parameters which are also extracted from the PPG signal (see Chapter 4), or by integrating PTT together to estimate BP. Future work on interpreting physiologically the relationship between these parameters and arterial BP will be important to improve this new method before it can finally be put into use practically.

Considering the importance of the beat-to-beat oscillatory BP, as well as the beat-to-beat varying nature of PTT, the new PPG model proposed in this study has been further modified by integrating the relationship between the heart rate and BP, and the nearly linear relationship between PTT and BP. Based on the physiological mechanism of baroreflex control and the empirical sigmoidal law, the modified PPG model is able to generate more realistic BP (SBP and mean BP) series. Furthermore, using the BP series as an input for the time delay generator, the PTT series were generated varying with each heart cycle. As a result, the discrepancy in phase between the simulated spectra and the spectra of experimental data from a normal subject has to some extent been addressed.

From the application point of view, the modified model could be a useful tool to investigate certain characteristics associated with PPG signals under different physiological conditions. For example, the effect after the administration of certain agents can be reflected by the change in PEP; and other variations in physiological status can possibly be interpreted by adjusting or further modifying the sigmoidal function between the heart rate and BP. Furthermore, the new model could be of certain importance in evaluating the PTT or FY interval based BP estimation from physiological point of view. It may be noticed that in the mathematical derivation of

the output PPG signal (see Eq. 5-5), not only PTT but the impulse response of the Windkessel model ($h(t)$) as well as the dynamic BP waveform ($p_{BP}(t)$) are to some extent associated the beat-to-beat arterial BP. Therefore, the accuracy of the PTT or FY interval based BP estimation can be enhanced by taking into account some other physiological parameters.

By realizing the generation of time-varying BP and PTT, the proposed model is improved to better mimic the PPG signal. As mentioned before, PTT is a valuable parameter for various applications. In other words, the new model consequently carries plenty of useful information related to PPG and ECG signals. However, the feasibility of the new model has not been fully tested for the generation of beat-to-beat SBP or mean BP. Also, DBP is so far simplified as a constant. Future research should further investigate the complex interaction between the heart rate and blood pressure, and it is desirable that the pulse generator in the current model could possibly be improved to more realistically render dynamic information of both SBP and DBP.

Chapter 6

A Novel Biometric Approach

6.1 Introduction

Automatic human authentication using biometrics is an emerging important technology to secure human interactions with safety systems. Its potential application can be great in many different areas such as telemedicine or e-banking. Nowadays, most systems that control access to financial transactions, computer networks, or secured locations still identify authorized persons by recognizing passwords, or ID cards. These systems are not reliable enough, because the information is easy to be stolen or forged. Being able to eliminate such common problems, biometric systems, which use unique human physical or behavioral characteristics to automatically identify a person, can ensure much greater security or confidentiality.

Biometric approaches used today have been made possible by the explosive advances in computing power, and have been made necessary by the widespread connection of computers all over the world. Certain characteristics of our bodies or features of our behaviors have been studied as means of human identification, such as fingerprint, face [69] [70], voice [71], retina/iris [72], lip movement [73], gait motion [74], electroencephalograph (EEG) [75], and ECG [76] [77]. New applications based on these biometric approaches would provide us with a promising and irrefutable future of human identification. However, fingerprint can be recreated in latex, face recognition can be fooled by a photo, voice can be imitated [78], and the methods based on EEG or ECG are to some extent cumbersome because several electrodes are required to pick up the bio-signals.

The PPG technique is under increasing recognition for extensive applications. In this chapter, it is proposed to use PPG signals for human verification. Compared with other biometric approaches, PPG technique has several distinct advantages including low development cost, easy to use without any complicated procedure or special skill, and conveniently accessible to various sites of human body, such as finger, ear lobe, wrist or arm. The specific aim of this work is to investigate the feasibility of this new approach. The preliminary results of the experiments performed on the fingertip of the subjects demonstrate that the PPG approach is promising for human verification.

6.2 Human Verification by PPG Signal

In this section, a new application of PPG signals for human verification is introduced. Different approaches for decision-making are used to study the feasibility of this new method.

6.2.1 Experiment

The PPG data were obtained from 17 healthy subjects, aged 23-30. During the experiment, all the subjects sat still on a chair and let their muscle relaxed. The PPG probe (reflective), consisting of a LED and a photodetector, was attached on the fingertip of the right index finger by a belt. PPG signals were recorded continuously for about one minute for each person, and converted into digital signals at the sampling rate of 1K samples/s.

The raw data were preprocessed by filtering the low frequency and high frequency components. The PPG signals from three different subjects are shown in Fig. 6-1, in which distinct features can be observed from each individual signal from a certain subject.

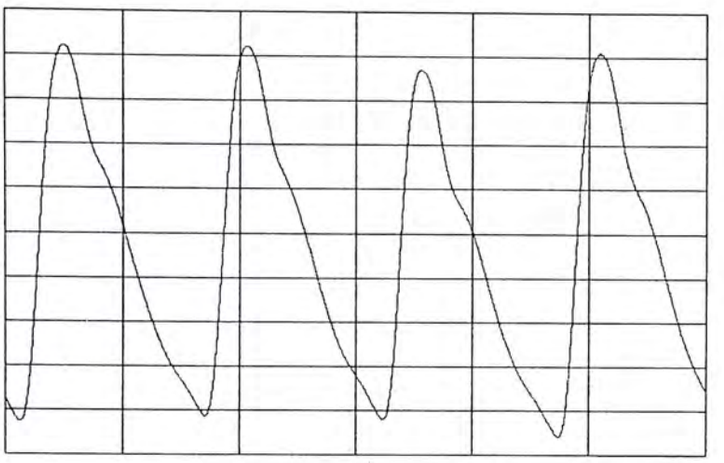

(a)

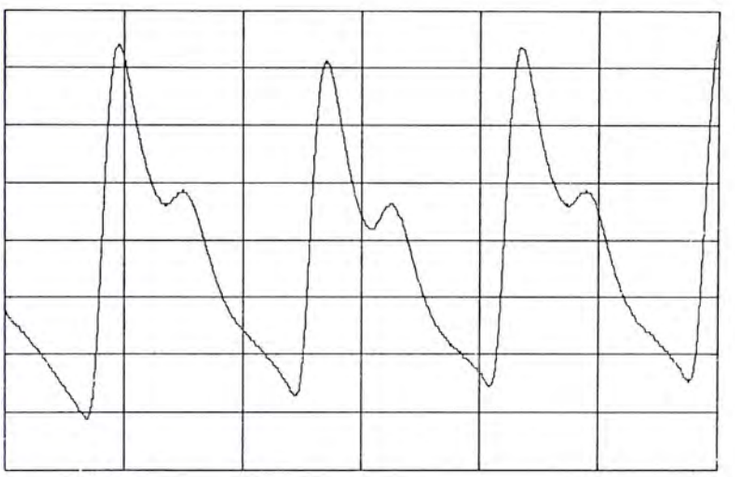

(b)

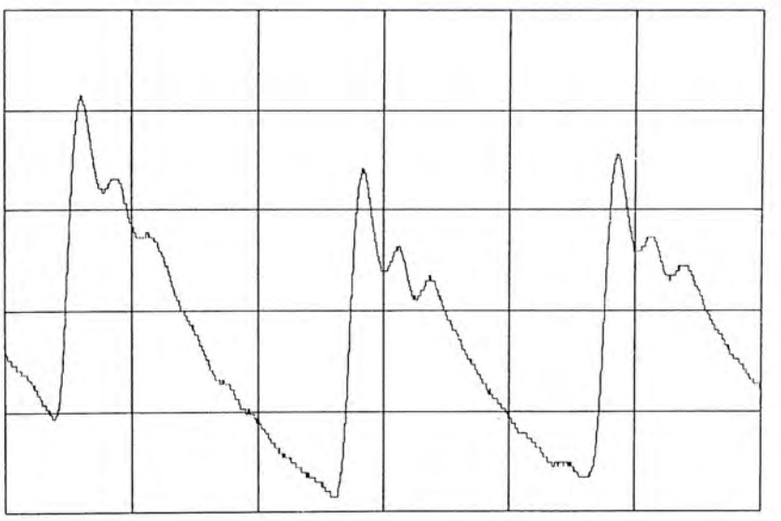

(c)

Fig. 6-1: PPG signals from three different subjects.

6.2.2 Feature Extraction

As shown in Fig. 6-1, distinct characteristics of the PPG signal can be observed in different subjects. Therefore, four feature parameters -- peak number, time interval, upward slope and downward slope -- were extracted from the PPG signals of each subject (see Fig. 6-2). The four features are defined as follows:

1) The peak number M : the number of peaks on each pulse;
2) The upward slope k_1: the slope between the bottom of each waveform and the first peak;
3) The downward slope k_2: the slope between the last peak of each waveform and the bottom;
4) The time interval t_1: the time interval between the bottom point and the first peak point;

The template vector consisting of four average feature parameters was then formulated for each subject.

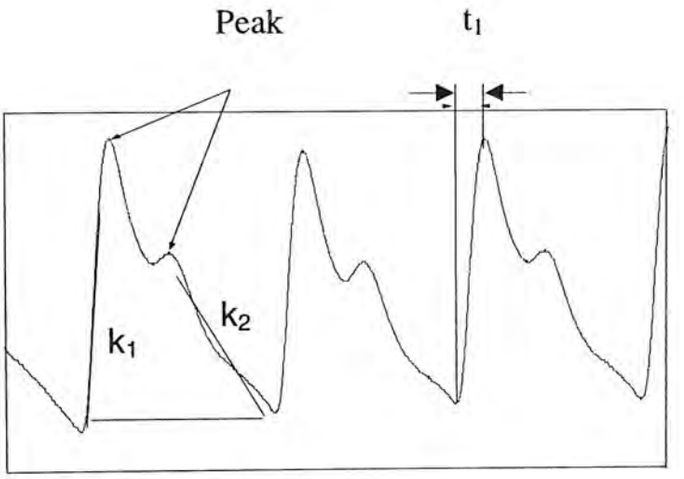

Fig. 6-2: The definitions of the four features extracted from the PPG waveform.

6.2.3 Decision-making

1) *Euclidean distance*

In order to determine the discriminability of the four features and the weight P_j of each parameter, a statistical analysis was performed. A ratio F_j between the interclass and intra-class variabilities as defined in Eq. (6-1) was calculated. The higher the ratio, the more discriminant the feature is.

$$F_j = \frac{Interclass\ Variability}{Intraclass\ Variability} = \frac{\sqrt{\frac{1}{N}\sum_{i=1}^{N}(\overline{y_{ij}} - \overline{u_j})^2}}{\frac{1}{N}\sum_{i=1}^{N}\sqrt{\frac{1}{K_i}\sum_{k=1}^{K_i}\left(y_{kij} - \overline{y_{ij}}\right)^2}} \quad , \tag{6-1}$$

where F_j is the ratio for the *jth* feature, $\overline{y_{ij}}$ is the mean of the *jth* feature of the *ith* subject, $\overline{u_j}$ is the mean of *jth* feature, y_{kij} is the *jth* feature of the *kth* pulse of the *ith* subject, N is the number of subjects, and K_i is the number of pulses used for feature extraction from the *ith* subject.

The verification was carried out by comparing the sample vector obtained at different periods of time with the template feature vector. The final decision was made based on the Euclidean distance, d, combined with the weight p_j of each feature parameter,

$$d = \sqrt{\sum_{j=1}^{L} p_j (x_j - t_j)^2} \quad , \tag{6-2}$$

where L being the dimension of the feature vector, P_j the weight coefficient which is determined by the percentage of F_j distributed to the *jth* feature, x_j the *jth*

component of the sample feature vector, and t_j the jth component of the template feature vector.

The Euclidean distance, d, between each sample vector and each template vector was calculated. The decision of the verification was done on the subject with the minimum value of d.

2) Fuzzy logic

Fuzzy logic was implemented for decision-making, in which an output score was generated as the result of the comparison between the enrollment template and the newly generated one. The Gaussian Function was selected as the membership function (MF), which can be expressed as follows:

$$G\{x;\mu_{ij},\sigma_{ij}\} = \exp(-(x-\mu_{ij})^2 / 2\sigma_{ij}^{\ 2}) \qquad (6\text{-}3)$$

where μ_{ij} is the average value of the jth feature parameter of the ith subject, and σ_{ij} is the standard deviation of jth feature parameter of the ith subject.

The degree of membership for each feature parameter was determined by the maximum value of the overlapped area created by the Gaussian curves of the two templates. Fig. 6-3 illustrates how the approach works: the enrollment template parameter is $t_i = 1.852 \pm 0.076$; while the newly generated template parameter is given by $s_i = 1.784 \pm 0.057$.

Inserting the two sets of parameters into (6-3) respectively generates two curves as shown in Fig. 6-3. The shadowed area is overlapped by the two curves and the maximum value is recorded as the membership degree. The values inclining towards 1

on the vertical axis indicate a good match, while those inclining towards 0 represent a poor match.

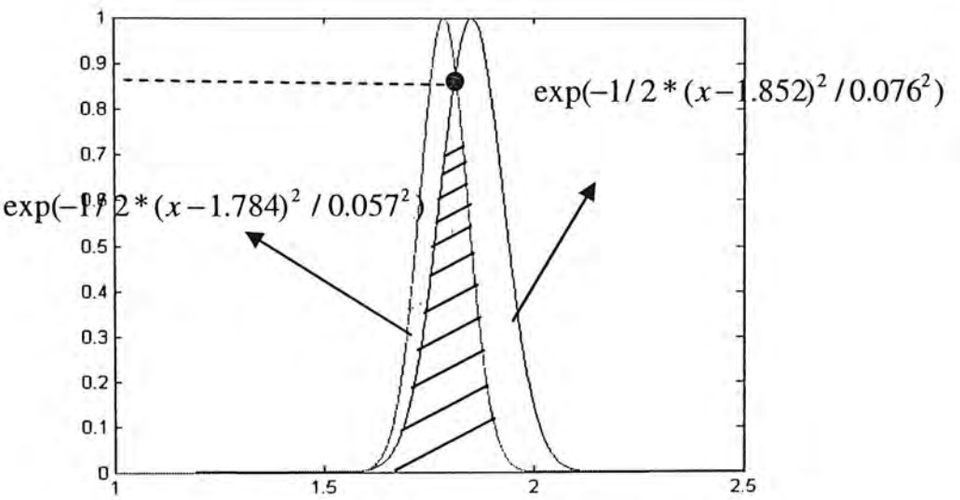

Fig. 6-3: The Gaussian curves generated by the two templates.

In this way, each newly generated feature parameter will produce a value comparing with the enrollment template parameter. This leaves four membership values for a single subject, which must be consolidated using an AND operator to obtain a final output score that lies between 0 and 1. Normally, the fuzzy logic AND operator takes the minimum value of all the membership values [80]. However, in practice it shows that the minimum value often does not reflect the true degree to which two templates match [81]. So finally, a type of MEAN operator was utilized, which takes the weighted average of the four membership values.

The verification was also carried out by comparing the two templates generated in the same trial but at different periods of time.

6.2.4 Results

1) *Euclidean distance*

Table 6-1 gives the results using Euclidean distance based decision-making. Each cell represents the calculated distance between the template and the sample. The shortest distances are shadowed.

Table 6-1: PPG Verification results using Euclidean distance based decision-making.

	d1	d2	d3	d4	d5	d6	d7	d8	d9	d10	d11	d12	d13	d14	d15	d16	d17
1	0.008	2.529	14.852	0.859	22.203	0.599	6.443	0.219	0.649	178.457	1.004	84.296	21.852	0.750	29.502	2.408	65.682
2	2.604	0	5.286	0.989	12.755	0.795	1.164	3.002	3.988	141.154	1.623	61.29	11.588	2.710	15.882	0.215	49.534
3		3.152	0.340	7.417	8.883	6.739	1.742	11.646	14.148	106.983	8.350	42.896	7.245	10.936	7.517	3.809	39.634
4	0.848	1.320	11.270	0.025	20.194	0.369	4.319	0.845	0.824	167.652	1.406	78.385	18.799	1.626	25.239	1.596	62.172
5	22.135	12.166	9.286	18.524	0.017	17.963	6.258	25.003	25.517	80.58	13.925	21.091	0.307	16.731	2.267	10.445	12.809
6	0.344	1.712	12.156	0.346	22.435	0.198	5.538	0.216	0.942	173.851	1.632	82.902	21.422	1.706	27.917	2.075	66.867
7	4.900	0.583	4.094	2.647	8.008	2.510	0.139	5.805	6.498	125.863	2.305	50.530	7.001	3.772	10.800	0.402	39.465
8	0.139	2.829	15.006	0.885	25.044	0.639	7.342	0.003	0.705	183.281	1.906	88.765	24.355	1.651	31.679	3.078	71.043
9	0.624	3.784	17.563	0.981	26.379	1.403	8.197	0.509	0.025	188.78	2.198	91.834	25.318	1.695	33.601	3.887	71.809
10	187.873	148.300	104.335	171.926	87.912	170.373	125.273	193.031	197.884	0.396	166.310	25.231	85.748	176.945	68.700	147.304	55.600
11	2.294	1.190	9.315	1.896	10.633	1.572	2.018	3.424	3.690	144.55	0.289	60.353	10.599	0.895	16.823	0.431	44.167
12	128.813	96.984	63.905	116.180	48.224	114.887	78.224	133.515	137.134	4.192	110.471	6.921	46.865	119.048	34.953	95.651	26.741
13	25.043	13.694	9.321	20.347	0.415	20.188	7.036	27.854	27.979	74.793	16.348	18.568	0.091	19.457	1.356	12.137	11.600
14	1.185	3.073	15.411	2.188	16.426	1.858	5.451	2.230	2.055	166.688	0.240	74.063	16.849	0.041	25.122	2.072	53.664
15	29.916	15.879	6.835	23.910	2.546	23.537	8.693	32.295	33.639	63.222	21.422	15.136	1.438	25.359	0	15.132	14.169
16	2.741	0.146	5.276	1.545	11.383	1.030	1.115	3.363	4.662	138.338	1.433	58.878	10.683	2.544	14.995	0.141	47.080
17	75.230	57.904	48.400	69.374	16.665	69.047	43.732	81.187	79.680	49.106	58.245	8.727	18.623	62.579	19.603	53.489	0.447

The performance of this approach is evaluated by the ROC curve, as shown in Fig. 6-4. The individual points on the curve represent the verification results as genuine acceptance rate vs false acceptance rate with different thresholds. The values of the thresholds are: 0.01, 0.02, 0.03, 0.05, 0.10, 0.14, 0.15, 0.20, 0.30, 0.34, 0.40, 0.45, 0.60, 1.0, 3.0, 6.0, 7.0, and 8.0. It is found that when the threshold is around 0.45, the best performance can be achieved. That is, the genuine acceptance equals to 16/17, while the false acceptance rate is less than 0.05.

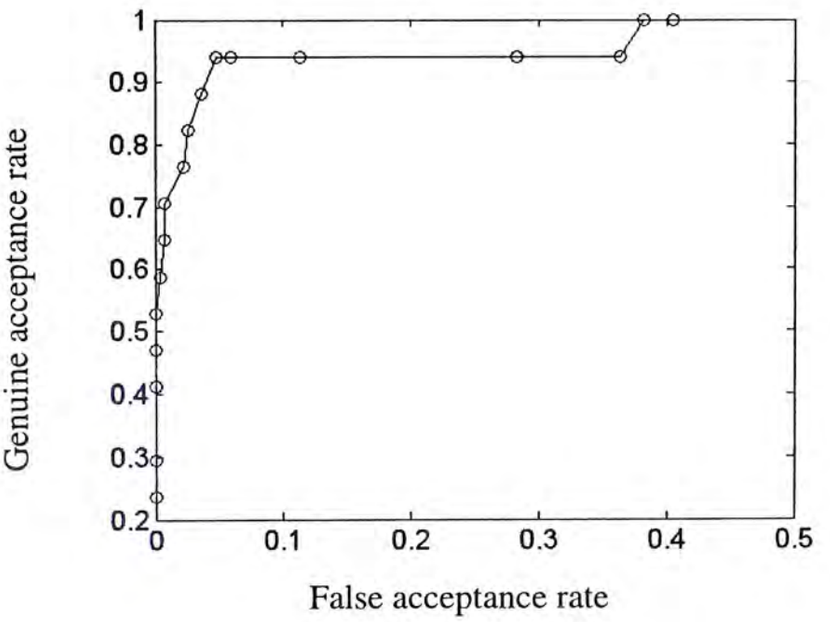

Fig. 6-4: Performance of the PPG verification using Euclidean distance.

2) Fuzzy logic

Table 6-2 gives the results using Fuzzy logic based decision-making. Each cell represents the averaged membership degree between the template and the sample. The largest final output scores are shadowed.

Table 6-2: PPG verification results using fuzzy logic based decision-making.

	1	2	3	4	5	6	7	8	9	10	11	12	13	14	15	16	17
1	0.982	0.478	0.388	0.492	0.291	0.532	0.168	0.699	0.322	0.064	0.407	0.299	0.075	0.330	0.298	0.263	0.053
2	0.575	1.000	0.508	0.638	0.369	0.538	0.519	0.475	0.413	0.232	0.481	0.468	0.256	0.477	0.466	0.581	0.205
3	0.380	0.310	0.839	0.168	0.264	0.253	0.339	0.463	0.105	0.102	0.276	0.228	0.162	0.253	0.377	0.315	0.155
4	0.414	0.315	0.062	0.674	0.203	0.548	0.226	0.281	0.635	0.329	0.083	0.250	0.371	0.098	0.210	0.167	0.253
5	0.415	0.664	0.431	0.475	0.995	0.584	0.672	0.420	0.397	0.368	0.450	0.472	0.863	0.374	0.680	0.635	0.516
6	0.903	0.675	0.433	0.847	0.610	0.905	0.572	0.895	0.845	0.402	0.688	0.479	0.480	0.609	0.421	0.716	0.409
7	0.599	0.808	0.841	0.715	0.723	0.712	0.963	0.609	0.667	0.475	0.782	0.585	0.716	0.672	0.644	0.908	0.666
8	0.945	0.482	0.452	0.615	0.335	0.654	0.221	0.998	0.557	0.107	0.551	0.327	0.125	0.477	0.302	0.366	0.072
9	0.658	0.396	0.342	0.645	0.321	0.425	0.493	0.697	0.970	0.457	0.441	0.438	0.470	0.427	0.496	0.343	0.382
10	0.003	0.012	0.001	0.025	0.145	0.156	0.108	0.001	0.420	0.942	0.173	0.162	0.487	0.044	0.009	0.225	0.404
11	0.799	0.731	0.661	0.767	0.549	0.894	0.626	0.802	0.565	0.328	0.897	0.438	0.402	0.737	0.403	0.844	0.268
12	0.398	0.542	0.528	0.552	0.519	0.388	0.550	0.409	0.463	0.687	0.280	0.723	0.537	0.231	0.671	0.412	0.507
13	0.287	0.488	0.418	0.395	0.709	0.449	0.617	0.262	0.591	0.537	0.4500	0.356	0.987	0.401	0.575	0.543	0.870
14	0.389	0.362	0.272	0.138	0.188	0.333	0.136	0.288	0.297	0.012	0.507	0.080	0.012	0.961	0.019	0.399	0.256
15	0.288	0.449	0.693	0.528	0.538	0.292	0.590	0.280	0.463	0.391	0.210	0.489	0.695	0.147	1.000	0.348	0.380
16	0.531	0.872	0.431	0.307	0.270	0.349	0.265	0.460	0.081	0.054	0.494	0.262	0.056	0.477	0.301	0.603	0.054
17	0.084	0.231	0.108	0.158	0.308	0.167	0.254	0.099	0.305	0.438	0.094	0.260	0.540	0.305	0.172	0.203	0.985

The ROC curve to evaluate the performance of this approach is shown in Fig. 6-5. The values of the thresholds are: 1, 0.99, 0.98, 0.96, 0.94, 0.92, 0.9, 0.85, 0.8, 0.75, 0.7, 0.65, 0.6, and 0.5.

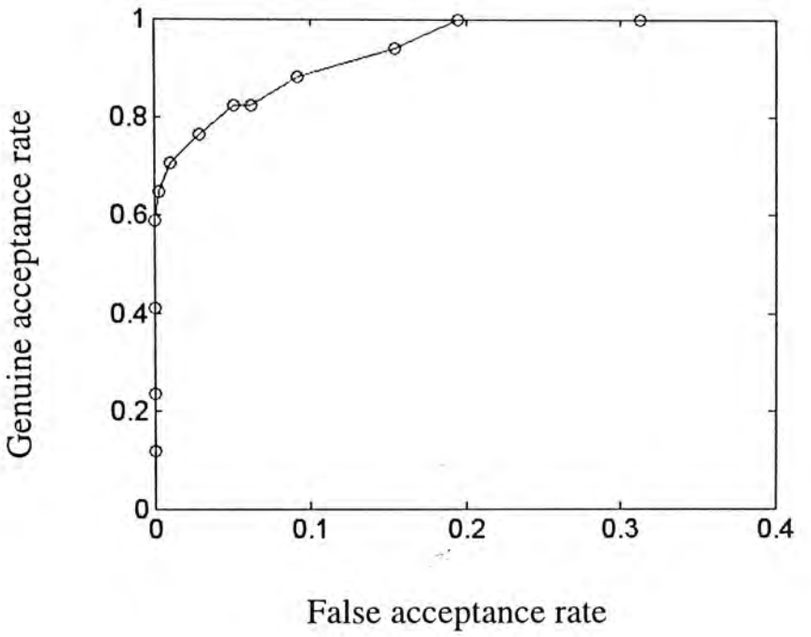

Fig. 6-5: Performance of the PPG verification using fuzzy logic.

6.3 Discussion

A new approach of using PPG signals for human verification is presented in this chapter. The verification is accomplished by simply putting the fingertip on the PPG sensors. The result of this study shows that the PPG signals have predominant characteristics that can be used to identify different persons. Considering the physiological mechanism of the PPG generation, as described in Chapter 3, the stability in features of the PPG signal can be a result of the almost unchanged physiological status as well as the properties of the arterial system under normal relaxed conditions for healthy subjects.

According to the experimental results, the rate of correct verification can reach up to 94% (one out of seventeen in errors), while the false acceptance rate is within 5%. The false authentications were mainly attributed to the poor quality of the signals from the subjects, perhaps due to respiration and motion artifacts, which resulted in some distortions in the template feature vector.

Two approaches for decision-making were implemented: 1) Euclidean distance;

and 2) Fuzzy logic. The performances of the verification under these two different approaches were evaluated by the ROC curve respectively, which indicates that the Euclidean distance approach seems to achieve better verification results. However, this might be due to the small size of database studied in this work. In other words, the fuzzy logic approach could be more efficient for a large number of subjects.

The results presented above are under the condition that the template and the sample were within the same trial. For those generated from different trials, the result is not yet satisfactory. This is perhaps mainly due to the variations in the contacting force applied on the PPG sensor during different trials, which could probably influence the contour of the PPG signal to a large extent. In the future development, a finger clip would be preferable, which is able to achieve relatively stable contacting force for each subject. Also, further research based on large database must be done to improve this new method before it can be finally put into use in practice.

Chapter 7

Conclusions

7.1 Conclusions of Major Contributions

The extensive use of PPG signals in various applications has attracted great interest in studying its physiological generation mechanism, and in investigating certain characteristics of the PPG waveform for the evaluation of clinically useful physiologic parameters. In this thesis, a new model is developed for the generation of the PPG signal based on its physiological mechanisms. The investigation on the features of the PPG waveform in this study has lead to two important new applications of this signal.

The first part of this thesis is focused on a theoretical study of spectral characteristics of the IPFM model. In this part, with a single sinusoidal signal as the input modulation signal to the IPFM model, an expression for the relationship between the instantaneous firing rate and the intensity of the input signals is derived. The corresponding output of the IPFM model and its spectra are also studied from demodulation point of view. It is found that the output of the IPFM demodulator without noise is actually the approximated instantaneous firing rate rather than the original input modulation signal as reported before in several literatures [5] [6] [7] [8]. Simulations with different patterns of the input modulation signals are carried out under certain restrictions on the modulation depth and frequencies. The result further demonstrates that without the knowledge of the threshold, it is practically implausible to recover precisely the input modulation amplitude or intensity information. Meanwhile, it is also found that the firing rate function can be reconstructed with

reasonable accuracy by a simple LPF, which can be even applicable to more generalized input signals.

Based on the simple but powerful structure of the IPFM model, a mathematical model is developed for the generation of PPG signals. Taking advantage of the two fundamental models, the IPFM model and the Windekessel model, together with the transmission properties of the pressure wave, the new model proposed in this study can reasonably mimic the physiological generation process of PPG signals. The simulation result indicates that though under certain simplifications, the model does correctly produce a number of important features of the PPG signal in both time and frequency domains, as well as the relationship between ECG and PPG signals with certain time delay. The relationship between the input modulating signal and the output of the proposed model is also studied. It is found that the modulation depth and the mean value in the fluctuant input signal are two important quantities that have an effect on HRV. It is also found that the PSD of ECG and PPG trains may serve as an alternative to evaluate the HRV by analyzing the power of the sidebands. These results could be of certain diagnostic value, and may be useful in explaining phenomena under some physiological and pharmacological conditions.

The features on the waveform of the PPG signal obtained from experimental data are studied from statistical point of view in the third part of this thesis. In this part, a significantly high correlation ($r = 0.962 \pm 0.029, \quad p < 0.0001$) was found between the RR interval of the ECG signal and the YG interval of the PPG signal. The FY interval of the PPG signal also exhibits a high correlation ($r = -0.8383 \pm 0.0912$, $p < 0.0001$) with the PTT at a relatively high contacting force between the finger and the sensor; while at low temperature and at the dynamic state, moderate correlations can be observed between these two parameters. The correlation between the PTT and the RR intervals, on the other hand, is not significant. The results of this study indicate that the YG

interval could reflect to a large extent the relevant rhythm information associated with the duration of a heart cycle, while the FY interval might provide valuable information about the cardiac dynamics and the properties of the arterial elasticity under certain conditions.

Based on the results of the correlation study and considering the previously reported relationship between PTT and arterial BP [36] [38], a new approach for the beat-to-beat BP estimation is proposed in the fourth part of this thesis. For either multi-beat or beat-to-beat estimation, the result of the FY-based approach is satisfactory in comparison with the AAMI standard on the non-invasive BP evaluation. The results of this new approach, comparable to or even better than under certain conditions those from the PTT-based method, demonstrate that the beat-to-beat BP monitoring can be implemented using the PPG technique only, which would provide much more convenience for the continuous non-invasive BP measurement. The analysis of the beat-to-beat BPV is also carried out using this new approach. By comparing with the result from FINAPRES device, it is concluded that the only possible error of the new method in the spectral estimation is the underestimation of the LF power. Taking advantage of the relationship between heart rate and BP, as well as the nearly linear relationship between BP and PTT under the resting condition, the new model is modified considering time-varying BP and PTT, which indeed makes this model more physiologically plausible.

Considering its semi-repetitive nature, another new application of PPG signals is proposed for human verification. Although with a simple waveform, the PPG signal does contain characteristics that can be considered as unique identifiers specific to different persons while they are similar enough to recognize the same person. The preliminary result with a reasonable successful rate shows that this method is promising for human verification.

In summary, this thesis deals with a comprehensive study on simple but useful PPG signal, which not only provides an insight into better understanding the underlying mechanism of the PPG signal, but also results in two important new applications of the PPG signal for the non-invasive continuous BP monitoring and the human authentication.

7.2 Work to Be Done

For the first part of work, taking into account the detailed properties of the output events, it is necessary to further explore proper processing techniques before LPF in order to recover the original neural information faithfully.

For the further improvement of the new model for the generation of the PPG signal, it might be important to focus on the specialization of the pulse generator and the time delay generator. In fact, both the pressure wave contour and the time delay (PTT) are associated with the arterial BP. Further research on the complex interaction among heart rate, BP, pulse wave contour, and pulse wave velocity in the cardiovascular and arterial systems would be crucial to improve our model. Ideally, the pulse generator in the current model could possibly be improved to more realistically carry dynamic information of both SBP and DBP and thereby some timing intervals, and the time delay generator in the current model could also be modified for more accurate generation of the time varying PTT. Furthermore, the refractory period may also be taken into account so that the new model is able to better interpret the underlying mechanism of heart beat generation.

In order to enhance the reliability of the beat-to-beat estimation of BP and BPV, further studies to explore the physiological indications of the FY interval are extremely useful. It is also necessary to improve the estimation equations, as well as the calibration approaches. It could be useful to include other parameters which are

also extracted from the PPG signal, or by integrating PTT together to estimate BP. Future work on interpreting physiologically the relationship between these parameters and arterial BP will be important to improve this new method before it can be finally put into use practically.

For the new application of the PPG signal in biometrics, further research based on large database must be done. Also, it is important to explore features that are more stable within the same person while they can still be used to identify different persons. It is also desirable to further explore a better decision-making approach to improve the performance of the PPG-based authentication.

References:

[1] Echeverria J.C., Crowe J.A., Woolfson M.S., and Hayes-Gill B.R., "Application of empirical mode decomposition to heart rate variability analysis," *Medical & Biological Engineering & Computing,* **9(4)**: 471-479, 2001.

[2] de Boer R.W., Karemaker J.M., and Strackee J., "Spectrum of a series of point events, generated by the integral pulse frequency modulation model," *Medical & Biological Engineering & Computing,* **23(2):** 138-142, 1985.

[3] Bayly, E. J., "Spectral analysis of pulse frequency modulation in the nervous systems," *IEEE Trans. Biomed. Eng.,* **BME-15**: 257-265, 1968.

[4] Hyndman, R. D. and Mohn, R. K., "A model of the cardiac pacemaker and its use in decoding the information content of cardiac intervals," *Automedica,* **1**: 239-252, 1975.

[5] Rompelman, O., Snijders, J. B. I. M., and Van Spronsen, C. J., "The measurement of heart rate variability spectra with the help of a personal computer," *IEEE Trans. Biomed. Eng.,* **BME-29**: 503-510, 1982.

[6] Berger, R. D., Akselrod, S., Gordon, D. Cohen, R.J., "An efficient algorithm for spectral analysis of heart rate variability," *IEEE Trans. Biomed. Eng.,* **BME-33**: 900-904, 1986

[7] Mainardi, L. T., Bianchi, A. M., Baselli, G.,and Cerutti, S., "Pole-tracking algorithms for the extraction of time-variant heart rate variability spectral parameters," *IEEE Trans. Biomed. Eng.,* **42**: 250-259, 1995.

[8] Seydnejad, S. R. and Kitney, R. I., "Real-time heart rate variability extraction using the kaiser window," *IEEE Trans. Biomed. Eng.,* **44**: 990-1005, 1997.

[9] Fusheng Yang and Wangcai Liao, "**Modeling** and decomposition of HRV signals with wavelet transforms," *IEEE Engineering in Medicine and Biology,* **16**: 17 – 22, 1997.

[10] Hung-Wen Chiu and Tsair Kao, "A mathematical model for autonomic control of heart rate variation," *IEEE Engineering in Medicine and Biology*, **20**: 69 – 76, 2001.

[11] TenVoorde, B. J., Ree, E. F., Hack, W. W. M., Bergschneider, V. M., Hoekstra, B.P.T., Faes, T. H. J. C., and Rompelman, O., "Spectral quantification of respiratory sinus arrhythmia in preterm and fullterm neonates: beyond half the mean heart rate," *Automedia,* **13**: 15-31, 1990.

[12] Pyetan, E. and Akselrod, S., "Do the High-Frequency Indexes of HRV Provide a Faithful Assessment of Cardiac Vagal Tone?" *IEEE Trans. Biomed. Eng.*, **50**: 777-783, 2003.

[13] John K-J. Li., The arterial circulation: physical principles and clinical applications, Totowa, N.J.: Humana Press, c2000.

[14] Frank, O. Die, Grundform des arterielien Pulses. Z. Biol. **37**: 483-526, 1899.

[15] Frank, O. Die, Theorie der Pulswellen. Z. Biol. **85**:91-130, 1926.

[16] Fry, D.L. and Greenfield, J.C., Jr., Mathematical approach to hemodynamics with particular reference to Womersley's theory. In: Attinger, E.O.ed., Pulsatile Blood Flow, pp. 85-99, McGraw-Hill, New York, 1964.

[17] Li, J. K-J., "Pressure-derived flow: a new method," *IEEE Trans. Biomed. Eng.*, **BME 30**: 244-246, 1983.

[18] Cavalcanti, S. and Belardinelli, E., "Modeling of cardiovascular variability using a differential delay equation," *IEEE Trans. Biomed. Eng.*, **43**: 982 – 989, 1996.

[19] Ferreira, A.S., Filho, J.B., and Souza, M.N., "Identification of vascular parameters based on the same pressure pulses waves used to measure pulse wave velocity," *Proc. of the 23rd Annual International Conference of the IEEE EMBS*, **4**: 3418 – 3421, 2001.

[20] Gnudi, G. and Zanella, A., "Arterial Windkessel parameter estimation: a new frequency-domain method," *Computers in Cardiology*, pp: 329 - 332, 1995.

[21] Robert M. Berne and Matthew N. Levy., Cardiovascular physiology, St. Louis: Mosby Year Book, c1997.

[22] Allam, M.E. and Greenleaf, J.F., "Isomorphism between pulsed-wave Doppler ultrasound and direction-of-arrival estimation. I. Basic principles," *IEEE Transactions on*

Ultrasonics, Ferroelectrics and Frequency Control, **43**: 911 – 922, 1996.

[23] Sorvoja, H.S.S., Myllyla, R.A., Nissila, S.M., Karja-Koskenkari, P.M., Koskenkari, J.K., Lilja, M.K., and Kesaniemi, Y.A., "Systolic blood pressure accuracy enhancement in the electronic palpation method using pulse waveform," *Proc. of the 23rd Annual International Conference of the IEEE EMBS*, **1**: 222 – 225, 2001.

[24] Stevanov, M.; Baruthio, J.; Gounot, D.; "Projective MR measurements of pulse-wave velocity in the presence of reflected waves on an arterial model," *Computers in Cardiology*, pp: 215 – 218, 2000.

[25] Risacher, F., Jossinet, J., McAdams, E., Eynard, C., McLaughlin, J., and Schmitt, M., "Computation of the Pulse Wave Velocity in Limbs from Multichannel Impedance Plethysmography," *Proc. of the Annual International Conference of the IEEE EMBS*, **5**: 1744 – 1745, 1992.

[26] Franchi, D., Bedini, R.; Manfredini, F., Berti, S.; Palagi, G., Ghione, S., and Ripoli, A., "Blood pressure evaluation based on arterial pulse wave velocity," *Computers in Cardiology*, pp: 397 – 400, 1996.

[27] Allen, J. and Murray, A., "Comparison of regional variability in multi-site photoplethysmographic pulse wave characteristics," *Proc. of 1st International Conference on Advances in Medical Signal and Information*, pp. 26 - 314-316, 2000.

[28] Okada, M., "Possible determinants of pulse-wave velocity in vivo," *IEEE Transactions on Biomed Eng.*, **35**: 357 – 361, 1988.

[29] Nitzan, M., Babchenko, A., Faib, I., Davidson, E., and Adler, D., "Assessment of changes in arterial compliance by photoplethysmography," *The 21st IEEE Convention of the Electrical and Electronic Engineers in Israel*, pp: 351 – 354, 2000.

[30] Olsson E., Ugnell H., Oberg PA., and Sedin G., "Photoplethysmography for simultaneous recording of heart and respiratory rates in newborn infants," *Acta Paediatrica.*, **89(7)**: 853-861, 2000.

[31] Kyriacou, P.A., Powell, S., Langford, R.M., and Jones, D.P., "Esophageal pulse oximetry utilizing reflectance photoplethysmography," *IEEE Transactions on Biomed Eng.*, **49**: 1360 – 1368, 2002.

[32] Bloom L.J., "An evaluation of finger pulse volume as a psycho-physiological measure of anxiety," *Psychophysiol.*, **13**: 40-42, 1976.

[33] Herztman A.B., "Photoplethysmography of the fingers and toes in man," *Proc. Soc. Exp. Biol. Med.*, **37**: 529-534, 1937.

[34] H. Ugnell and P. Å. Öberg, "The time-variable photoplethysmographic signal; dependence of the heart synchronous signal on wavelength and sample volume," *Medical Engineering & Physics*, **17**: 571-578, 1995.

[35] Iketani Y., Iketani T., Takazawa K., and Murata M., "Second derivative of photoplethysmogram in children and young people," *Japanese Circulation Journal.*, **64(2)**:110-116, 2000.

[36] Geddes L.A., Voelz M.H., Babbs C.F., Bourland J.D., and Tacker W.A., "Pulse transit time as an indicator of arterial blood pressure," *Psychophysiol.*, **18**: 70-75, 1981.

[37] Loukogeorgakis S., Dawson R., Phillips N., Martyn CN., and Greenwald SE, "Validation of a device to measure arterial pulse wave velocity by a photoplethysmographic method," *Physiological Measurement.*, **23(3)**:581-596, 2002.

[38] Paul A. Obrist, Kathleen C. Light, James A. Mccubbin, J. Stanford Hutcheson, and J. Lee Hoffer, "Pulse transit time: relationship to blood pressure and myocardial performance," *Psychophysiology*, pp. 292-301, 1979.

[39] Nitzan, M., Babchenko, A., Turivnenko, S., and Khanokh, B., "Spontaneous fluctuation in the tissue blood volume and the systolic blood volume increase," *Nineteenth Convention of Electrical and Electronics Engineers in Israel*, pp. 228-230, 1996.

[40] M. Di Rienzo, Blood pressure and heart rate variability: computer analysis, modeling and clinical applications, Amsterdam: IOS Press, 1993.

[41] U.S. National Library of Medicine, Medical Encyclopedia—Pulse, U.S.A., 2003; http://www.nlm.nih.gov/medlineplus/ency/article/003399.htm.

[42] Pallas-Areny, R., Colominas-Balague, J., and Rosell, F.J., "The effect of respiration-induced heart movements on the ECG," *IEEE Trans. Biomed. Eng.*, **36**: 585-590, 1989.

[43] Winter, I. M., D. Robertson, D., and Yates, G. K., "Diversity of characteristic frequency rate-intensity functions in guinea pig auditory nerve fibers," *Hearing Research*, **45(3)**: 191-202, 1990.

[44] Yates, G. K., "Basilar membrane nonlinearity and its influence on auditory nerve rate-intensity functions," *Hearing Research*, **50(1-2)**: 145-162, 1990.

[45] Sherebrin, M.H.; Sherebrin, R.Z., "Frequency analysis of the peripheral pulse wave detected in the finger with a photoplethysmograph," *IEEE Trans. Biomed. Eng.*, **37**: 313 – 317, 1990.

[46] J. Weinman, A. Hayat, and G. Raviv, "Reflection plethysmography of arterial blood volume pulses," *Med. Biol. Eng. Comput.*, **124**: 22-31, 1977.

[47] Moyle, John T. B., Pulse oximetry, London: BMJ, 2002.

[48] Wilmer W. Nichols and Michael F., McDonald's blood flow in arteries: theoretical, experimental and clinical principles, London: Arnold; New York: Oxford University Press, 1998.

[49] Li J. K-J, Comparative cardiovascular dynamics of mammals, CRC Press, New York, 1996.

[50] Ward, S., Heneghan, C., and Nolan, P., "An integrate-and-fire based model of PP and PR variability in the human electrocardiogram," *Proc. of 1st International IEEE EMBS Conference on Neural Engineering*, pp: 297 – 300, 2003.

[51] Gnudi, G., "Estimation of arterial system parameters from noninvasive measurements," *Proc. of Computers in Cardiology*, pp: 661 – 664, 1991.

[52] Cappello, A. and Gnudi, G., "Analysis of the arterial pressure-volume curve in the three-element windkessel model," *Proc. of Computers in Cardiology*, pp: 385 - 388, 1993.

[53] Melgers, M.C., Swenne, C.A., van De Vooren, H., and van der Wall, E.E., "Interaction between the arterial baroreflex and a hypertensive stressor: a mathematical model," *Computers in Cardiology*, pp: 45 – 48, 2002.

[54] Joannides R., Richard V., Haefeli WE., Benoist A., Linder L., Luscher TF., and Thuillez C., "Role of nitric oxide in the regulation of the mechanical properties of peripheral conduit arteries in humans," *Hypertension.* **30(6)**:1465-1470, 1997.

[55] Heron E., Chemla D., Megnien JL., Pourny JC., Levenson J., Lecarpentier Y., and Simon A., "Reactive hyperemia unmasks reduced compliance of cutaneous arteries in essential hypertension.," *Journal of Applied Physiology,* **79(2)**:498-505, 1995.

[56] Hedman AE, Hartikainen JEK, Tahvanainen KUO, and HakumakiMOK, "The high frequency component of heart rate variability reflects cardiac parasympathetic modulation rather than parasympathetic 'tone'," *Acta Physiol Scand*, **155**: 267-273, 1995.

[57] Malik M and Camm AJ, "Components of heart rate variability- what they really mean and what we really measure," *Am J Cardiol,* **72**: 821-822, 1993.

[58] Berger RD, Saul JP, and Cohen RJ, "Transfer function analysis of autonomic regulation I. Canine atrial rate response," *Am J Physiol* 256: H142-H152, 1989.

[59] X.F. Teng and Y.T. Zhang, "The effect of contacting force on photoplethysmographic signals," submitted to *Physiological Measurement.*

[60] C.M. Lee and Y.T. Zhang, "Effect of the local temperature change on pulse transit time," submitted to *Physiological Measurement.*

[61] Moyle, John T. B., Pulse oximetry, London: BMJ, 2002.

[62] Carta, D.R., "Parameter estimation of a physiological model for heat exchange during cardio-pulmonary bypass," *in Proc. 17th Annual Conference IEEE Engineering in Medicine and Biology Society*, **2**: 1427-1428, 1995.

[63] Marek Malik and A. John Camm, Heart rate variability, Armonk, NY: Futura Pub. Co., c1995.

[64] Golub; Howard L., Method and apparatus for non-invasive, cuffless, continuous blood pressure determination, US patent 5,865,755, 1999.

[65] U. Zwiener, "Physiological interpretation of autospectra, coherence and phase spectra of blood pressure, heart rate and respiration in man," *Automedica,* **2**: 161-169, 1978.

[66] B. Fiser, N. Honzikova, and J. Penaz, "Power spectra of spontaneous variations of indirectly recorded blood pressure, heart rate and acral blood flow," *Automedica*, **2**: 143-147, 1978.

[67] Maestri, R., Pinna, G.D., Gobbi, E., Robbi, E., and La Rovere, M.T., "Spectral analysis of arterial blood pressure variability: assessing the accuracy of the finometer device," *Computers in Cardiology*, pp: 505 – 508, 2003.

[68] deBoer RW., Karemaker JM., and Strackee J. "Hemodynamic fluctuations and baroreflex sensitivity in humans: a beat-to-beat model," *American Journal of Physiolog,* **253**: H680-9, 1987.

[69] Brunelli, R. and Poggio, T., "Face recognition: Features versus templates", *IEEE Trans. on Pattern Analysis and Machine Intelligence*, **15**: 1042-1052, 1993.

[70] A. Samal and P. A. Iyengar, "Automatic recognition and analysis of human faces and facial expressions: A survey," *IEEE Transactions Pattern Recognition*, **25**: 65-67, 1992.

[71] D. Dunn, "Using a multi-layer perceptron neural for human voice identification," *Proc. of the 4th Int. Conf. Signal Process. Applicat. Technol.*, Newton, MA, USA, 1993.

[72] Negin, M., Chmielewski, T.A., Jr., Salganicoff, M., von Seelen, U.M., Venetainer, P.L. and Zhang, G.G., "An iris biometric system for public and personal use," *Computer*, **33**: 70-75, 2000.

[73] Kyong Seok Paik, Chin Hyan Chung, Jin Ok Kim and Dae Jun Hwang, "On a lip print recognition by the pattern kernels with multiresolution architecture," *Proc. of*

International Conference on Image Processing, **2**: 246-249, 2001.

[74] ChewYean Yam, Nixon, M.S. and Carter, J.N., "Performance analysis on new biometric gait motion model," *Proc. of the 5th IEEE Southwest Symposium on Image Analysis and Interpretation*, pp. 31-34, 2002.

[75] Paranjape, R.B., Mahovsky, J., Benedicenti, L. and Koles', Z., "The electroencephalogram as a biometric," *Canadian Conference on Electrical and Computer Engineering*, **2**: 1363-1366, 2001.

[76] Biel, L., Pettersson, O., Philipson, L. and Wide, P., "ECG analysis: a new approach in human identification," *IEEE Transactions on Instrumentation and Measurement*, **50**: 808-812, 2001.

[77] Biel, L., Pettersson, O., Philipson, L. and Wide, P., "ECG analysis: a new approach in human identification," I*MTC/99, Proc. of the 16th IEEE Instrumentation and Measurement Technology Conference*, **1**: 557-561, 1999.

[78] T. W. Shen, W. J. Tompkins and Y. H. Hu, "One-Lead ECG for Identify Verification," *2nd Joint Conference of the IEEE EMBS and the Biomedical Engineering Society*, Huston, 2002

[79] Ruud.M Bolle, Sharath Pankanti and Nalini K. Ratha, "Evaluation Techniques for Biometric-based Authentication System (FRR)," *Proc. of the 15th International Conference on Pattern Recognition*, **2**: 831-837, 2000.

[80] D. McNeil and P. Freiberger, Fuzzy Logic, Touchstone, Simon & Schuster, Old Tappan, N.J., 1994.

[81] De Ru, W.G. and Eloff, J.H.P., "Enhanced password authentication through fuzzy logic," *IEEE Expert*, **12**: 38-45, 1997.

Publication List:

Journal Paper:

Y. Y. Gu and Y. T. Zhang,, "A Study on the Correlations between the Features of Photoplethysmographic Signal" submitted to *Physiological Measurement.*

Conference Papers:

Y. Y. Gu, Y. Zhang, and Y. T. Zhang, "A Novel Biometric Approach in Human Verification by Photoplethysmographic Signals," in *4th Annual IEEE EMBS Special Topic Conference on Information Technology Applications in Biomedicine,* Birmingham, UK, 2003.

T. Ma, ***Y. Y. Gu,*** and Y. T. Zhang, "A Novel Biometric approach by Evoked Action Potential," in *1st International IEEE EMBS Conference on Neural Engineering,* Capri Island, Italy, 2003.

Y. T. Zhang, K. Hung, L. Yip, and ***Y. Y. Gu,*** "Telemedicine: Opportunities and Challenges," in *5th Asia Pacific Conference on Medical and Biological Engineering and 11th International Conference on Biomedical Engineering*, Singapore, 2002.

Y. Y. Gu and Y. T. Zhang, "Reducing the Influence of Contacting Force Applied on Photoplethysmographic Sensor on Heart Rate Variability Estimation," in *25th Annual International Conference of the IEEE EMBS*, Mexico, 2003

Y. Y. Gu *and* Y. T. Zhang, "Photoplethysmographic Authentication through Fuzzy Logic," in IEEE EMBS Asian-Pacific Conference on Biomedical Engineering, Japan, 2003.

Y. Y. Gu, Y. T. Zhang,, and T. Ma, "A theoretical analysis of the firing rate function based on an integral pulse frequency modulation model," in IEEE EMBS Asian-Pacific Conference on Biomedical Engineering, Japan, 2003.

Y. Y. Gu, and Y. T. Zhang, "Effects of neural dynamics on information decoding," Proceedings of Chinese Biomedical Engineering Conference (in press), Wuxi, China, 2003.

Y. Y. Gu and Y. T. Zhang, "发展远程医疗及家庭保健仪器," Proceedings of Chinese Biomedical Engineering Conference, Xiamen, China, 2002.

Patent

Y. Y. Gu, Y. T. Zhang,, Y. Zhang, and T. Ma, "A Method for Human Verification Using Evoked Action Potential Signal".

Y. Zhang, Y. T. Zhang, and ***Y. Y. Gu,***, "A Method for Human Verification Using Photoplethysmographic Signal".